Aalborg Universitet

AALBORG UNIVERSITY
DENMARK

Electric Vehicle Batteries State Estimation Under a Wide Range of Test and Aging Conditions

Gismero, Alejandro

DOI (link to publication from Publisher):
10.54337/aau510574496

Publication date:
2022

Document Version
Publisher's PDF, also known as Version of record

Link to publication from Aalborg University

Citation for published version (APA):
Gismero, A. (2022). *Electric Vehicle Batteries State Estimation Under a Wide Range of Test and Aging Conditions*. Aalborg Universitetsforlag. https://doi.org/10.54337/aau510574496

General rights
Copyright and moral rights for the publications made accessible in the public portal are retained by the authors and/or other copyright owners and it is a condition of accessing publications that users recognise and abide by the legal requirements associated with these rights.

- Users may download and print one copy of any publication from the public portal for the purpose of private study or research.
- You may not further distribute the material or use it for any profit-making activity or commercial gain
- You may freely distribute the URL identifying the publication in the public portal -

Take down policy
If you believe that this document breaches copyright please contact us at vbn@aub.aau.dk providing details, and we will remove access to the work immediately and investigate your claim.

Downloaded from vbn.aau.dk on: April 26, 2024

ELECTRIC VEHICLE BATTERIES STATE ESTIMATION UNDER A WIDE RANGE OF TEST AND AGING CONDITIONS

BY
ALEJANDRO GISMERO GALIATSATOS

DISSERTATION SUBMITTED 2022

AALBORG UNIVERSITY
DENMARK

Electric Vehicle Batteries State Estimation Under a Wide Range of Test and Aging Conditions

Ph.D. Dissertation

Alejandro Gismero Galiatsatos

Dissertation submitted September, 2022

Dissertation submitted: September, 2022

PhD supervisor: Assoc. Prof. Erik Schaltz
Aalborg University

Assistant PhD supervisor: Assoc. Prof. Daniel-Ioan Stroe
Aalborg University

PhD committee: Professor Huai Wang (chairman)
Aalborg University, Denmark

Professor Julia Kowal
Technische Universität Berlin, Germany

Associate Professor Chresten Træholt
Technical University of Denmark, Denmark

PhD Series: Faculty of Engineering and Science, Aalborg University

Department: AAU Energy

ISSN (online): 2446-1636
ISBN (online): 978-87-7573-813-7

Published by:
Aalborg University Press
Kroghstræde 3
DK – 9220 Aalborg Ø
Phone: +45 99407140
aauf@forlag.aau.dk
forlag.aau.dk

© Copyright: Alejandro Gismero Galiatsatos

Printed in Denmark by Stibo Complete, 2022

Abstract

The performance of the battery is not invariable throughout its lifetime. Degradation causes a persistent decay in performance that increases over time leading to the end of its useful life. The impact of the degradation will depend on the application and performance requirements. Stationary batteries are generally oversized and can provide the required performance until very advanced states of degradation. However, this is an especially critical aspect in electric vehicles since a loss of capacity will directly affect the driving range. Similar vehicles may be exposed to very different operating conditions, i.e. frequent use of a work or shared vehicle versus light use of a car intended for commuting; fast charges vs. slow overnight charges; or large temperature differences between countries or seasons during the year. Therefore, in this thesis, a thorough set of tests is developed considering the different factors that affect battery degradation. These tests include both cycling and calendar profiles, at different temperatures and charge/discharge currents. To analyze the degradation, the cells are subjected to periodic performance tests in order to evaluate parameters such as capacity and resistance, as well as changes in the open circuit voltage (OCV) curves.

The state estimation is a fundamental task in most applications based on battery storage. The voltage, current and temperature measurements are essential to delimit the zone of safe operation of the batteries. However, information about the remaining capacity or battery degradation cannot always be measured directly during normal battery operation. State of charge (SOC) and state of health (SOH) are very useful parameters for the user and are relatively easy to obtain through specific tests. Although, when this is not possible, it is necessary to estimate them indirectly by using a model of the battery. For further improvement of the SOC estimation, the impact of different operating conditions on the estimate accuracy is analyzed. With the knowledge acquired, a robust method of SOC and SOH estimation is proposed, allowing to estimate the state of the battery accurately under variable working conditions.

Although SOH estimation of electric vehicle is highly relevant, it also has great limitations. The data from the previous history of the vehicle is not

usually known, in addition the access to the battery and the tests that can be carried out are limited. To deal with these handicaps, different techniques based on impedance measurement, such as the electrochemical impedance spectroscopy (EIS) or the hybrid pulse power characterization (HPPC); and the analysis of the voltage curve as the incremental capacity analysis (ICA) are analyzed. Moreover, the impact of charging rate and battery temperature are studied through an extensive set of tests in which the cells are subjected to different aging conditions as well as on real vehicles, providing evidence that it is possible to improve accuracy when these factors are considered.

Therefore, throughout this dissertation, the impact of different aging conditions is analyzed, as well as the influence of the operating conditions during the tests on the battery state estimation, which is especially focused on electric vehicles.

Resumé

Et batteris egenskaber forandrer sig i løbet af dets levetid. Degradering forårsager et vedvarende fald i ydeevnen, hvilket bevirker, at batteriet på et tidspunkt ikke kan opfylde sin primære funktion længere. Virkningen af degraderingen afhænger af anvendelsen og kravene til ydeevnen. Stationære batterier er generelt overdimensionerede og kan levere den nødvendige ydeevne selv ved stor slitage. Dette er et særligt kritisk aspekt i elektriske køretøjer, da et tab af kapaciteten direkte vil påvirke rækkevidden. Lignende køretøjer kan blive udsat for meget forskellige driftsforhold, f.eks. hyppig brug af arbejdskøretøjer eller delebiler i forhold til let brug af en bil beregnet til pendling; hurtige opladninger i forhold til langsomme opladninger natten over; eller store temperaturforskelle mellem lande eller årstider i løbet af året. Derfor er der i denne afhandling udviklet omfattende test, der tager højde for de forskellige faktorer, som påvirker batteridegraderingen. Disse test omfatter både cykliske profiler og kalenderprofiler, ved forskellige temperaturer og op- og afladningsstrømme. For at analysere degraderingen udsattes cellerne for periodiske ydelsestest til at evaluere parametre som kapacitet og modstand, samt ændringer i kurven for åbenkredsløbsspændingen (OCV).

Tilstandsestimering er en grundlæggende nødvendighed i de fleste applikationer, hvor der indgår batterier. Måling af spænding, strøm og temperatur er afgørende for at afgrænse området for sikker brug af batterierne. Oplysninger om den resterende kapacitet eller batteridegradering kan dog ikke altid måles direkte under normal batteridrift. Ladningstilstand (SOC) og sundhedstilstand (SOH) er meget nyttige parametre for brugeren og er relativt nemme at opnå gennem specifikke tests. Selvom det ikke er muligt, er det nødvendigt at estimere dem indirekte ved at bruge en model af batteriet. For yderligere forbedring af SOC-estimatet, analyseres indvirkningen af forskellige driftsforhold For nøjagtigheden af estimereingen. Med den opnåede viden foreslås en robust metode til SOC- og SOH-estimering.

Selvom SOH-estimering af elektriske køretøjer er yderst relevant, har den også store begrænsninger. Dataene fra køretøjets tidligere historie er normalt ikke kendt, desuden er adgangen til batteriet og de test, der kan udføres,

begrænset. For at håndtere disse handicap analyseres forskellige teknikker såsom impedansmåling, elektrokemisk impedansspektroskopi (EIS), hybrid pulse power characterization (HPPC) samt incremental capacity analysis (ICA). Desuden studeres virkningen af opladningshastighed og batteritemperatur gennem et omfattende sæt af test, hvor cellerne udsattes for forskellige ældningsforhold såvel som på rigtige køretøjer, hvilket viser, at det er muligt at forbedre nøjagtigheden, når disse faktorer tages i betragtning.

Derfor, i denne afhandling analyseres påvirkningen af forskellige ældningsforhold, samt påvirkningen af driftsbetingelserne under testene på batteritilstandsestimeringen, som især er rettet mod elektriske køretøjer.

Preface

This Ph.D. thesis has been submitted to the Faculty of Engineering and Science at Aalborg University to fulfill the requirements for the Ph.D. degree in Energy Technology. This thesis compiles the results from three different research projects:

- eVolution2Grid - "Innovative Vehicle to Grid model for electric mobility deployment in Europe". Supported by the Electric Mobility Europe (EMEurope) programme and Innovation Fund Denmark.
- BATNOSTIC - "Adaptive BATtery diagNOSTIC tools for lifetime assessment of EV batteries". Funded by EUDP Denmark (Grant number: 64015-0611) .
- WABAT - "Workshop Automated BAttery Tester". Funded by EUDP Denmark (Grant number: 64019-0056) .

I would like to acknowledge the above-mentioned institutions and the consortium partners involved.

First of all, I would like to thank my main supervisor, Assoc. Prof. Erik Schaltz, who offered me the opportunity to work in the department and whose support has been essential for the achievement of this project. Also thank him for his patience and dedication, whatever my problem was, it quickly became one of his priorities. I am equally grateful to my co-supervisor, Assoc. Prof. Daniel-Ioan Stroe for his guidance and sincere feedback as well as for his knowledge and dedication in the laboratory, without which this work would not have been possible.

Special thanks to Kjeld Nørregaard, Bjarne Johnsen and Lasse Stenhøj from the Danish Technological Institute, for all the interesting discussions and the valuable data provided during the course of the project.

I would also like to thank Matthieu Dubarry from Hawaii Natural Energy Institute for providing me their external cooperation and valuable comments on my research work.

I am also grateful to my colleagues Václav Knap, Jia Guo and Yaqi Li for their help in practical matters and with laboratory related work.

I would like to extend my sincere thanks to Elisa Braco, whose support and energy reached me when I needed it most.

Finally, I would like to express my most sincere gratitude to my family and friends for their essential encouragement and patience to undertake this long journey. Especially to my partner, Beatriz, who despite the distance did not stop inspiring or supporting me for a single day.

Alejandro Gismero Galiatsatos
Aalborg University, September 28, 2022

Contents

Abstract iii

Resumé v

Preface vii

I Summary 1

1 Introduction 3
1.1 Background . . . 3
1.2 Research Objectives and limitations . . . 5
1.2.1 Objectives . . . 5
1.2.2 Limitations . . . 6
1.3 Battery cells used in this research . . . 7
1.4 Thesis Outline . . . 8
1.5 List of Publications . . . 9

2 Degradation Analysis of Electric Vehicle Lithium-Ion Batteries 11
2.1 Introduction . . . 12
2.2 Methodology . . . 12
2.2.1 Calendar Aging Tests . . . 13
2.2.2 Cycling Aging Tests . . . 14
2.2.3 Reference Performance Test . . . 15
2.3 Accelerated Aging Results . . . 18
2.3.1 Cell A . . . 18
2.3.2 Cell B . . . 20
2.3.3 Cell C . . . 24
2.3.4 Cell D . . . 28
2.4 Summary . . . 31

3 Online Battery State Estimation **33**
3.1 Introduction . . . 34
3.2 Methodology . . . 36
3.3 Temperature and Current Influence . . . 38
3.4 Proposed Method . . . 42
3.5 Summary . . . 45

4 Offline SOH Estimation **47**
4.1 Impedance Based SOH Estimation . . . 48
4.1.1 Electrochemical Impedance spectroscopy . . . 48
4.1.2 Hybrid Pulse Power Characterization . . . 55
4.2 Open Circuit Voltage Based Estimation . . . 60
4.3 Summary . . . 75

5 Conclusions and Future Work **77**
5.1 Conclusions . . . 77
5.2 Main Contributions . . . 79
5.3 Future Work . . . 80
References . . . 81

II Papers **89**

J1 Recursive State of Charge and State of Health Estimation Method for Lithium-Ion Batteries Based on Coulomb Counting and Open Circuit Voltage **91**

J2 Electric Vehicle Battery State of Health Estimation Using Incremental Capacity Analysis **93**

J3 Influence of Test Conditions in the Incremental Capacity Analysis for the State of Health Estimation of Lithium-ion Batteries for Electric Vehicles **95**

C1 Calendar Aging Lifetime Model for NMC-based Lithium-ion Batteries Based on EIS Measurements **97**

C2 Comparative Study of State of Charge Estimation Under Different Open Circuit Voltage Test Conditions for Lithium-Ion Batteries **99**

Acronyms

ANN Artificial Neural Network.

BEV Battery Electric Vehicle.

BMS Battery Management System.

BOL Beginning of Life.

CC Constant Current.

CV Constant Voltage.

DOD Depth of Discharge.

DRV Driving Profile.

DV Differential Voltage.

DVA Differential Voltage Analysis.

EEC Electrical Equivalent Circuit.

EIS Electrochemical Impedance Spectroscopy.

EKF Extended Kalman Filter.

EOL End of Life.

EV Electric Vehicle.

FEC Full Equivalent Cycle.

FOI Feature of Interest.

HPPC Hybrid Pulse Power Characterization.

IC Incremental Capacity.

ICA Incremental Capacity Analysis.

ICEV Internal Combustion Engine Vehicle.

KF Kalman Filter.

LAM Loss of Active Material.

LLI Loss of Lithium Inventory.

LMO Lithium Manganese Oxide.

MAE Mean Absolute Error.

NCA Lithium Nickel Cobalt Aluminum Oxide.

NMC Lithium Nickel Manganese Cobalt Oxide.

NRMSE Normalized Root Mean Squared Error.

OCV Open Circuit Voltage.

ORI Ohmic Resistance Increase.

RMSE Normalized Root Mean Squared Error.

RPT Reference Performance Test.

SEI Solid Electrolyte Interphase.

SOC State of Charge.

SOH State of Health.

SVM Support Vector Machine.

V2G Vehicle to Grid.

WLTP Worldwide Harmonized Light Vehicles Test Procedure.

Part I

Summary

Chapter 1

Introduction

1.1 Background

In the last decade, concern about global warming and emissions has increased, compelling governments to reach agreements with increasingly demanding goals. In the context of the European Green Deal, the European Commission has set the goal of achieving climate neutrality by 2050. To this end, other mid-term goals have been set, such as reducing emissions by at least 55% compared to 1990 by the year 2030 [1]. The transport sector has a great impact on greenhouse gas emissions. In Europe, transport in general accounts for 27% of the emissions and 22% are caused by road transport. These emissions are mainly due to the type of energy used during the use phase, which in the EU more than 90% corresponds to fossil fuels [2].

In addition, road transport is responsible for more than a third of NOx emissions, which have a high negative impact on the health of population, especially in urban areas, and is responsible for thousands of premature deaths every year [3]. Due to the relevance of road transport emissions, new proposals have been launched suggesting to accelerate the transition towards clean mobility to a 100% reduction in new passenger and light commercial vehicles by 2035 [4].

To meet these quotas, a strong growth in electric vehicle sales is expected, with estimates of 60% of new car sales [5]. In the following decades, the recycling industry will have to expand accordingly in order to absorb a large number of batteries from vehicles at the end of their useful life. In [6], the authors forecast recycling needs within 12 and 138 GWh annually from 2030. However, before this occurs, there will be a great potential for second-hand or repurposing as stationary storage for grid and buildings [7].

Currently in the EU countries, the used car market is considerably larger than the new car market in terms of number of vehicles. Despite the differ-

ences among EU countries, on average a vehicle has 3-4 owners throughout its life, estimating a used/new car ratio for the EU greater than 3 [8].

Unlike combustion vehicles, the second-hand market for electric vehicles is not yet established. In contrast to internal combustion engine vehicles (ICEVs), the cost structure is different in battery electric vehicles (BEVs). The battery is the most expensive element of the vehicle, it accounts for a third of the total cost and, although the cost of batteries is expected to decrease, it will continue to account for a large part of the total cost of the vehicle in 2030 [9].

The lack of means to reliably diagnose the state of the batteries can generate uncertainty to potential buyers of a used EV since the driving range and useful life are the aspects that most concern people when purchasing an electric vehicle [10, 11]. Therefore, due to the special conditions of the electric vehicles market, the development of accurate tools to evaluate the performance and degradation of the batteries is essential.

Battery Management Systems (BMS) are responsible for controlling and monitoring the state of the battery and play an important role in guaranteeing safety and avoiding the hazards related to lithium-ion technology when operated outside of the limits set by the manufacturer [12].

The BMS is also in charge of estimating the short-term capabilities of the battery, depending on the operation of the battery and external conditions. The main parameter is the State of Charge (SOC), which represents the amount of energy available in the battery compared to when it is fully charged and its knowledge is particularly important in EV applications as it indicates the driving range of the vehicle.

The definition of SOC refers to the actual capacity of the battery which is likely to change with degradation, therefore, for certain applications it is necessary to use models that also provide information about the long-term capabilities of the battery.

The State of Health (SOH) indicates the battery degradation and performance capabilities compared to a fresh battery. There is no absolute definition of the SOH and it depends on the variables used to estimate it, being the two most common the capacity and the internal resistance.

There are numerous methods to estimate the battery SOH that can be classified according to the way data is processed and what data is required for the estimation.

These methods are divided into online or offline methods depending on whether the data is processed in real time or retroactively. The offline approaches generally provide large sets of data gathered in the laboratory from different pre-established test conditions. On the other hand, online methods use measurements obtained in real time and are often embedded in the BMS thus, with a more limited amount of data and processing capacity [13, 14]. Depending on the data used, the methods can be classified as experimental

methods or adaptive methods [15]. Experimental methods use previously stored data and relate certain parameters to battery degradation such as internal resistance [16, 17], partial capacity [18, 19] or parameters derived from the open circuit voltage (OCV) curve [20, 21]. On the other side, adaptive methods use equivalent circuit models or black box approaches to monitor battery degradation. The Kalman filter is the most widespread method that allows updating the parameters of the equivalent circuit through measurements observed over time [22, 23].

The scientific literature on battery SOH estimation methods is very extensive, however, its actual application in electric vehicles is very limited. Most of the proposed methods require a large amount of vehicle usage data, which is often not available or accessible by third parties. Therefore, the purpose of this work is to investigate how to improve and apply the existing methods to the specific application of electric vehicles.

1.2 Research Objectives and limitations

1.2.1 Objectives

The electrification of transport and the implementation of renewable energies are introducing a large number of batteries into the market and their useful life is one of the greatest concerns of users. There is a great potential in the second hand or second life of EVs or their batteries, but this must be supported by certain guarantees. To achieve satisfactory performance throughout the entire battery life and towards the ecological transition, reliable methods must be developed in order to allow users to know what they can expect from their batteries at any time during their useful life. The aim of this thesis is to investigate how to improve the current estimation methods by evaluating the operating conditions during the tests. Therefore, the work focuses on the following objectives:

O1. Evaluate the degradation of the cells under different conditions to subsequently identify path independent estimators.

The degradation performance of the cells studied will be analyzed. The cells will be subjected to calendar and cycling aging tests under different conditions of temperature, SOC and current profiles. The degradation behavior of the different cells should be studied in depth to identify possible trends and relations.

O2. Analyze the impact of different operating conditions on the online battery state estimation and propose a robust estimation method for electric vehicles.

The OCV curves and the impact of aging, temperature and the methods used to obtain them will be compared. The effect that OCV curves and the different working conditions have on the SOC estimation accuracy will be discussed and, according to the results obtained, a reliable SOC and SOH estimation method for electric vehicles should be proposed.

O3. Analyze the performance of different methods to assess the degradation of electric vehicles with data collected from similar cells or vehicles.

Different methods of SOH estimation for electric vehicles based on different parameters will be evaluated. Two techniques to obtain impedance such as EIS and HPPC will be compared, analyzing their performance to estimate capacity fade from the variation of the internal resistance. The use of vehicle chargers to estimate the batteries SOH during charging will be also discussed. The ICA technique will be applied to both cells and vehicles to verify its feasibility and the main factors that affect its performance will be studied.

1.2.2 Limitations

This Ph.D. project has several limitations as described below:

- All vehicles and cells analyzed are NMC-based with the exception of cell D which is NCA. Other chemistries are not investigated and, therefore, the results may not be applicable to other types of cells.
- The study of degradation is limited to capacity and resistance. Different operating conditions can lead to different aging modes, however this will not be investigated in this PhD project.
- Due to the difficulty of access to real vehicles, the data obtained is limited and, unlike the cells analyzed in the laboratory, it is not possible to control or monitor the aging conditions.
- The use of heavy-computational methods, such as neural networks, has a growing interest in academia, however these methods are outside the scope of this project.

1.3 Battery cells used in this research

The lithium batteries used in this work come from new battery packs of electric vehicles or are intended for them. Three of these batteries are lithium nickel manganese cobalt oxide ($LiNiMnCoO_2$) cathode based, also referred as NMC. Figure 1.1 shows some of the cells during the tests. This type of batteries has a great specific energy and provide high power, thus it is at present the preferred chemistry for electric vehicles, although manufacturers are starting to move towards lower cobalt configurations due to its high price.

The first battery is a cylindrical cell of the Samsung brand with 3.4 Ah capacity. This battery was studied for its application in light vehicles for industrial use with V2G capabilities. The second cell comes from a new spare module belonging to the first generation BMW i3. The pack was purchased and disassembled to analyze the individual cells separately. The third cell comes from second generation Nissan Leaf modules. The last cell chemistry is lithium nickel cobalt aluminum oxide ($LiNiCoAlO_2$) cathode based, also referred as NCA. It offers similar characteristics to NMC, moderately improving specific energy and lifespan, although it is a more hazardous chemistry in the event of thermal runaway [24]. The specifications of the cells are listed in detail in Table 1.1.

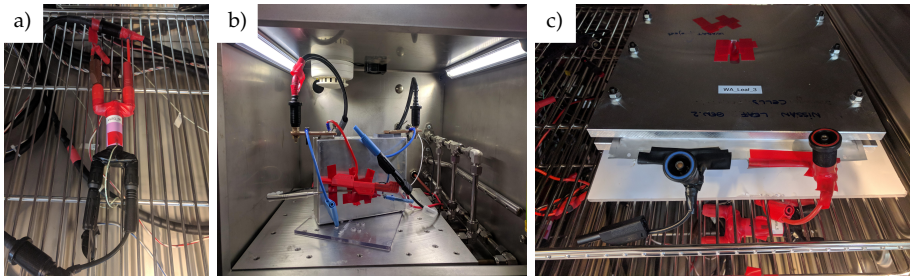

Fig. 1.1: The cells under study being tested in a climatic chamber. a) Cylindrical A-cell. b) Prismatic B-cell. c) Pouch C-cell mounted on a test fixture.

Table 1.1: Main specifications of the batteries used in the research.

Cells Specifications				
Item	**A**	**B**	**C**	**D**
Format	Cylindrical	Prismatic	Pouch	Cylindrical
Cathode	NMC	LMO/NMC	NMC	NCA
Nominal capacity	3.4 Ah	63 Ah	57.5 Ah	4.0 Ah
Max voltage	4.2 V	4.125 V	4.2 V	4.2 V
Cut-off voltage	2.65 V	3 V	2.6 V	2.6 V
Corresp. vehicle	Prototype	BMW-I3 2013	Nissan Leaf 2020	-

1.4 Thesis Outline

This Ph.D. thesis summarizes the outcomes and findings from the research of the Ph.D. project, including a report and a collection of publications. The structure of the thesis is presented in Figure 1.2, relating the chapters of the report with the corresponding outcomes, and is distributed as follows:

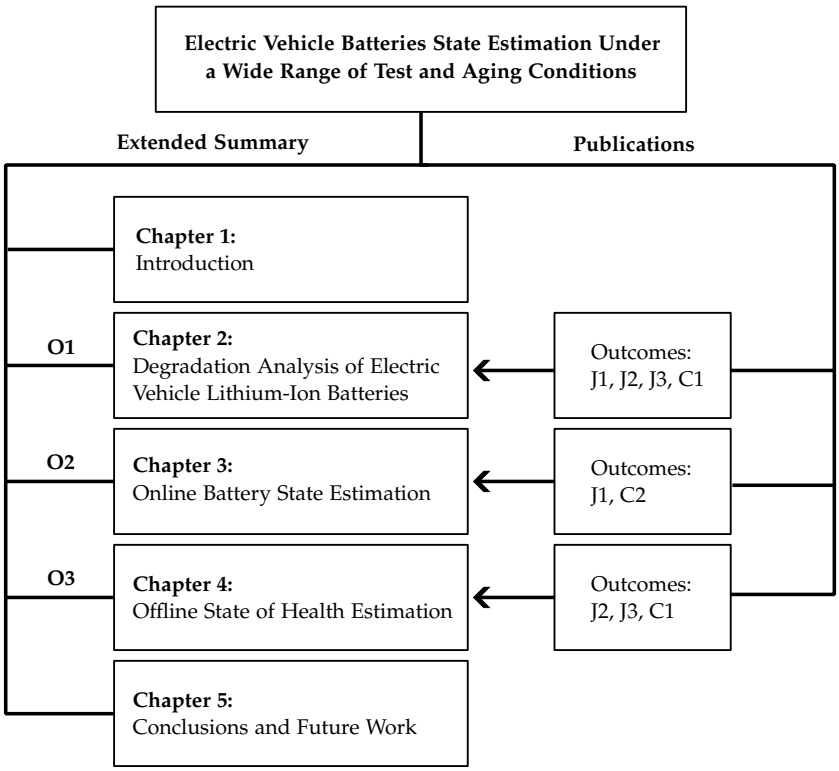

Fig. 1.2: Thesis structure with related project objectives (O1-O3) and outcomes.

Chapter 1 introduces the background, objectives and limitations of the project. Chapter 2 describes the methodology used for the aging tests and discusses the degradation results obtained from the analyzed cells when exposed to different conditions. Chapter 3 considers the influence of current and temperature on the online battery state estimation and proposes an estimation method to improve the estimate accuracy under variable conditions. Chapter 4 investigates the performance of different state of health estimation methods applied to both single cells and commercial vehicles. Chapter 5 concludes the outcomes and findings of the Ph.D. project and summarizes the main contributions and future research opportunities.

1.5 List of Publications

Journal Papers

J1. **A. Gismero**, E. Schaltz and D. -I. Stroe, "Recursive State of Charge and State of Health Estimation Method for Lithium-Ion Batteries Based on Coulomb Counting and Open Circuit Voltage," *Energies*, 2020, 1811, 13(7).

J2. **A. Gismero**, K. Nørregaard, B. Johnsen, L. Stenhøj, D. -I. Stroe, E. Schaltz. "Electric Vehicle Battery State of Health Estimation Using Incremental Capacity Analysis". *Journal Of Energy Storage*, under review, 2022.

J3. **A. Gismero**, M. Dubarry, J. Guo, D. -I. Stroe, E. Schaltz. "Influence of Test Conditions in the Incremental Capacity Analysis for the State of Health Estimation of Lithium-ion Batteries for Electric Vehicles". *Applied Energy*, under review, 2022.

Conference Papers

C1. **A. Gismero**, D. -I. Stroe and E. Schaltz, "Calendar Aging Lifetime Model for NMC-based Lithium-ion Batteries Based on EIS Measurements," *2019 Fourteenth International Conference on Ecological Vehicles and Renewable Energies (EVER)*, 2019, pp. 1-8.

C2. **A. Gismero**, D. -I. Stroe and E. Schaltz, "Comparative Study of State of Charge Estimation under Different Open Circuit Voltage Test Conditions for Lithium-Ion Batteries," *IECON Proceedings (Industrial Electronics Conference)*, 2020-October, 1767–1772.

Other Publications not included in the thesis

J4. A. Barragán-Moreno, E. Schaltz, **A. Gismero**, and D. I. Stroe, "Capacity State-of-Health Estimation of Electric Vvehicle Batteries Using Machine Learning and Impedance Measurements," *Electronics 2022*, Vol. 11, Page 1414, vol. 11, p. 1414, 4 2022

J5. F. Naseri, E. Schaltz, D. I. Stroe, **A. Gismero**, and E. Farjah, "An Enhanced Equivalent Circuit Model With Real-Time Parameter Identification for Battery State-of-Charge Estimation," *IEEE Transactions on Industrial Electronics*, vol. 69, pp. 3743–3751, 4 2022

J6. Q. Zhang, D. Wang, E. Schaltz, D.-I. Stroe, **A. Gismero**, and B. Yang, "Degradation Mechanism Analysis and State-of-Health Estimation for Lithium-ion Batteries Based on Distribution of Relaxation Times," *Journal of Energy Storage*, vol. 55, p. 105386, 11 2022

C3. V. Knap, L. Vestergaard, **A. Gismero**, and D.-I. Stroe, "Evaluation of the battery degradation factors for nano-satellites at LEO", *Proceedings of the International Astronautical Congress, IAC* vol. 2020-Octob, 2020.

C4. F. Naseri, E. Schaltz, D. I. Stroe, **A. Gismero**, E. Farjah, and S. Karimi, "State-of-Charge Estimation of NMC-based Li-ion Battery Based on Continuous Transfer Function Model and Extended Kalman Filter", *2021 12th Power Electronics, Drive Systems, and Technologies Conference, PEDSTC 2021*, 2 2021.

C5. V. Knap, M. Molhanec, **A. Gismero**, and D.-I. Stroe, "Calendar Degradation and Self-Discharge Occurring During Short and Long-Term Storage of NMC Based Lithium-ion Batteries," *ECS Transactions*, vol. 105, pp. 3–11, 11 2021.

Chapter 2

Degradation Analysis of Electric Vehicle Lithium-Ion Batteries

This chapter describes the methodology used for the aging tests and discusses the degradation results obtained from the studied cells when subjected to different working conditions. The results presented in this chapter are extracted from the following outcomes:

J1. **A. Gismero**, E. Schaltz and D. -I. Stroe, "Recursive State of Charge and State of Health Estimation Method for Lithium-Ion Batteries Based on Coulomb Counting and Open Circuit Voltage," *Energies*, 2020, 1811, 13(7).

J2. **A. Gismero**, K. Nørregaard, B. Johnsen, L. Stenhøj, D. -I. Stroe, E. Schaltz. "Electric Vehicle Battery State of Health Estimation Using Incremental Capacity Analysis". *Journal Of Energy Storage*, under review, 2022.

J3. **A. Gismero**, M. Dubarry, J. Guo, D. -I. Stroe, E. Schaltz. "Influence of Test Conditions in the Incremental Capacity Analysis for the State of Health Estimation of Lithium-ion Batteries for Electric Vehicles". *Applied Energy*, under review, 2022.

C1. **A. Gismero**, D. -I. Stroe and E. Schaltz, "Calendar Aging Lifetime Model for NMC-based Lithium-ion Batteries Based on EIS Measurements," *2019 Fourteenth International Conference on Ecological Vehicles and Renewable Energies (EVER)*, 2019, pp. 1-8.

2.1 Introduction

The operation of batteries involves reversible chemical reactions, which allow energy to be stored during charging and released during discharge. Electrolyte instability also causes side reactions with the electrodes that can result in the formation of solid electrolyte interphase (SEI). These side reactions lead to the progressive degradation of the battery performance, reducing the capacity and increasing its internal resistance [25]. Therefore, the battery lifetime is given by the number of cycles that the battery can withstand while maintaining adequate performance. However, in many applications the battery is subjected to prolonged idle times compared to when it is in use. In these cases, it is also necessary to know the lifetime in years.

Capacity decay during rest (idling or storage) and cycling is one of the major concerns related to the real life use of lithium batteries. Therefore, the prediction of the lifetime is usually based on the present capacity of the battery in relation to its original capacity. In general, it is considered that a battery is at the end of its useful life when it reaches 80% of the original capacity [26, 27] although batteries can continue functional far beyond that limit [7].

The knowledge about the expected batteries lifetime is mandatory in order to ensure the techno-economic feasibility of the application, however battery manufacturers are providing limited information about the lifetime and degradation performance of the battery. Also, the test needed at normal operating conditions are time demanding due to the relatively long life of the battery. Therefore, it is essential the development of accelerated aging test and battery lifetime models that provide reliable predictions.

2.2 Methodology

Throughout this work, three types of fresh batteries for electric vehicles have been used. In this type of application, the batteries are subjected to a combination of use (cycling) and rest times (idling). In order to design models that accurately predict the lifetime of the batteries, it is necessary to analyze both situations.

Battery degradation does not only depend on usage but it is the result of a combination of different physical and chemical mechanisms. These mechanisms produce different effects in the cell that can be summarized as loss of lithium inventory (LLI), loss of active material (LAM) of the positive and the negative electrodes and ohmic resistance increase (ORI) [28]. These modes of degradation depend on the stress factors to which the battery is subjected, so it is necessary to identify these factors correctly.

In the case of calendar aging, the most significant are the temperature and the storing SOC [29]. While for cycling aging, in addition to temperature and average SOC, is also affected by the number of equivalent cycles, as well as by the cycle depth and C-rate of these cycles [30].

The effects of stress factors on the lifetime of batteries can be non-linear. For this reason, it is advisable to apply sufficient levels of the stress factor in order to interpolate correctly and obtain an accurate lifetime model [31].

The tests were carried out following the procedure shown in Figure 2.1.

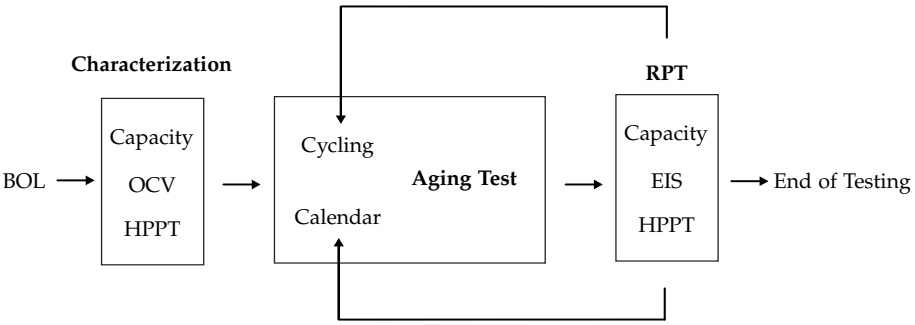

Fig. 2.1: Procedure for testing and aging assessment.

Firstly, the pristine cells at beginning of life (BOL) are subjected to preconditioning through the application of five successive cycles of charge and discharge. This allows checking that the cell performance corresponds to that indicated by the manufacturer, detect discrepancies between cells of the same batch and homogenize the capacity measurements after prolonged storage times.

Next, a characterization of the cells is carried out, in which the capacity at different temperatures and C-rates is measured, the open circuit voltage (OCV) recorded and the internal resistance measured.

Once the preliminary tests are finished, the aging tests are carried out. In the case of calendar aging tests, the cells are stored for a specific period of time at a specific temperature and SOC. Meanwhile the cycling aging cells are subjected to a charge/discharge profile for an equivalent number of cycles and at a controlled temperature. Once completed, a reference performance test is carried out and the procedure is repeated until the End of Life (EOL) or until the tests are concluded. Details about the RPT are described in Section 2.2.3.

2.2.1 Calendar Aging Tests

As previously explained, temperature and voltage have an important influence on degradation due to calendar aging. Depending on the application,

calendar aging may be the main contributor to degradation.

To evaluate the effect that these conditions have on the lifetime of the cells, the matrix test exposed in Table 2.1 was adopted. This procedure consists of the combination of at least three temperatures and three SOC levels designed to broadly cover the operating conditions. The cells are charged up to the established SOC level and stored in temperature-controlled chambers until the next RPT.

Table 2.1: Calendar aging test matrix.

Cell Type	Cell ID	Calendar aging test conditions	
		T [°C]	SOC [%]
A	-	-	-
B	Cal-01	35	50
	Cal-02	40	50
	Cal-03	45	50
	Cal-04	45	10
	Cal-05	45	90
	Cal-06	05	50
C & D	Cal-01	05	90
	Cal-02	25	90
	Cal-03	35	10
	Cal-04	35	50
	Cal-05	35	90
	Cal-06	45	90
	Cal-07	45	50

2.2.2 Cycling Aging Tests

In addition to the calendar aging tests, cycling aging tests were also performed to determine the behavior of the cells studied when operated under different conditions. As in the case of calendar aging, environmental conditions such as temperature as well as different charge and discharge profiles were analyzed. Also, the effect of different charging currents as well as different discharge profiles, some based on constant current (CC) and others based on driving profiles (DRV), were studied. The cells were tested in temperature-controlled chambers and the temperature of the cells was monitored through thermocouples located on their surface.

The test conditions used for the different cells are summarized in Table 2.2.

Table 2.2: Cycling aging test matrix.

Cell Type	Cell ID	Cycling aging test conditions		
		T [°C]	C-rate (Cha/Dis)	DOD [%]
A	Cyc 01-03	35	0.5 / 0.5 DRV	20
	Cyc 04-06	25		
	Cyc 07-09	15		
B	Cyc-01	10	1.5 / 1.5 CC	70
	Cyc-02	25	1.5 / 1.5 CC	
	Cyc-03	45	0.5 / 1.5 CC	
	Cyc-04	45	1.0 / 1.5 CC	
	Cyc-05	45	1.5 / 1.5 CC	
C & D	Cyc-01	10	0.3-1 / 0.5 DRV	65
	Cyc-02	25	0.3-1 / 0.5 DRV	
	Cyc-03	25	0.3-1 / 0.5 CC	
	Cyc-04	35	0.3-1 / 0.5 DRV	
	Cyc-05	35	0.3-1 / 0.5 DRV	

2.2.3 Reference Performance Test

The aging tests can take months or even years depending on the applied conditions. To study the incremental degradation of the battery performance parameters, periodic RPTs are performed. The test intervals depend on the applied conditions and the resolution requirements during the experiment. In some cases, shorter intervals were used at the beginning of the experiments to achieve higher resolution in the first battery life and were extended at the end to save resources. Table 2.3 shows the temperatures and test interval used for the four batteries analyzed. The test interval is given in days for the calendar aging tests and in full equivalent cycles (FEC) for the cycling aging tests.

Table 2.3: RPT, frequency and test temperatures.

Cell Type	Test interval		Test Temperature [°C]			
	Calendar	Cycling				
A	30 days	20 / 60 FEC			25	35
B		100 / 200 FEC			25	
C		150 FEC	10	17.5	25	35
D		150 FEC	10	17.5	25	35

Not all the batteries in this work were subjected to the same RPT due to different test purposes. Cell A is intended to be used in a fleet vehicle with V2G capabilities and therefore the cycling performance takes relevance. Shorter test frequencies were initially planned and changed during the aging test due to the low degradation measured. Cell B was used to develop a method for vehicle SOH estimation based on the voltage curve analysis and Cells C and D to verify the robustness of this method under different test conditions, and therefore the RPT was performed at a wide range of temperatures. The general procedure is presented in Figure 2.2 and described as follows:

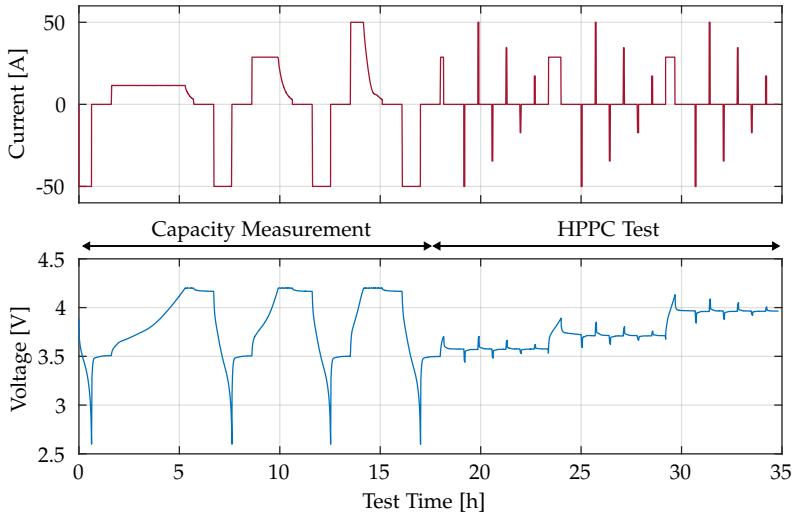

Fig. 2.2: RPT current profile and voltage response.

The RPT consists of two stages, in the first one, the capacity is measured. After a full discharge, the cell is charged and discharged at different rates to measure the capacity. The discharge is performed at constant current until reaching the cut-off voltage. The charging is performed following the constant current - constant voltage (CC-CV) procedure, while the cell is considered fully discharged by applying a constant current of 1C (or lower) until the cut-off voltage is reached. Each step is followed by a 1-hour rest period.

In the second stage, the impedance is determined by applying a Hybrid Pulse Power Characterization (HPPC) test as described in [32] and detailed in Chapter 3. Electrochemical Impedance Spectroscopy (EIS) is also used for cell B. These tests are applied at different SOCs to evaluate the impedance in the whole working range. A thermal chamber is used to ensure a constant ambient temperature during the test. The influence of the temperature is

investigated by repeating the same test multiple times. Table 2.3 shows the different temperatures considered during the RPTs.

Table 2.4 shows the capacity values measured in the first RPT for each of the analyzed cells and the mean and standard deviation of these values. Similarly, Table 2.5 shows the resistance values measured at the first RPT. The values were obtained by applying a one-second C/2 charging pulse. Except for cell D-Cyc-02 that shows an unusual high resistance value, the values obtained within each group are rather homogeneous. The differences between similar cells subjected to calendar or cycling aging are mainly due to the use of different measurement equipment. The graphs presented in the rest of the chapter show values obtained under the same conditions, relative to these first measurements of capacity and resistance.

Table 2.4: BOL capacity [Ah] of the tested cells measured at 25ºC and C/5.

Cal-	**A**	**B**	**C**	**D**	**Cyc-**	**A**	**B**	**C**	**D**
01	-	61.03	54.46	3.83	**01**	3.40	61.72	52.42	3.90
02	-	61.30	54.47	3.88	**02**	3.38	60.94	51.69	3.85
03	-	61.42	54.09	3.91	**03**	3.38	61.22	52.07	3.96
04	-	61.26	54.02	3.97	**04**	3.38	61.28	51.70	3.93
05	-	61.68	54.05	4.07	**05**	3.37	61.20	51.97	3.94
06	-	61.47	54.15	4.09	**06**	3.38	-	-	-
07	-	-	54.34	4.02	**07**	3.38	-	-	-
	-	-	-	-	**08**	3.36	-	-	-
	-	-	-	-	**09**	3.35	-	-	-
μ		61.36	54.23	3.97	μ	3.376	61.27	51.97	3.92
σ		0.217	0.193	0.098	σ	0.013	0.282	0.299	0.042

Table 2.5: BOL resistance [mΩ] of the tested cells measured at 25ºC and 50% SOC.

Cal-	**A**	**B**	**C**	**D**	**Cyc-**	**A**	**B**	**C**	**D**
01	-	0.823	1.131	23.20	**01**	46.27	0.599	0.964	44.26
02	-	0.857	1.032	23.27	**02**	48.44	0.615	1.022	66.70
03	-	0.890	0.986	24.61	**03**	47.51	0.607	0.955	38.66
04	-	0.891	1.090	23.35	**04**	46.87	0.607	1.004	36.09
05	-	0.856	0.990	22.99	**05**	47.25	0.581	1.022	46.77
06	-	0.861	0.954	22.90	**06**	47.06	-	-	-
07	-	-	0.994	23.99	**07**	47.17	-	-	-
	-	-	-	-	**08**	46.50	-	-	-
	-	-	-	-	**09**	47.74	-	-	-
μ		0.863	1.025	23.47	μ	47.20	0.602	0.993	46.49
σ		0.025	0.064	0.612	σ	0.653	0.013	0.032	12.071

2.3 Accelerated Aging Results

2.3.1 Cell A

Cycling Aging

Cell A was intended for usage in a vehicle with Vehicle to Grid (V2G) capabilities, so it would be active most of the time, therefore all efforts were focused on the cycling aging test. In order to determine the degradation behavior, three different temperatures (15ºC, 25ºC and 35ºC) and a discharge profile based on the WLTP driving cycle were used. For each aging condition, three identical cells were tested, making a total of nine cells. The cells were subjected to a total of 800 FECs over a period of 18 months. The aging procedure is detailed in [J1] and Chapter 3. Initially, an RPT was performed every 20 FEC. As little degradation was observed during the first 300 FEC, the separation between RPTs was increased. Cells Cyc-03, 06 and 09 were removed from the aging tests after 300 FEC for further analysis.

Capacity Fade

The capacity measured in the RPTs is shown in Figure 2.3 as a function of the cycles performed.

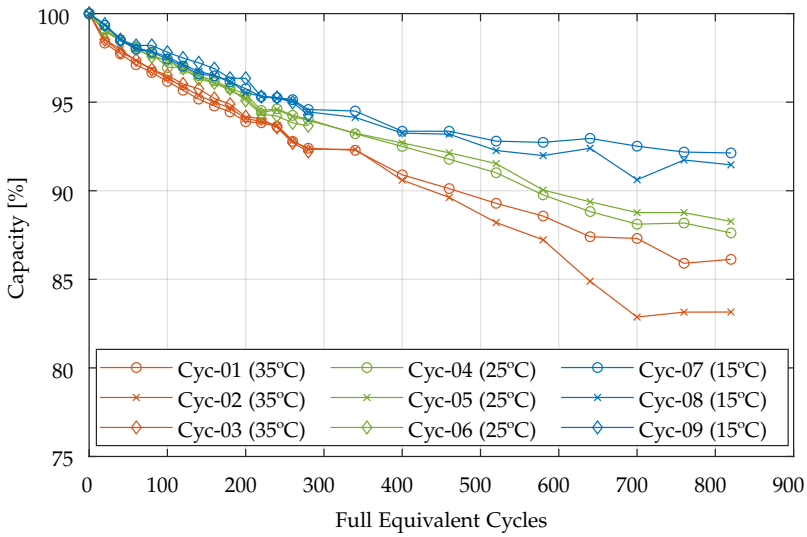

Fig. 2.3: Capacity fade of "Cell A" under cycling aging conditions. Measured at 25ºC and C/5.

In the cells subjected to higher temperatures, a greater loss of capacity

is observed, approximately 15%, after 800 cycles. When the temperature decreases, the loss of capacity is reduced, resulting in 12% for cells at 25ºC and 8% for cells at 15ºC

It is also observed that at lower temperatures the loss of capacity seems to slow down with time as expected. In the case of cells at 15ºC, most of the capacity fade (7%) occurred in the first 400 cycles, while in the next 400 only 1% more was measured.

Internal Resistance

The results of the internal resistance measurements are shown in Figure 2.4. The cells cycled at 15ºC show a similar resistance increase, accumulating a 10-15% increase after 800 cycles. Again, similar to capacity, the resistance increase slows after 400 cycles.

On the contrary, the cells subjected to 25ºC and 35ºC show a greater dispersion in the results than the cells at lower temperature. The resistance increments at the end of the test were between 25% and 45% and no significant difference was observed between the two test conditions.

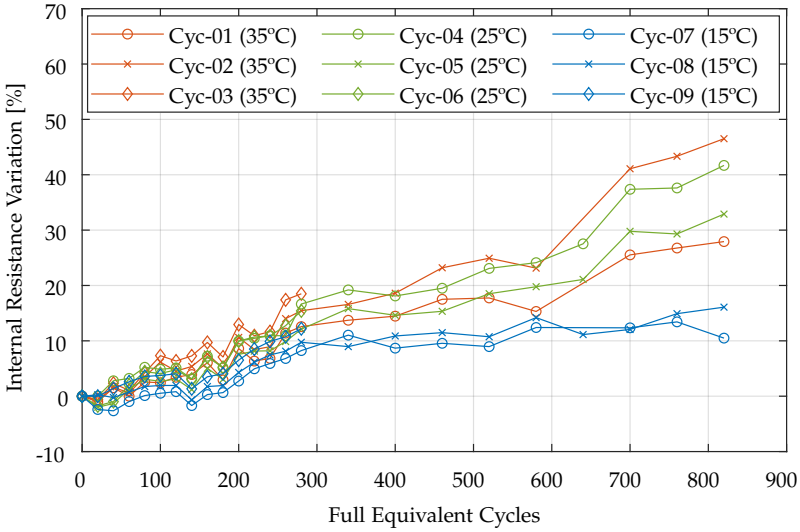

Fig. 2.4: Internal resistance of "Cell A" under cycling aging conditions. Measured at 25ºC and 50% SOC.

2.3.2 Cell B

Calendar Aging

To determine the calendar lifetime of cell B, six cells were subjected to calendar aging under the conditions stated in Table 2.1. To observe the influence of temperature, cells Cal-01 to Cal-03 were stored at 50% SOC and at three different temperatures (35, 40 and 45ºC). A fourth cell was stored at 5°C to investigate low temperature behavior. On the other hand, to observe SOC level influence Cal-03 to Cal-05 cells were stored at the same temperature (45ºC) but at three different SOC levels (10%, 50% and 90%).

Capacity Fade

The results obtained from the capacity measurements are shown in Figure 2.5. Observing the data obtained from the cells stored at 50% SOC, the influence of temperature can be analyzed. Taking the Cal-01 cell, stored at 35ºC, as a reference, it can be observed that after 20 months of testing, it has lost more than 15% of its initial capacity. When the storage temperature is increased by 5ºC, the loss of capacity almost doubles (Cal-02), reaching triple if the temperature increase is 10ºC (Cal-03). On the other hand, reducing the storage temperature to 5ºC allows the capacity loss during this time to be kept below 5%. As expected, the results agree with previous studies on the same type of battery. In [33] a similar degradation behaviour is reported for the same aging conditions.

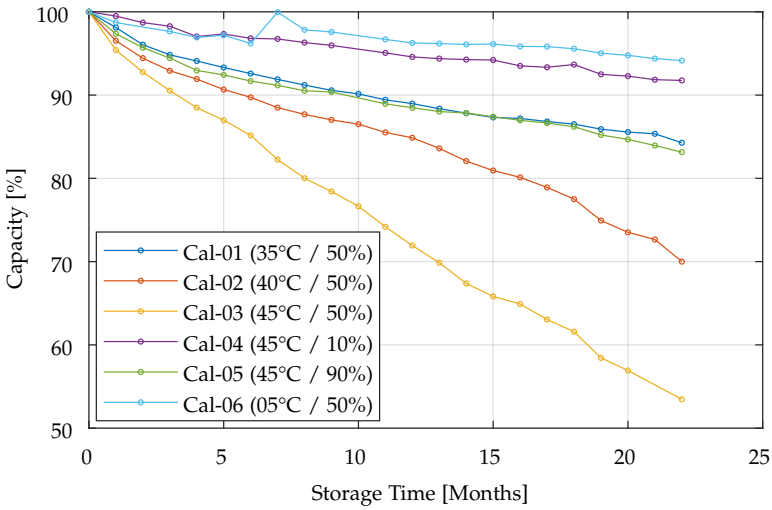

Fig. 2.5: Capacity fade of "Cell B" under calendar aging conditions. Measured at 25ºC and C/5. Source [J2].

Regarding the influence of SOC, the analysis of the cells stored at 45ºC (Cal-03, Cal-04 and Cal-05) shows that 50% SOC is the most harmful for the cells, as reported in [20]. On the contrary, the cell stored at 10% SOC (Cal-04) shows the least degradation, keeping 90% of its capacity. In general, a similar behaviour is observed regardless of the aging conditions, a first stage where the capacity fade slows down with the aging process and a second stage with a linear dependency between the capacity fade and the storage time.

Therefore, the results indicate that high temperatures in addition to medium levels of SOC would produce the most unfavorable conditions for battery storage, causing a large loss of capacity in a short period of time. Similar degradation behaviour is reported in [34].

Internal Resistance

During the RPTs the internal resistance was measured for various levels of SOC. Figure 2.6 shows the results for 50% SOC.

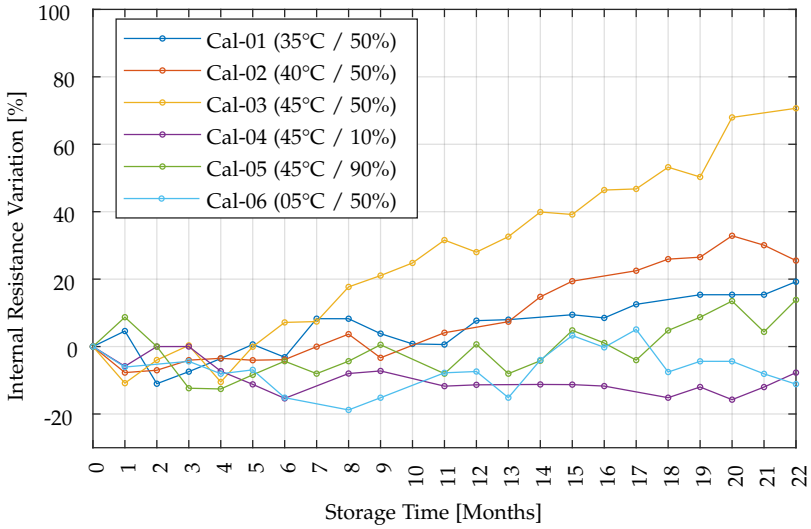

Fig. 2.6: Internal resistance of "Cell B" under calendar aging conditions. Measured at 25ºC and 50% SOC.

The results show two phases in the evolution of resistance. First, there is a decrease in internal resistance of up to 10% compared to BOL, similar behaviour is reported in [35]. After a few months of storage, the resistance increases again and continues with a positive trend until the end of the tests. In this second phase, the resistance returns to levels similar to those of BOL when reaching approximately 85% of capacity fade. Cells Cal-04 and Cal-06,

which did not reach such a degradation, maintained a negative resistance increase for almost the entire duration of the tests. For the rest of the cells, the increase in resistance in this second phase exhibits a similar trend to that observed with the capacity fade. The Cal-03 cell, with the greatest degradation, reaches an increase in internal resistance of 70%.

Cycling Aging

To determine the cycling lifetime of cell B, five cells were used and subjected to different aging conditions as shown in Table 2.2. To analyze the influence of the current used during charging, cells Cyc-03, Cyc-04 and Cyc-05 were subjected to identical temperature conditions (45ºC) but different charging rates (0.5C, 1C and 1.5 C). Furthermore, to compare the effect of temperature, Cyc-01 and Cyc-02 cells were tested at 10ºC and 25ºC, respectively, and 1.5C.

Capacity Fade

Under these conditions, more than 2000 cycles were carried out in all the cells. Figure 2.7 shows the capacity results as a function of the cycles performed.

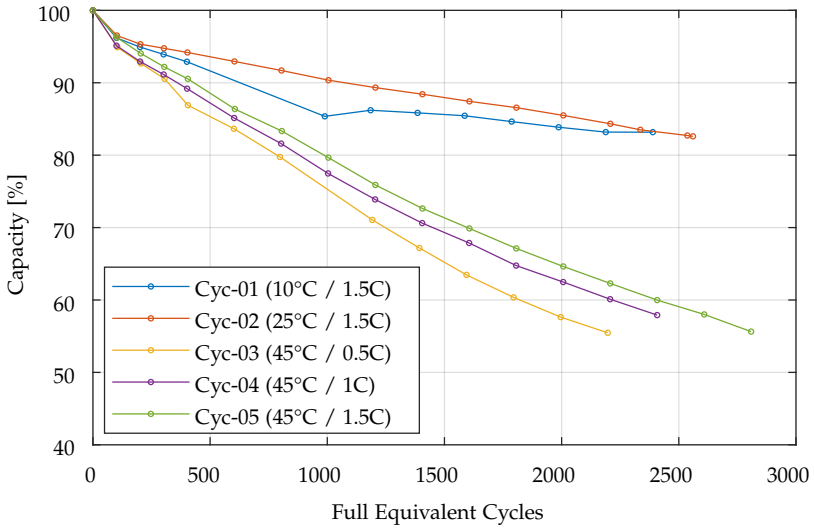

Fig. 2.7: Capacity fade of "Cell B" under cycling aging conditions. Measured at 25ºC and C/5. Source [J2].

First, a greater degradation is observed at high temperatures. After 2000 cycles, the cell cycled at 25ºC keeps approximately 80% of its initial capacity, while cells tested at 45ºC have lost at least 40% of capacity compared to

BOL, hence, the loss of capacity is almost doubled. Unlike the calendar aging tests, it is observed that reducing the temperature from 25ºC to 10ºC does not present benefits concerning degradation. After 2000 cycles, the loss of capacity is similar to that observed at 25ºC, in addition, a more accelerated loss of capacity is observed during the first 1000 cycles. Regarding the influence of the C-rate on the degradation, it is observed that the three cells tested at different charging currents present similar shaped degradation curves. A greater degradation is observed at lower rates, which seems counterintuitive, however, the reason for this difference can probably be found in the way the test was carried out. Lower currents imply longer charging times, and thus longer test duration. Therefore, this greater degradation is probably due to a longer exposure time to high temperatures.

Internal Resistance

The results of the internal resistance measurements at 50% SOC are shown in Figure 2.8. As in the results of calendar aging, a first phase in which there is a resistance drop is observed in all the cells, followed by a linear increase with the cycles number. In cells subjected to medium temperatures (Cyc-01 and Cyc-02), the internal resistance barely increases with respect to their BOL value after 2000 cycles. However, in cells aged at 45ºC there is a resistance increase between 40% and 70%.

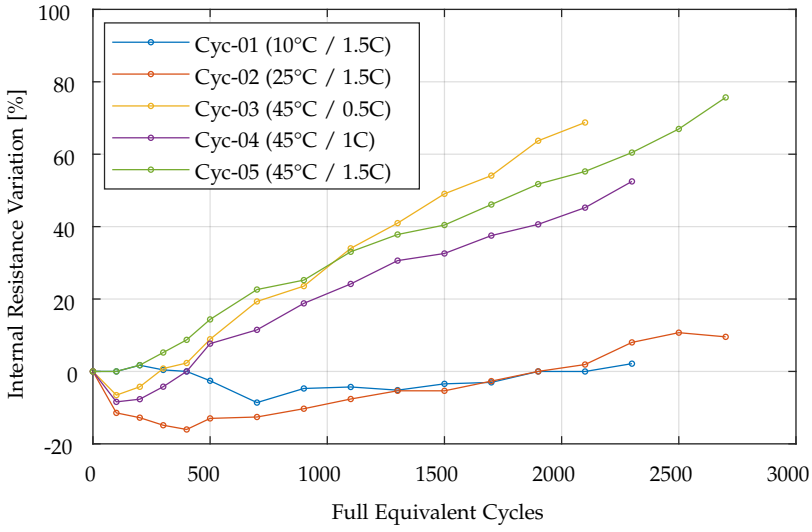

Fig. 2.8: Internal resistance of "Cell B" under cycling aging conditions. Measured at 25ºC and 50% SOC.

2.3.3 Cell C

Calendar Aging

To study the calendar lifetime of battery C, seven cells were exposed to different SOC and temperature conditions as explained in Table 2.1. The tests lasted 13 months. In order to evaluate the effect of SOC, three cells (Cal-03, Cal-04 and Cal-05) were subjected to the same temperature (35ºC) and different SOC levels (10%, 50% and 90%). Similarly, the influence of temperature was studied by exposing another three cells (Cal-02, Cal-05 and Cal-07) to identical SOC conditions but different temperatures (25ºC, 35ºC and 45ºC). Additionally, one cell was tested at 5ºC as reference. Cell Cal-06 was also added to investigate possible interactions between temperature and SOC level conditions.

Capacity Fade

The results obtained from the capacity fade tests are shown in Figure 2.9.

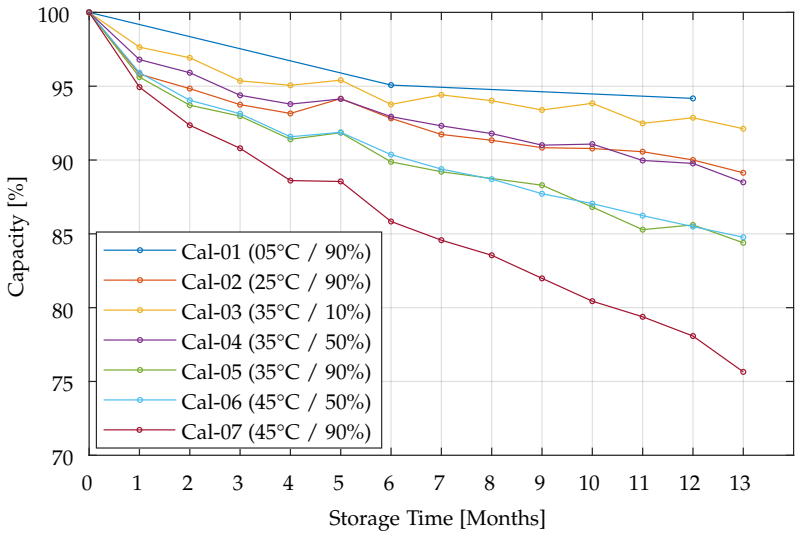

Fig. 2.9: Capacity fade of "Cell C" under calendar aging conditions. Measured at 25ºC and C/5. Source [J3].

To evaluate the effect of temperature, cell Cal-02, stored at 25ºC and 90% SOC, can be used as reference. Just over a year later, a loss of capacity of 10% compared to the initial capacity is observed in this cell. When the temperature rises to 35ºC, the capacity fade increases by 50% (Cal-05) and by 150% if temperature rises to 45ºC (Cal-07). When the influence of temperature in

cells stored at 50% SOC is analyzed, an increase in degradation with temperature is also observed, although this is significantly lower. The Cal-04 cell stored at 35ºC, has a capacity fade of 12% by the end of the tests while for the Cal-06 cell at 45ºC, it is 15%. This represents a 25% capacity loss increase when temperature rises from 35ºC to 45ºC with 50% SOC, while at 90% SOC this temperature increase represents 65% more capacity lost.

Contrasting with cell B, in this case it is more damaging to store the batteries at high SOC. Cell Cal-03, stored at 10% SOC, showed a capacity loss of 7% at the end of the tests, while for the cells stored at 50% and 90%, the capacity loss was 12% and 15% respectively.

Internal Resistance

Figure 2.10 shows the internal resistance trend of the cells tested with the storage time.

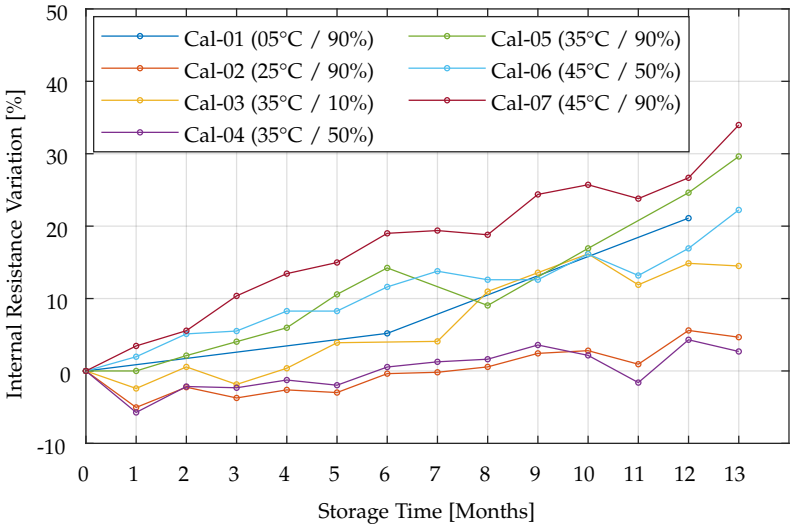

Fig. 2.10: Internal resistance of "Cell C" under calendar aging conditions. Measured at 25ºC and 50% SOC.

In this case only three of the cells show a slight resistance drop before it starts to increase with storage time. Cells Cal-02, Cal-03 and Cal-04 do not return to BOL levels until after 4-6 months of storage, while the resistance of the other cells increases from the beginning of the tests. In general, the resistance increase follows a similar trend to the capacity loss, however cells Cal-03, stored at 10% SOC and Cal-01 stored at 5ºC, show a higher resistance increase than expected, tripling that of cells with higher capacity loss.

Cycling Aging

In addition to the calendar aging tests, another five cells were tested to investigate the cycling lifetime. Four of these cells were subjected to discharge cycles following a WLTP-based driving profile with an average C-rate of 0.5C. The other cell (Cyc-03) was charged and discharged at constant current at 0.5C as well. To evaluate the effect of temperature, the test matrix was set up with three different working temperatures, 10ºC, 25ºC and 35ºC, as shown in Table 2.2. All cells were tested until failure or until they were no longer considered safe to operate.

Capacity Fade

The results of the capacity evolution of the cells tested are presented in Figure 2.11. Except for cell Cyc-01, the rest of the cells present two different stages during their aging. Firstly, a linear loss of capacity with the number of cycles, which, depending on the aging conditions, lasts from BOL to between 600 and 950 cycles. This stage is followed by an abrupt capacity drop, in which in a matter of a few tens of cycles the battery loses more than 50% of its capacity.

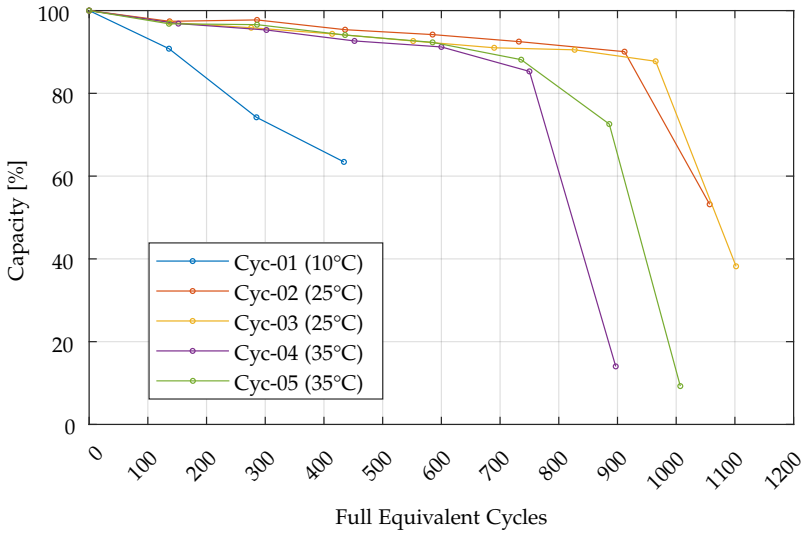

Fig. 2.11: Capacity fade of "Cell C" under cycling aging conditions. Measured at 25ºC and C/5.

The beginning of the nonlinear behavior, also known as “knee-point” indicates a change in the dominating aging mechanism. The lithium inventory loss due to SEI growth gives way to the loss of active material as the main cause of battery degradation [28, 36].

The cells cycled at 25ºC (Cyc-02 and Cyc-03) show a similar degradation trend, regardless of the discharge profile used, reaching 900 cycles before the sudden capacity drop. On the other hand, the cells subjected to 35ºC show a significantly faster loss of capacity, reaching the knee-point around 700 cycles.

Finally, cell Cyc-01, cycled at 10ºC, showed a rapid deterioration of its performance since the beginning of the tests. Other authors have studied the effect of low temperature on cycling aging lifetime [37, 38], but in general this effect begins at subzero temperatures, so further tests would be needed to determine the actual reasons behind the aging behavior of this cell.

Internal Resistance

The results of the internal resistance measurements at 50% SOC are shown in Figure 2.12

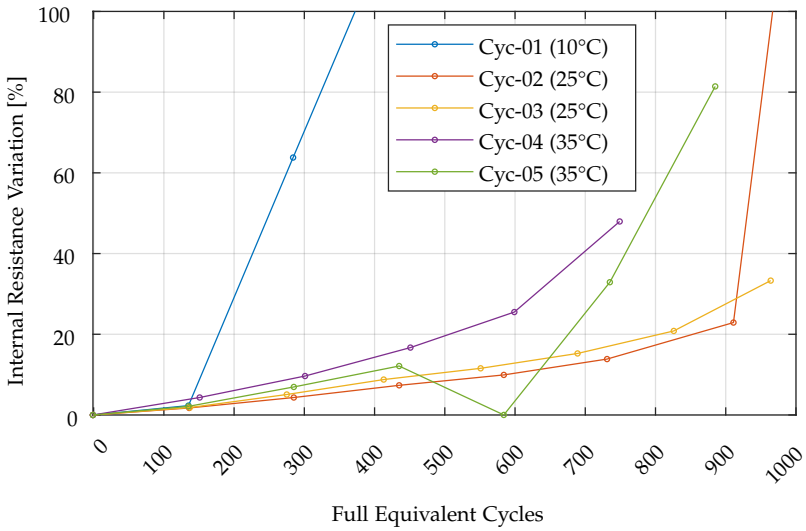

Fig. 2.12: Internal resistance of "Cell C" under cycling aging conditions. Measured at 25ºC and 50% SOC.

Again, a smooth increase in resistance is observed up to 20-30%, at which the knee-point occurs and the resistance shoots up. The growth of the resistance is in agreement with the capacity fade, cells aged at 25ºC show a lower growth rate than the cells at 35ºC.

The Cal-01 cell increases its resistance by more than 100% between 140 and 400 cycles, indicating some type of failure or accelerated aging mechanism in this cell.

2.3.4 Cell D

Calendar Aging

For cell D, the same test matrix was used as for cell C, as shown in Table 2.1.

Capacity Fade

Figure 2.13 shows the evolution of the cell capacity for different storage conditions.

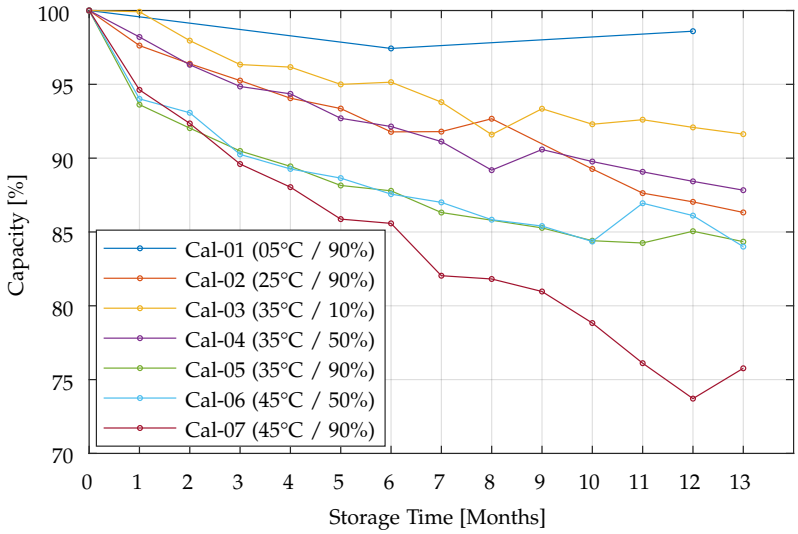

Fig. 2.13: Capacity fade of "Cell D" under calendar aging conditions. Measured at 25ºC and C/5.

Despite having a different chemistry, the results from cell D show many similarities with those from cell C. Again, the most harmful conditions for calendar lifetime would be high SOC levels and high temperatures. Compared to the type C battery, cells Cal-02 to Cal-04 show a slower degradation while in cells Cal-05 and Cal-06 it is more accelerated during the first 3 months of testing. However, after one year under the same conditions, cells C and D show very similar levels of capacity fade. The only exception is the cell Cal-01, stored at 10ºC, which suffered 4 times less degradation than its analogous of type C.

Internal Resistance

The results of the internal resistance evolution at 50% SOC are shown in Figure 2.14

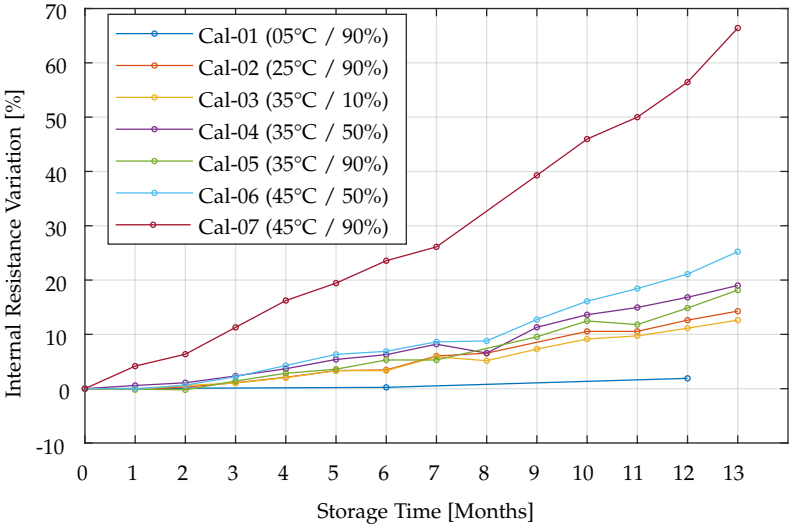

Fig. 2.14: Internal resistance of "Cell D" under calendar aging conditions. Measured at 25ºC and 50% SOC.

In the case of this cell type, a first stage with reduction of the internal resistance is not observed. Cell Cal-01, stored at 5ºC, barely experiences a resistance increase after one year storage. Cell Cal-07, which accumulates the greatest degradation, increases its resistance by 65% after 13 months of testing. Its resistance increases at a much higher rate than the other cells since the beginning of the test. The rest of the cells show a trend, in general, in agreement with their capacity lost.

Cycling Aging

For cell D, it was used the same test matrix as for cell C, as shown in table 2.2. The cells were tested until failure or until it was not safe to continue operating them.

Capacity Fade

Figure 2.15 shows the capacity evolution of cell D during the cycling aging tests.

The results show again two different stages in the lifetime of the cells as in section 2.3.3. A first stage in which the capacity fade evolves linearly until the knee-point is reached and where the capacity drops abruptly. In the case of cells Cyc-01, Cyc-02 and Cyc-03, the knee-point is not visible because, after it occurred, it was not possible to continue with the tests.

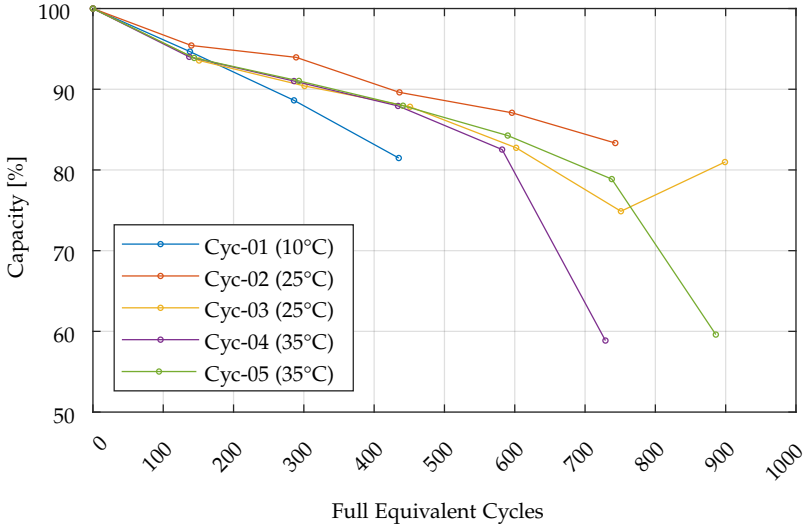

Fig. 2.15: Capacity fade of "Cell D" under cycling aging conditions. Measured at 25ºC and C/5.

Cell Cal-01, tested at 10ºC, shows a faster capacity loss than the rest. The rest of the cells reach the knee-point between 600 and 900 cycles. Cells subjected to 35ºC show a similar capacity fade trend in the linear stage, but when they reach the knee-point they begin to diverge. Cells Cal-02 and Cal-03 were tested at the same temperature, however, the cell subjected to CC discharge showed faster capacity loss than the one cycled by the WLTP profile.

Internal Resistance

The internal resistance results are shown in Figure 2.16.

The Cyc-03 cell with a CC profile shows the greatest resistance increase during the tests, reaching up to 95% and then decreasing again. This non-linear behavior, similar to what occurs in the case of capacity, could be a possible indicator of the end of battery life [39].

Cells Cyc-04 and Cyc-05, aged under the same conditions, start out with a similar trend, however, between 300 and 600 cycles, cell Cyc-05 maintains a constant internal resistance, which may explain the differences in life-cycle. In both cells, an increase in the slope prior to the knee-point in the capacity fade is observed.

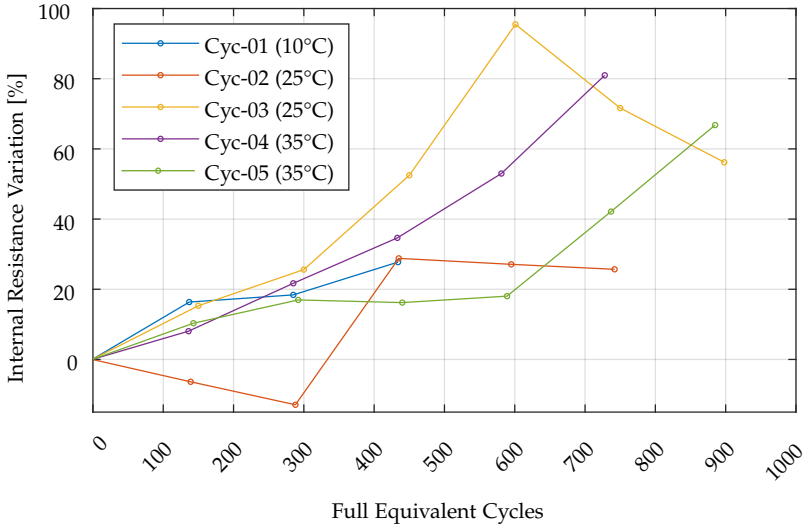

Fig. 2.16: Internal resistance of "Cell D" under cycling aging conditions. Measured at 25ºC and 50% SOC.

2.4 Summary

In this section the degradation behavior of four different cells used in electric vehicles has been investigated. The cells were exposed to different conditions of temperature, SOC, charge current and discharge profiles. The results show that the optimal conditions to store batteries would be low temperature (<=10ºC) and low SOC, which lead to the minimum degradation over time for all the cells, below 5% in the first year for the tested cells. However, for other storage conditions, it is observed that the tested batteries show very different behaviors. In general, a more accelerated loss of capacity is observed at higher temperatures; the results indicate that an increase of 10ºC can double the loss of capacity in the same period of time, which is in good agreement with Arrhenius law. Though, this is not always the determining factor, the SOC also seems to have a key role on the degradation. Most results in the literature show that calendar aging increases with the SOC [29, 40], although this study has revealed that this may not be extended to all cells and aging conditions. In the case of cell B, the analysis shows that elevated temperatures in combination with medium SOCs results in a substantially accelerated capacity fade. Regarding cycling aging, a moderate degradation rise is observed at increasing temperatures, although there are significant differences among the tested batteries. An accelerated capacity loss at low temperature was also observed in two of the cells analyzed. The charging rate however

does not seem to have a significant effect on cells performance, as very similar results are obtained between 0.5C and 1.5C.

Chapter 3

Online Battery State Estimation

This chapter focuses on the analysis of different parameters that affect online battery state estimation and its implementation on a simple and accurate ad-hoc algorithm for electric vehicles. The results presented in this chapter are extracted from the following outcomes:

J1. **A. Gismero**, E. Schaltz and D. -I. Stroe, "Recursive State of Charge and State of Health Estimation Method for Lithium-Ion Batteries Based on Coulomb Counting and Open Circuit Voltage," *Energies*, 2020, 1811, 13(7).

C2. **A. Gismero**, D. -I. Stroe and E. Schaltz, "Comparative Study of State of Charge Estimation under Different Open Circuit Voltage Test Conditions for Lithium-Ion Batteries," *IECON Proceedings (Industrial Electronics Conference)*, 2020-October, 1767–1772.

3.1 Introduction

The state of charge of a cell indicates the ratio between the available capacity and the actual full capacity so that a fully discharged battery corresponds to 0% SOC and a fully charged battery corresponds to 100% SOC.

There are basically three methods to estimate the SOC of a lithium-ion battery: those based on direct current measurements, those based on direct voltage measurements and those based on models.

SOC estimation based on battery current measurement is one of the most used methods. In this method, the charge added to or removed from the cell is measured and integrated over time to calculate the actual SOC [41]. This method is commonly called coulomb counting and is expressed as indicated in Equation 3.1.

$$SOC_t = SOC_0 + \frac{1}{Q}\int_0^t \eta_t I_t dt \tag{3.1}$$

Where I_t is the incoming or outgoing current of the battery, Q is the capacity and η_t is the coulombic efficiency, which depends, among others, on the temperature of the battery and the applied current. This method is accurate and simple to implement, however, it relies on the initial estimate of SOC (SOC_0) with no feedback mechanism, so it is very influenced by the accuracy of the current sensors; even small errors, due to the integration will result in high SOC deviations.

The battery voltage depends on the applied current and the impedance, which in turn depends on factors such as temperature or aging. Therefore, if the battery is considered at rest and the effect of hysteresis negligible, a direct relationship between SOC and voltage (u_t) can be established through the OCV curve, as expressed in Equation 3.2:

$$SOC_t = OCV^{-1}(u_t) \tag{3.2}$$

This method allows good results when the battery is at rest providing a sufficient relaxation time, although it leads to large errors when the cell is under load [42]. Equation 3.2 can be modified to also model the dynamic behavior of the cell by adding more or less complexity, as shown in Equation 3.3. When the ohmic drop ($R_0 I$) and one or more impedances are included to model the charge transfer resistance and the diffusion phenomena it is possible to achieve acceptable estimates for reasonable values of current and cell resistance.

$$SOC_t = OCV^{-1}(u_t - R_0 I) \tag{3.3}$$

Model based methods are an alternative to the direct measurement methods in which the system input (current) is used to predict the system output

(voltage). The measured and predicted outputs are compared and the difference can be used as a feedback to update the model estimate. In addition to the system parameters, these methods also allow to estimate internal states of the battery such as SOC and SOH. The Kalman filter (KF) is a widely used algorithm when the objective is to analyze hidden variables [22, 23, 43].

In Paper C2 an extended Kalman filter (EKF) is implemented to analyze the variations in the OCV curves obtained under different conditions and its effect on SOC estimation. In the proposed method, the dynamics of the battery are modeled through a first-order RC circuit illustrated in Figure 3.1 and described by the state Equations 3.4. The EKF allows a recursive estimation of the parameters of the model as well as the state of the battery defined by the OCV. Further details about the EKF implementation can be found in Paper C2.

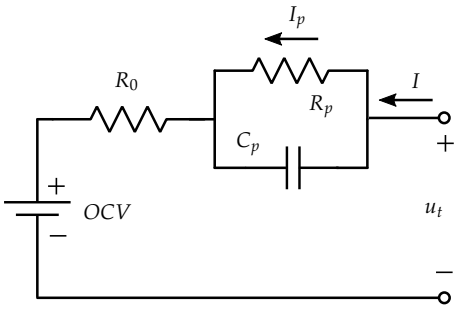

Fig. 3.1: First order equivalent circuit. Source [C2].

$$\begin{cases} \dot{I}_p = \frac{I}{R_p C_p} - \frac{I_p}{R_p C_p} \\ u_t = OCV + R_0 I + R_p I_p \end{cases} \tag{3.4}$$

As an alternative to battery model based methods, data-driven methods are gaining interest due to their flexibility and adaptability to non-linear systems. These methods consider the battery system as a black-box and allow to estimate its state using large aging datasets. The performance and accuracy of the estimation greatly depend on the quality of these datasets. There are numerous statistical and computational approaches, including artificial neural network (ANN) [44, 45] and support vector machine (SVM) [46, 47].

3.2 Methodology

The batteries used in this research are the A-cells of 3.4 Ah and cylindrical format 18650. These batteries were subjected to cycling aging at three different temperatures, 15ºC, 25ºC and 35ºC. Both the test matrix and the degradation results are detailed in Chapter 2.

The driving cycle adopted for this research, both to emulate a real aging scenario and to verify the estimation methods developed was the World Harmonized Light-duty Vehicle Test Procedure (WLTP) for class 2 vehicles. This test consists of three parts for low, medium and high speed, with a duration of 1477 seconds, i.e. 24.6 minutes [48]. The vehicle velocity is transformed into a current test profile depending on the characteristics of the vehicle as indicated in Equation 3.5.

$$I = \frac{(\frac{1}{2}\rho S C_x v^2 + C_r m_t g + m_t a)v}{\eta V} \tag{3.5}$$

The current is determined by calculating the power needed by the electric motor (VI) to overcome the drag force, rolling resistance and inertia (first, second and third terms in the numerator). It is assumed that the drag force is proportional to the square of the vehicle speed (v), being ρ the air density, S the frontal area and C_x the aerodynamic coefficient. For the calculation of the rolling resistance, the total mass of the vehicle (m_t), the gravity (g) and the rolling coefficient (C_r) are considered. Finally, a is the acceleration of the vehicle and η is the efficiency of the powertrain.

After each driving cycle, the cells are recharged to 90% SOC at a constant rate of 0.2C, leaving a rest period before the next cycle so that the entire process takes two hours. Figure 3.2 shows the current profile of a complete cycle and the voltage response of the cell.

In this research, two different methods were used to obtain the OCV curves, incremental and continuous charge/discharge cycle.

In the incremental method, the battery is fully charged and discharged by current pulses at regular SOC intervals allowing a fixed time for relaxation, OCV is measured at the end of this rest time. In the literature, SOC increases between 1% and 5% and relaxation times between 1h and 5h are recommended [49, 50]. Figure 3.3 illustrates the procedure followed to obtain the charge and discharge OCV curves, using a ΔSOC of 5% and a rest time of 4h. The charge and discharge curves form a loop due to hysteresis [51]. The voltage difference of both curves depends on the battery chemistry, SOC, and battery degradation [52]. For the cells used in this work, it was considered the average between charge and discharge curves as a reasonable approximation.

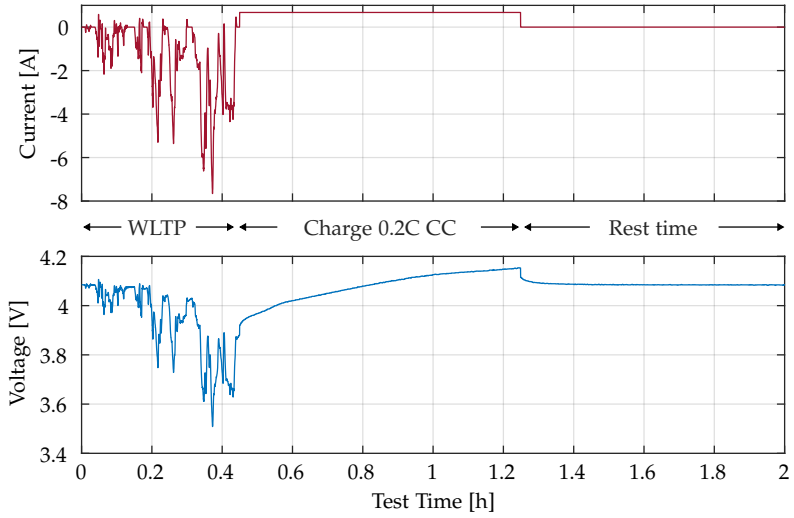

Fig. 3.2: WLTP-based mission profile and voltage response. Source [J1].

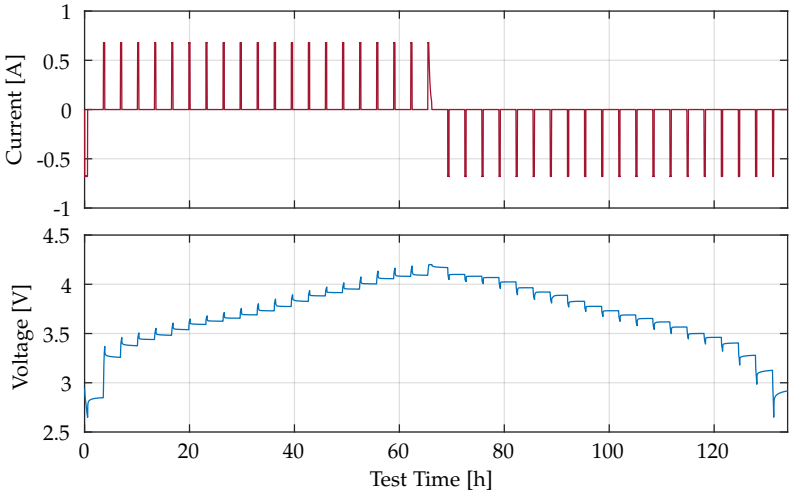

Fig. 3.3: Incremental OCV test profile and voltage response. Adapted from [C2].

On the other hand, in the continuous method, OCV curves are obtained through charging and discharging at very slow rates. This procedure is an alternative to the incremental method that allows to obtain the OCV faster, though it is considered less reliable [53]. Figure 3.4 illustrates the test profile used to measure the OCV at different charging rates, from 0.2C to 1C.

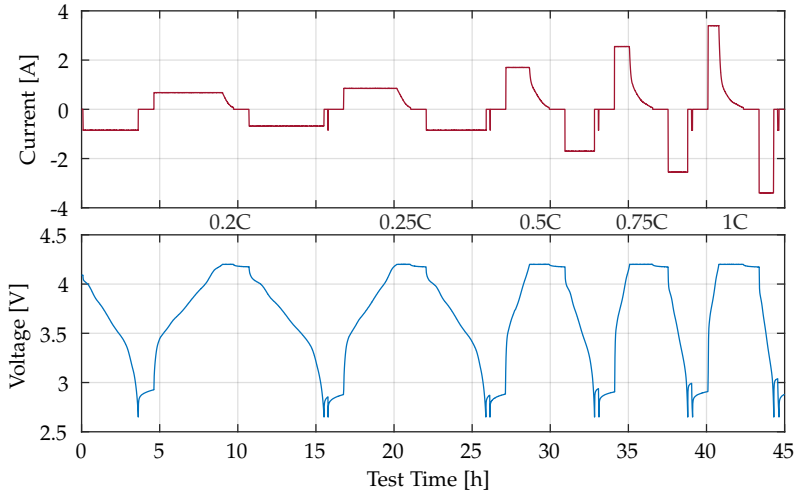

Fig. 3.4: Continuous OCV test profile for different rates (0.2C, 0.25C, 0.5C, 0.75C and 1C) and voltage response. Adapted from [C2].

As in the incremental method, the OCV curve is computed as the average of the charge and discharge curves obtained. In Paper C2 the OCV curves were obtained by both methods at five different temperatures (5ºC, 15ºC, 25ºC, 35ºC and 40ºC) for later comparison.

3.3 Temperature and Current Influence

The available capacity depends on the operating conditions. High currents or low temperatures reduce the usable capacity of the battery leading to considerable errors if not considered in the estimation. A compensation factor is defined in Paper J1 as the ratio between the capacity measured under reference conditions and under actual conditions. Figure 3.5 shows the discharge capacity at different temperature conditions and the corresponding values assigned to the compensation factor.

The OCV curve can also have an impact on the SOC estimate. Paper C2 analyzes how temperature, aging or even the method used to obtain the curve affect the estimation.

Figure 3.6 shows the difference between the OCV obtained with the incremental and continuous method at different charging rates. As expected, when current increases, the error obtained using the incremental curve as a reference increases, being greater in the areas of the curve with lower slope. However, rates of 0.2C and 0.25C produce adequate results, with an error below 3% between 5% and 85% SOC.

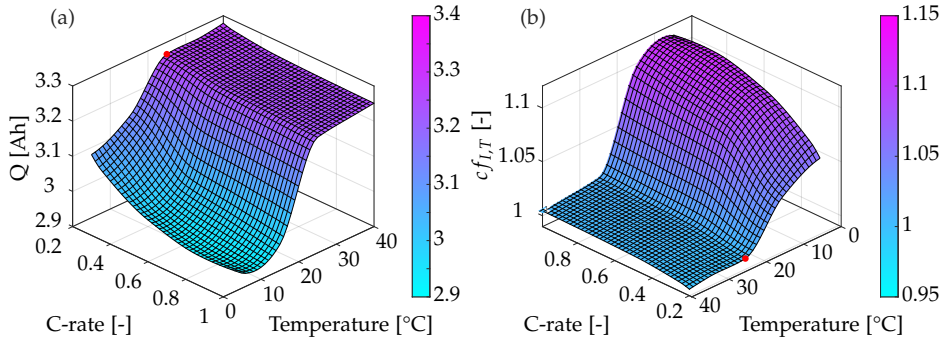

Fig. 3.5: (a) Discharge capacity under different rates and temperatures and (b) discharge compensation factor for those conditions. The red dot represents the reference conditions (0.2C and 25ºC). Adapted from [J1].

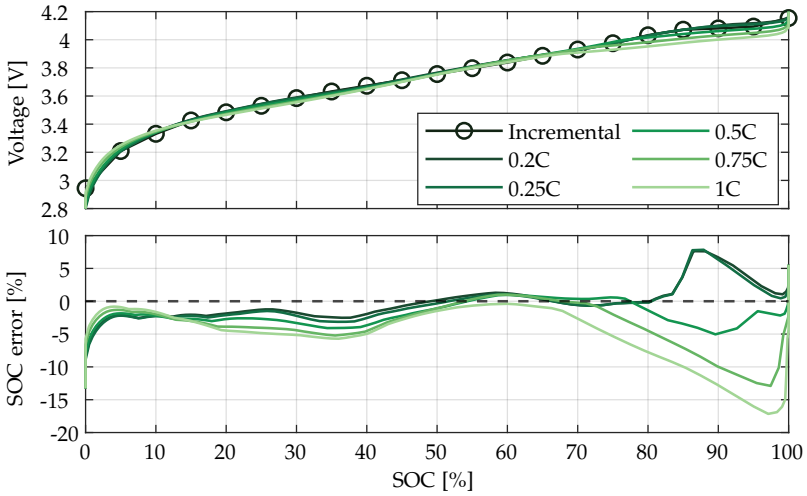

Fig. 3.6: Comparative of the OCV curves obtained using the incremental and continuous methods at different rates. Source [C2].

The evolution of the curve after 350 equivalent cycles, corresponding to a 7% capacity fade, was also analyzed. Figure 3.7 shows the comparison between both curves obtained by the incremental method. It is observed that the error between 5% and 100% SOC does not exceed 2%. Hence, using the curve at BOL does not drastically affect the accuracy of the estimate, at least in the SOH range analyzed.

The effect of different temperatures on the OCV curve is illustrated in Figure 3.8. The SOC error obtained for various temperatures is compared to the curve at 25ºC.

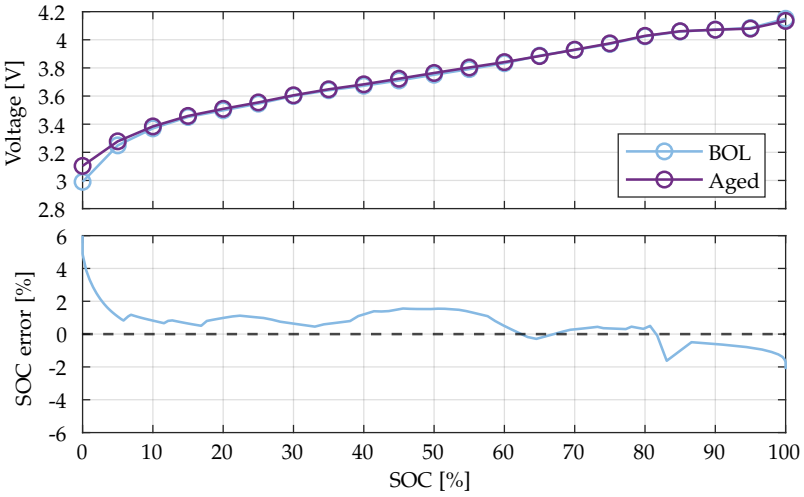

Fig. 3.7: Comparative of the OCV curves obtained at BOL and after aging (93% SOH) [C2].

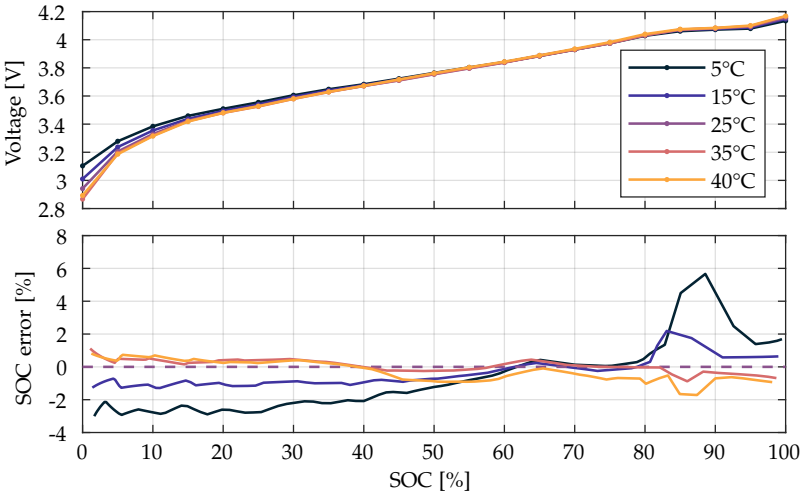

Fig. 3.8: Comparative of the OCV curves obtained using the incremental method at different temperatures. The OCV at 25ºC is used as reference. Source [C2].

Although the largest differences in voltage are below 20% SOC, the greatest SOC error occurs again above 80% because of the plateau in that area. Temperatures above 25ºC maintain an error below 2% throughout the curve, however, at lower temperatures the error increases, especially above 80%

SOC.

Paper C1 also compares the resulting error when using the OCV curves obtained under different conditions to estimate the SOC through an EKF. The test consists in discharging a fully charged cell, with four WLTP cycles separated by three hours rest periods, as shown in Figure 3.9.

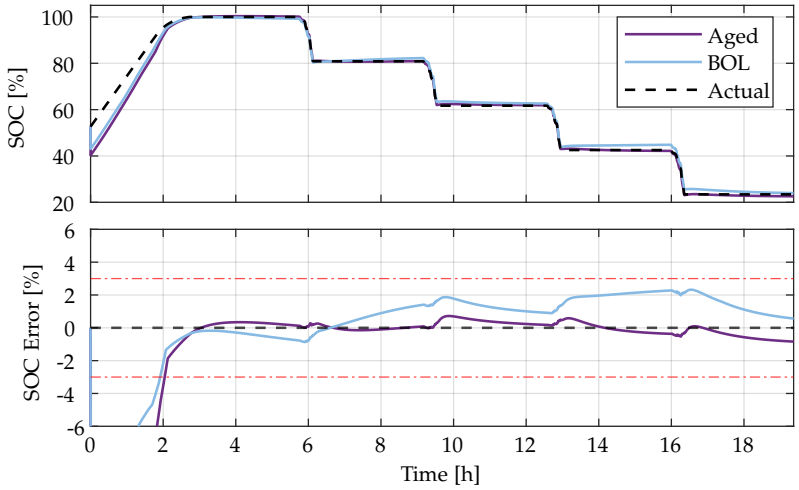

Fig. 3.9: SOC estimation of an aged cell (93% SOH) using the EKF and the OCV curves obtained at BOL and after aging. Source [C2].

In conclusion, SOC estimation results are more accurate using the curves obtained with the incremental method. However, for currents up to 0.25C, the error obtained through the continuous method is acceptable, not exceeding 2%. Regarding the effect of degradation, a cell with 7% capacity fade was used to compare the SOC estimation performance of two OCV curves, one corresponding to its current state of degradation and the other at BOL. Although the SOC error remained below 3% in both cases, the use of the OCV curve corresponding to the aging state of the cell achieved an estimation with an RMSE and a MAE between 3 and 4 times lower. Therefore, for higher levels of degradation it would be convenient to update the OCV curve used in the SOC estimation. Finally, regarding temperature, the greatest variation was observed at low temperatures below 15ºC, while at high temperatures, the OCV curves present similar results. The largest variation of the curves is also located below 20% SOC, a region with a high slope, hence, with no significant effect on SOC.

3.4 Proposed Method

Paper J1 proposes a SOC and SOH estimation method that combines the current based estimation with an OCV lookup update. Figure 3.10 illustrates the operation of this estimation method. While the battery is charging or discharging, SOC is calculated by integrating the current flowing through it. Depending on the temperature and C-rate, the correction factor is applied as explained in Section 3.3. When the battery is at rest, after 25 minutes, the OCV curve is used to estimate the SOC.

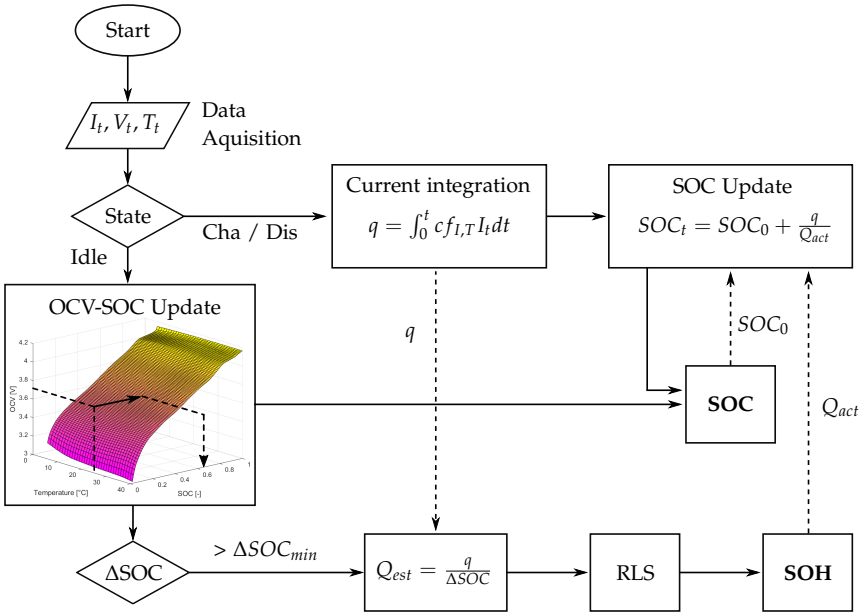

Fig. 3.10: Flowchart of the proposed SOC-SOH estimation algorithm. Adapted from [J1].

To estimate the SOC through current based methods, it is necessary to know the current capacity of the battery. The proposed method applies the partial capacity method [18, 19], by which the net capacity variation between two rest periods is measured and divided by the SOC variation, obtaining an estimate of the total capacity, as indicated in Equation 3.6.

$$Q_{est} = \frac{q}{\Delta SOC} \tag{3.6}$$

The accuracy of this estimate depends not only on the magnitude of the ΔSOC but also on the q measurement error, which in turn is influenced by the operating conditions (current and temperature) and the self-discharging effect [J1]. To minimize the error, multiple estimates are used to obtain the

capacity value using a recursive least squares (RLS) filter with a forgetting factor to give greater weight to the most recent estimates.

To verify the proposed method, a test consisting of multiple charges and discharges was used, using WLTP driving cycles up to different SOC levels. Overall, 58 cycles were carried out at different temperatures with one hour of resting time between cycles and charge periods and a total duration of 140 hours. Figure 3.11 illustrates the current and temperature profiles of the test and the estimated SOC.

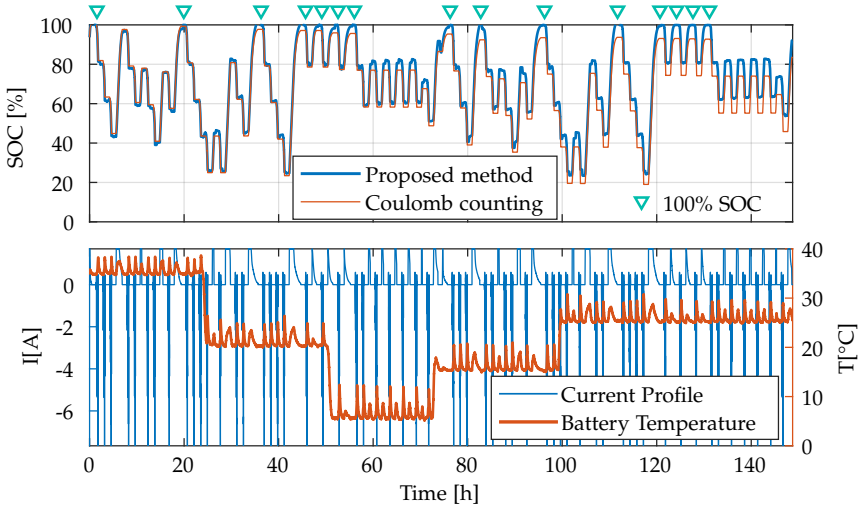

Fig. 3.11: Validation test. (Above) SOC estimation with the proposed method and with a traditional Coulomb counting method. (Below) Current and temperature profiles. Source [J1].

To evaluate the error in the estimation, the cell is fully charged to the 100% SOC several times during the test. The test is performed with three cells (Cyc-03, Cyc-06 and Cyc-09), aged at 35ºC, 25ºC and 15ºC respectively and with different degradation levels.

Figure 3.12 compares the SOC error of the traditional coulomb counting and the proposed method when a 100% SOC is reached. It can be observed that the coulomb counting error exceeds 7% due to cumulative errors. The error before the OCV is also shown, both with and without the compensation factor. It can be noted that when the current and temperature are compensated, the error obtained is reduced by half. Finally, after the OCV update, as expected, the error is similar in most of the estimates.

Finally, the system was fed with incorrect capacity values at the beginning of the test to verify the accuracy of the SOH estimation. Figure 3.13 shows the results for Cell-06. In all cases, the capacity converged to the real value,

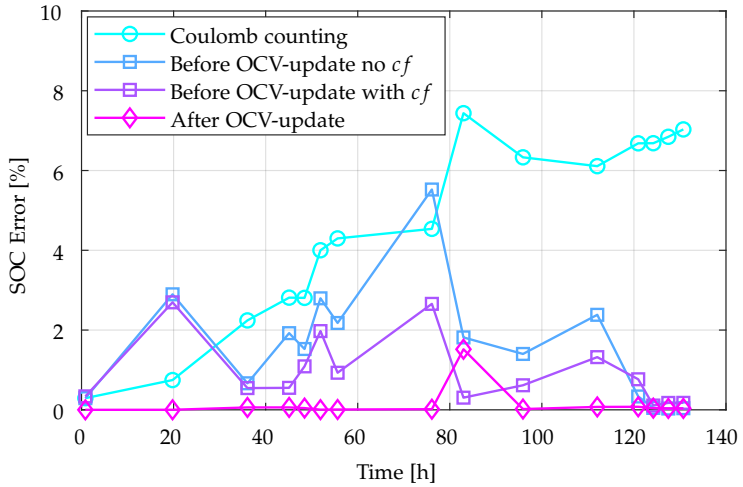

Fig. 3.12: SOC error during the validation test using the cell A-Cyc-06. Source [J1].

with a maximum error of 1.5%. The speed of convergence depends on the value assigned to the forgetting factor. However, as the capacity of a cell used under normal conditions varies gradually, a slower but stable convergence is preferable.

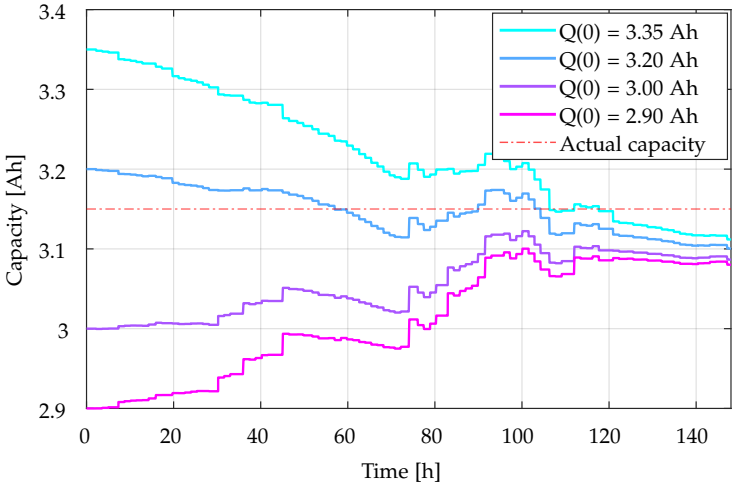

Fig. 3.13: Capacity estimation during the validation cell with different starting values for the cell A-Cyc-06. Source [J1].

3.5 Summary

This chapter studies how different parameters such as the current or the temperature affect the battery state estimation. Many estimation methods rely on the OCV-SOC relationship to estimate the state of the batteries. However, the OCV varies with aging, temperature or even the method used to obtain it. As a result of the analysis performed in Paper C2, it can be concluded that although the incremental method is the most accurate, the continuous method at low rates of up to 0.25C allows to obtain practical results. Regarding the aging, using the OCV curve obtained at BOL would be, in general, the most straightforward way, however it has been observed that the SOC error quadruples with aging before reaching 90% SOH. Although in the tests the error remained around 2%, it could increase when higher degradation levels are reached or when using another battery chemistry.

The temperature does not seem to have a big impact on the OCV as long as it stays above 15ºC. Lower working temperatures would alter OCV more drastically, so it would be advisable to know the OCV as a function of temperature. The proposed method uses current, voltage and temperature measurements to accurately estimate both SOC and SOH. The effect of different working conditions on the charging and discharging efficiency was analyzed enabling SOC estimation during battery operation under variable conditions. The use of OCV allows to obtain a first estimate of the SOC. Hence avoiding the characteristic cumulative errors of the Coulomb counting method and achieving SOC errors of less than 3%. Furthermore, using partial capacity, an estimate of the SOH is obtained each time the battery is at rest. The SOH error obtained after testing three different batteries during 140 hours of operation was below 1.5%.

Chapter 4

Offline SOH Estimation

This chapter focuses on the application of different methods to assess the degradation of electric vehicle batteries using data collected from cells or batteries from similar vehicles. In addition, the factors that affect the accuracy of the estimation during the tests are investigated. The results presented in this chapter are extracted from the following outcomes:

J2. **A. Gismero**, K. Nørregaard, B. Johnsen, L. Stenhøj, D. -I. Stroe, E. Schaltz. "Electric Vehicle Battery State of Health Estimation Using Incremental Capacity Analysis". *Journal Of Energy Storage*, under review, 2022.

J3. **A. Gismero**, M. Dubarry, J. Guo, D. -I. Stroe, E. Schaltz. "Influence of Test Conditions in the Incremental Capacity Analysis for the State of Health Estimation of Lithium-ion Batteries for Electric Vehicles". *Applied Energy*, under review, 2022.

C1. **A. Gismero**, D. -I. Stroe and E. Schaltz, "Calendar Aging Lifetime Model for NMC-based Lithium-ion Batteries Based on EIS Measurements," *2019 Fourteenth International Conference on Ecological Vehicles and Renewable Energies (EVER)*, 2019, pp. 1-8.

4.1 Impedance Based SOH Estimation

The impedance is, in addition to the capacity, one of the most relevant parameters of a battery since it has a critical role in its performance. The impedance determines the power capability of the cell, that is, the current that it is capable of supplying continuously without exceeding the undervoltage limits. Nevertheless, the resistance increase is also related to the capacity fade and hence a widely used parameter to estimate the battery capacity [16, 17, 54, 55]. This section studies two of the main techniques used to determine the impedance in electric batteries, electrochemical impedance spectroscopy (EIS) and hybrid pulse power characterization (HPPC); and its use to evaluate the SOH. The batteries used in this research are the B-cells of 63 Ah from the BMW i3. In order to evaluate the performance of this method, several cells were subjected to different aging condition. The test matrix and the results of the aging test are detailed in Chapter 2.

4.1.1 Electrochemical Impedance spectroscopy

EIS is a widely used non-destructive technique to characterize the electrochemical dynamics that occur in cells. The impedance spectrum obtained through EIS is very useful not only to characterize the behavior and develop cell models [56–59] but also to analyze the performance and identify the different processes and aging mechanisms occurring in the cell [60–62].

Methodology

To obtain the impedance spectrum, a small sinusoidal current of different frequencies is applied to the cell and the voltage response is measured (galvanostatic mode). This mode is more suitable for batteries as it provides better control and fewer errors in data acquisition [63].

The impedance spectra of the cells are represented in a Nyquist diagram, which shows the locus of the real and the imaginary parts of the impedance. Figure 4.1 presents a typical Nyquist diagram of a lithium-ion battery, from which the different electrochemical processes that occur in the cell can be inferred [61, 62]. The frequency range used in this work spans from 10 kHz to 10 mHz.

The highest frequencies capture the inductive behavior of the battery, related to the skin effect of the cell as well as the terminals and cables used in the measurement. This is reflected in the quadrant with positive imaginary part of the impedance in the Nyquist diagram.

At medium and low frequencies, one or several semicircles can be observed in the negative imaginary part of the impedance quadrant, these correspond to capacitive phenomena such as solid electrolyte interphase (SEI), the

double layer capacitances and the effect of the charge transfer resistance. The lower frequencies capture diffusion phenomena which appear as a straight line on the right of the spectrum [61, 62]. Finally, the ohmic resistance is located at the intersection of the spectrum with the real impedance axis.

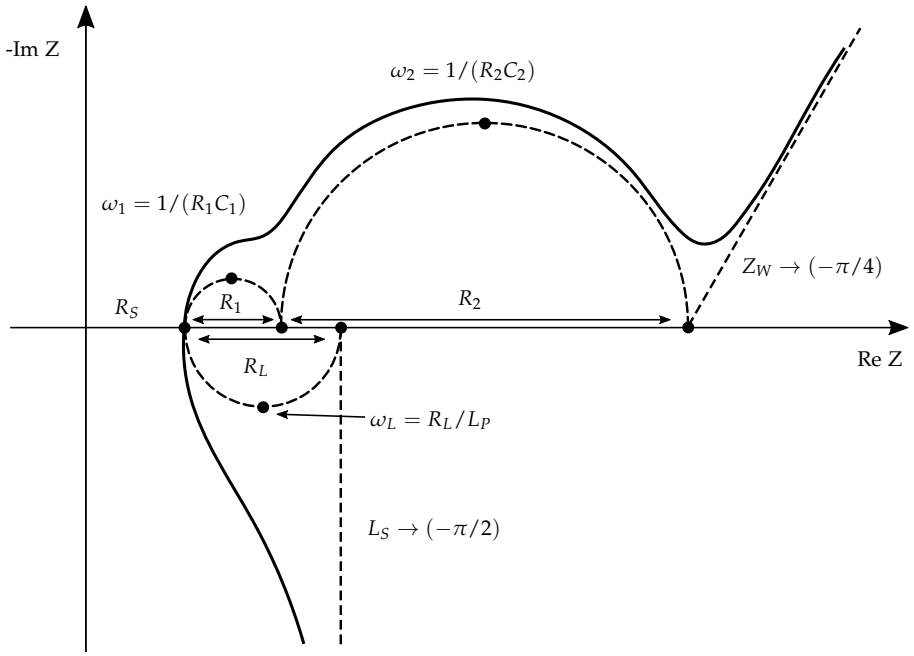

Fig. 4.1: Typical Nyquist diagram of Li-ion batteries. Adapted from [C1].

Cell Model Parametrization

To model the battery impedance, the obtained results are fitted into an electrical equivalent circuit (EEC) as illustrated in Figure 4.2. The EEC parameters are obtained through non-linear fitting of the real and imaginary parts of the impedance for each RPT performed.

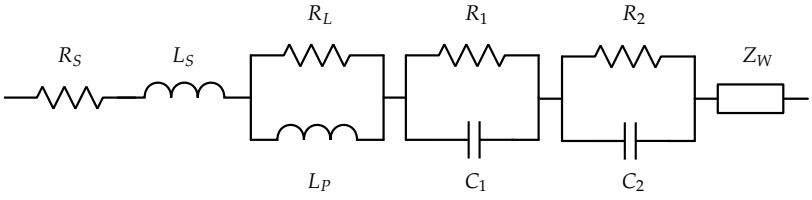

Fig. 4.2: Equivalent electrical circuit used for fitting the Nyquist plot in paper [C1].

The metric used to evaluate the accuracy of the non-linear fitting was the normalized root mean square error (NRMSE) calculated as indicated in Equation 4.1. In this equation, Z refers to the real or imaginary part of impedance as fitting is performed separately for both components. The maximum error obtained using the EEC shown in Paper C1 for all Nyquist curves was below 1%.

$$NRMSE = \frac{1}{Z_{max} - Z_{min}} \sqrt{\frac{\sum_{i=1}^{n} (\widehat{Z}_i - Z_i)^2}{n}} \tag{4.1}$$

The EEC consists of different elements in series and parallel that reproduce the electrochemical processes that occur inside the cell. The impedance of these elements is calculated as expressed in Equations 4.2 to 4.6.

$$Z_L = (j\omega)L_s + \frac{R_L(j\omega)L_p}{R_L + (j\omega)L_p} \tag{4.2}$$

$$Z_{RC1} = \frac{R_1}{1 + R_1(j\omega)C_1} \tag{4.3}$$

$$Z_{RC2} = \frac{R_2}{1 + R_2(j\omega)C_2} \tag{4.4}$$

$$Z_W = \frac{1}{Y_w\sqrt{(j\omega)}} \tag{4.5}$$

$$Z_{EEC} = R_s + Z_L + Z_{RC1} + Z_{RC2} + Z_W \tag{4.6}$$

R_s represents the ohmic resistance of the electrolyte and the cell electrodes. Z_L models the inductive behavior of the battery and other elements such as cables and connectors used in the measurement. The two semicircles that represent the capacitive phenomena are modeled by two RC elements, Z_{RC1} and Z_{RC2}; while the diffusion phenomena are emulated with a Warbrug impedance, where Y_w is the Warbrug capacitance.

As an example of the curve fitting process, Figure 4.3 illustrates the measured frequency response and the corresponding fitting curve through both Bode (magnitude and phase of impedance) and Nyquist diagrams.

Test SOC influence

To study the influence of the SOC of the cell during the measurement of the impedance spectrum, the tests in Paper C1 were performed at three different levels of SOC. Figure 4.4 shows the results for cell Cal-01. At BOL the SOC does not have a noticeable effect on impedance. An increase in the radius of the semicircles is observed when SOC decreases, which would indicate a

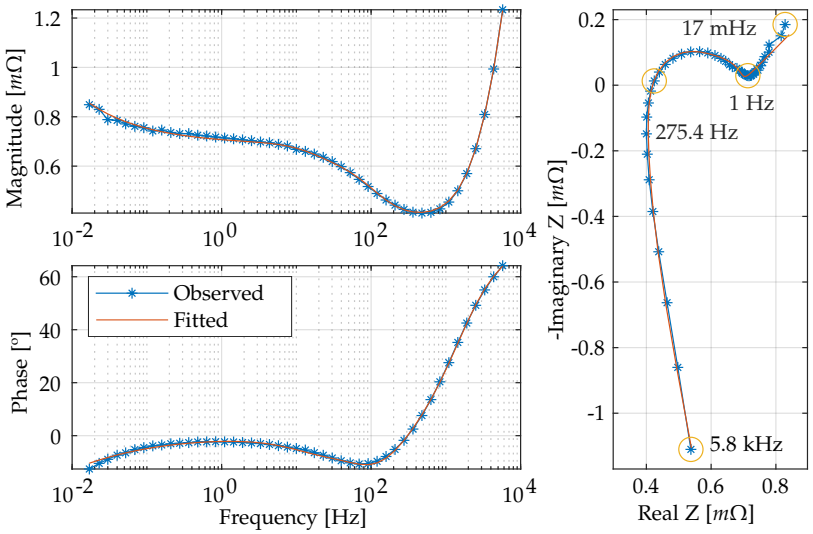

Fig. 4.3: Measured frequency response and fitted curve of a B-cell at BOL. Adapted from [C1].

rise of the charge transfer resistance. As the battery ages, an ohmic resistance increase with the SOC can be observed, while the radius of the semicircles keeps increasing at low SOC levels.

SOH Estimation

To estimate the degradation of the batteries, the evolution of the impedance spectra and the EEC parameters are analyzed, pursuing those that have a monotonic relationship with capacity. Figure 4.5 shows the evolution of the impedance spectrum for the five cells analyzed and compares the curves obtained at BOL with those obtained after 12 months of calendar aging. In general, a shift to the right is observed in all the curves, indicating an increase of the internal resistance. However, this does not occur evenly for all cells. Although the ohmic resistance increases in all cases, the radius of the semicircles is considerably reduced in the case of batteries aged at 10% and 90% SOC, which suggests a charge transfer resistance decrease for these aging conditions.

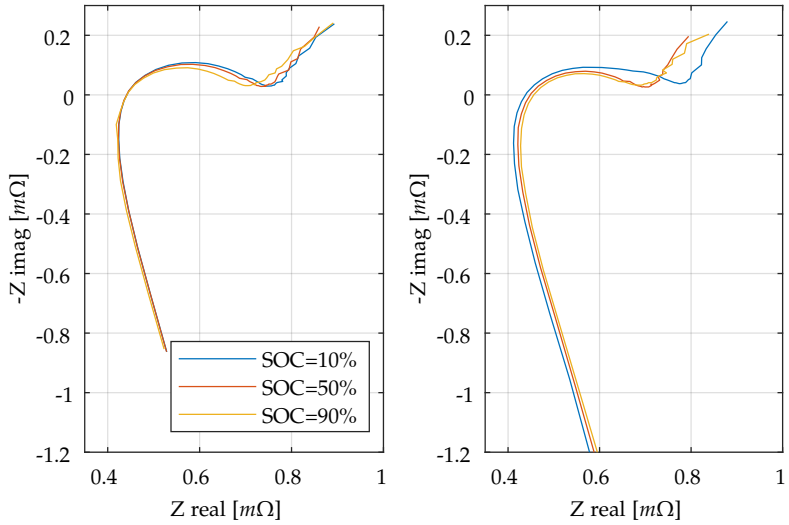

Fig. 4.4: Impedance spectrum of cell B-Cal-01 at three different SOC levels. BOL state (left) and after 12 months of calendar aging (right). Adapted from [C1].

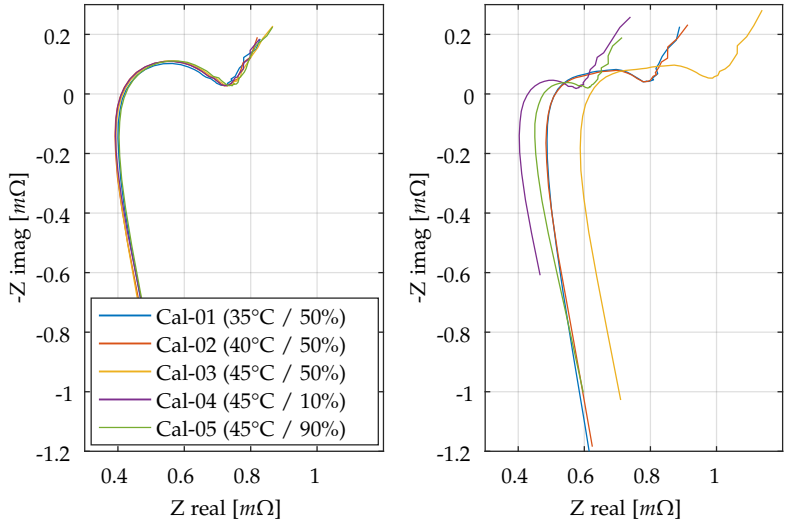

Fig. 4.5: Impedance spectrum of the five cells analyzed at 50% SOC. BOL state (left) and after 12 months of calendar aging (right). Adapted from [C1].

According to the results obtained in Paper C1, ohmic resistance increases progressively with time, showing a greater increase in cells subjected to high

temperatures and average SOH values, as occurs with capacity fade. Figure 4.6 shows the R_S evolution for the five cells tested.

Inductive elements generally show erratic values, without a clear trend with storage time or capacity fade. This is probably due to the influence that external elements such as cables used in the measurement have on these parameters.

Regarding the RC elements, the parameter R_2 shows a dependency with the aging conditions. In cells stored at 50% SOC, R_2 increases progressively with storage time. On the contrary, in cells Cal-04 and Cal-05, this value is reduced up to 50% of the initial value, which could indicate different degradation mechanisms depending on storage conditions. Figure 4.7 shows the different behaviours of R_2 with the aging conditions.

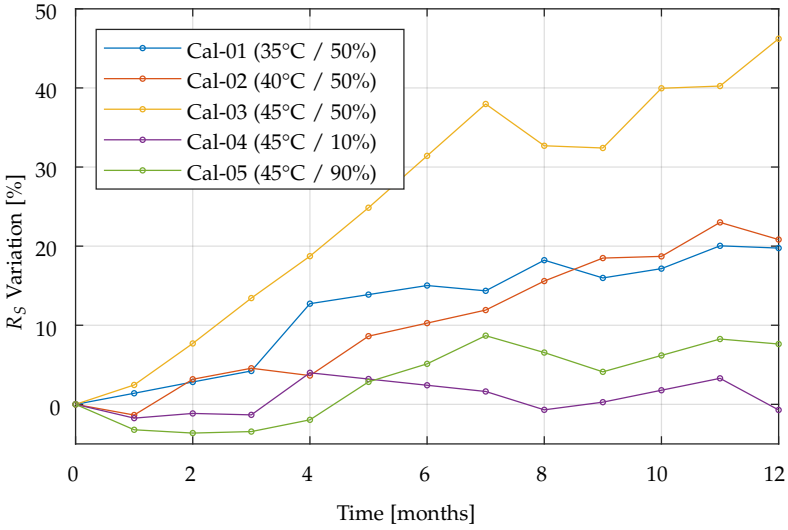

Fig. 4.6: Ohmic resistance (R_S) variation for the five cells analyzed, measured at 50% SOC. Adapted from [C1].

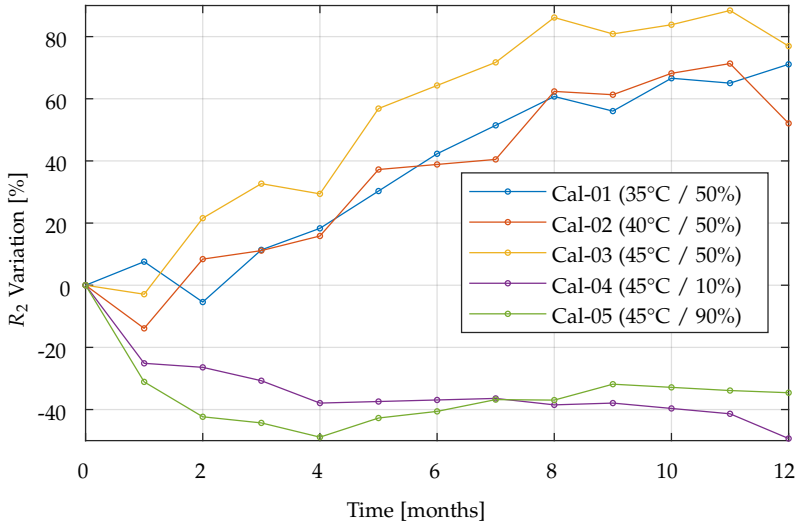

Fig. 4.7: Variation of R_1 for the five cells analyzed at 50% SOC. Adapted from [C1].

According to the results, R_S is the only parameter that shows a linear and monotonic dependence with the battery capacity regardless of the aging condition. Figure 4.8 shows the relationship between the ohmic resistance increase obtained for each SOC and the capacity of all the cells tested in Paper C1.

To compare the accuracy of the linear model, the metrics R^2, MAE and RMSE are used, whose values are indicated in Table 4.1. A linear relationship between ohmic resistance and capacity is observed for the three cases of SOC. However, as SOC increases, R_s explains better the SOH variation, reaching an R^2 of 0.89 for 90% of SOC.

Table 4.1: Statistic metrics of R_S as SOH estimator at different SOC levels.

SOC	**R^2**	**MAE**	**RMSE**
10%	0.81	2.80	3.27
50%	0.86	2.38	2.85
90%	0.89	2.04	2.45

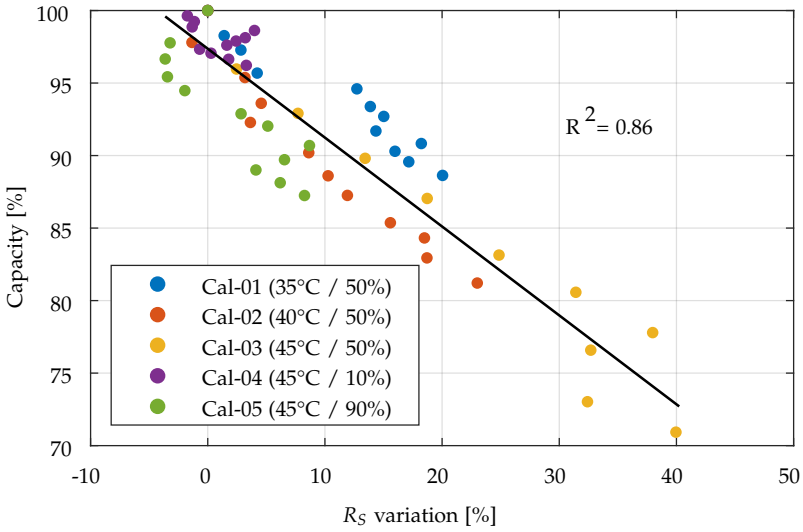

Fig. 4.8: Variation of R_s with the capacity for the five cells analyzed at 50% SOC.

4.1.2 Hybrid Pulse Power Characterization

The HPPC test is a widely used alternative to determine the internal resistance of the battery [64]. There are numerous works in the literature in which HPPC is used to determine the resistance, either directly or through simple EEC circuits [32, 65, 66]. This section studies the performance of this method to estimate the SOH of EV batteries.

Methodology

The HPPC consists of a succession of short duration pulses followed by a relaxation time. Three different values of current 0.5C, 1C and 1.5C were used, with a duration of 18 seconds. The minimum recommended relaxation time between pulses is 10 minutes [64], in this experiment the time was extended up to 30 minutes. Discharge pulses were alternated with charge pulses of equal current value so as not to alter the SOC during the test, though this is not always possible due to cell voltage limits. This procedure, illustrated in Figure 4.9, was repeated at three different SOC levels, 10%, 50% and 90%.

Through this procedure the resistance is calculated after 1, 10 and 18 seconds of pulse, as indicated in Equation 4.7.

$$R_t = \frac{U_t - U_0}{\Delta I}, \quad [t = 1, 10, 18]. \tag{4.7}$$

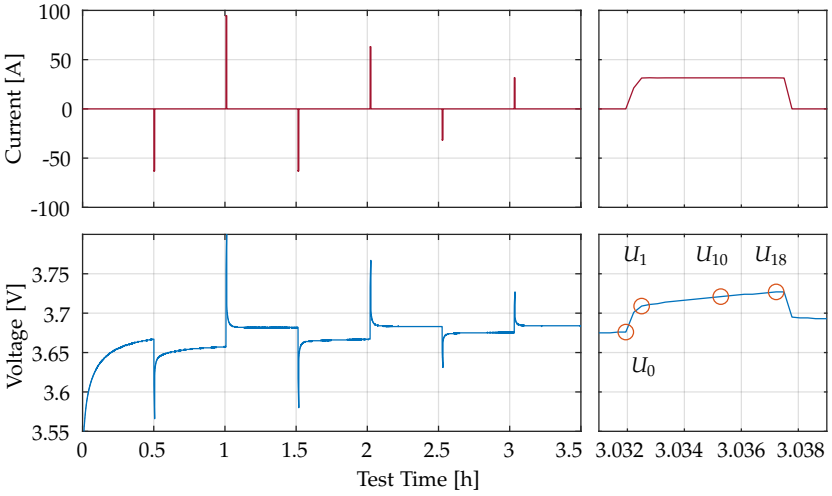

Fig. 4.9: HPPC procedure at 10% SOC with detail of the voltage measurements used for the internal resistance determination.

Pulse Parameters Influence

Figure 4.10.a shows the evolution of the internal resistance with the degradation measured by pulses of different current. In general, a higher resistance is observed when measured by lower current pulses. However, the variation on the results obtained by pulses of different currents is not significant and the trend in the three cases analyzed is very similar.

The influence of the pulse duration on the resistance measurement is illustrated in Figure 4.10.b. It is clearly observed how the resistance increases with the pulse duration. This is because, as time increases, the resistance due to other phenomena such as solid electrolyte interphase (SEI), double layer capacitances or the effect of charge transfer resistance is added to the ohmic resistance. The difference between the three resistances obtained increases as the battery ages due to the degradation caused by different aging mechanisms [61, 62].

Figure 4.11 shows the evolution of the resistance obtained as a function of the SOC. In the early stages of battery life, a higher resistance is observed at low SOC levels, while the minimum resistance is obtained at 50% SOC. However, this difference fades below 70% SOH.

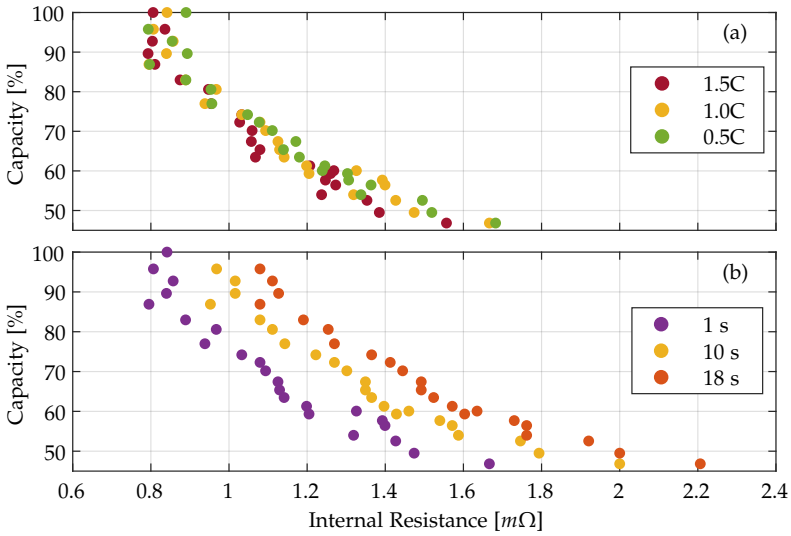

Fig. 4.10: Variation of internal resistance of cell Cal-03 with the capacity for different (a) pulse rates and (b) pulse duration.

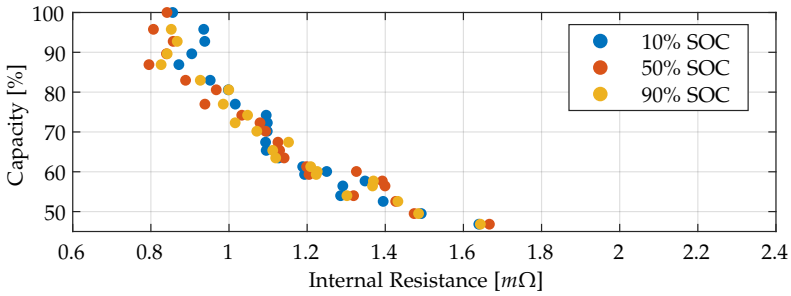

Fig. 4.11: Variation of internal resistance of cell Cal-03 with the capacity for different SOC levels.

SOH Estimation

According to the results, it is observed that the resistance obtained by HPPC is dependent on the capacity fade, as it occurred in the case of the ohmic resistance obtained through EIS. However, the relationship between both variables fluctuates with the aging conditions. Figure 4.12 shows the results of the evolution of the one-second resistance with the capacity of the cells subjected to calendar aging. Cells Cal-01 to Cal-03, stored at 50% SOC, show a similar trend in their resistance values. However, cells Cal-04 and Cal-05

do not exhibit the same behaviour with degradation. This is more clearly noticed by looking at the resistance results obtained at 90% SOC. In Figure 4.13 it is observed that cell Cal-05 has a parallel trend to the rest of the cells though separated by an initial capacity drop of around 15% with a negative resistance variation.

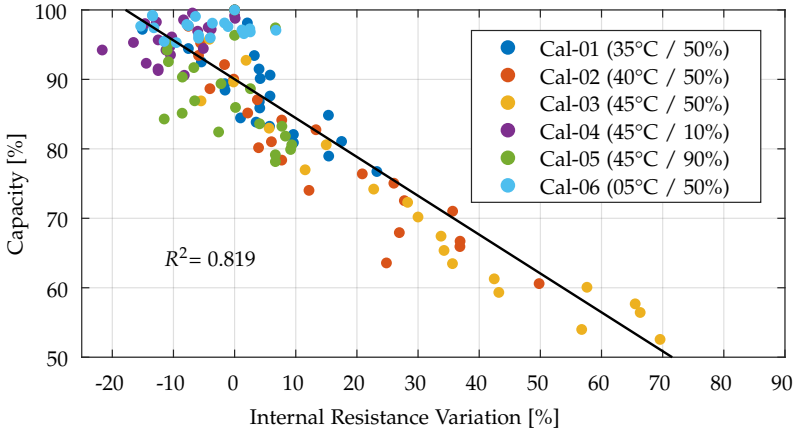

Fig. 4.12: Variation of R_{1s} with capacity for the calendar aged cells. Resistance obtained at 50% SOC and 1C pulse rate.

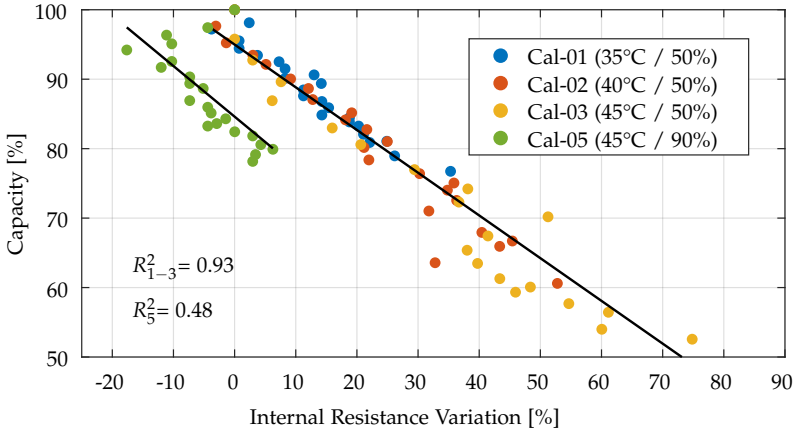

Fig. 4.13: Variation of R_{18s} with capacity for the calendar aged cells. Resistance obtained at 90% SOC and 1C pulse rate.

The results obtained by cycling aging also show discrepancies depending on the aging conditions. Figure 4.14 illustrates the evolution of the one-

second resistance for the five cells subjected to cycling aging. Cells Cyc-03 to Cyc-05 follow a very similar trend, with an accelerated increase in resistance with capacity fade. Cell Cyc-02 again shows a similar trend after an initial capacity drop, similar behavior as the cells subjected to calendar aging. Finally, the resistance of the cell Cyc-01 does not reveal a clear relationship with the capacity.

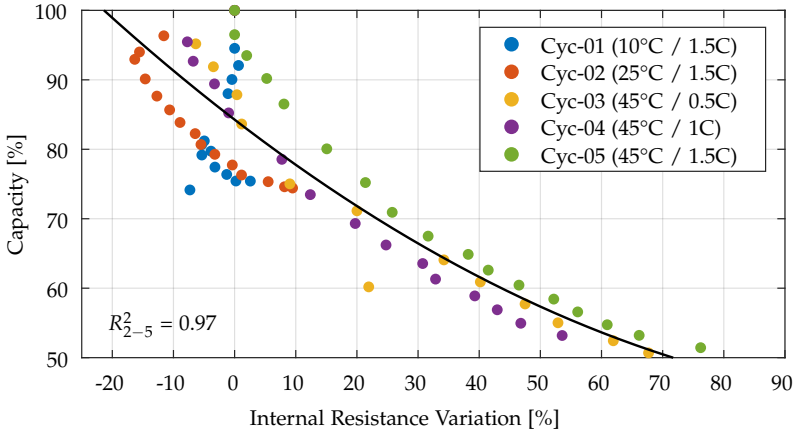

Fig. 4.14: Variation of R_{1s} with capacity for the cycling aged cells. Resistance obtained at 50% SOC and 1C pulse rate.

The metrics R^2, MAE and RMSE are compared to analyze the performance of the resistances obtained by HPPC. Table 4.2 shows the values obtained except for cells Cal-04, Cal-05, Cyc-01 and Cyc-02 which have been omitted due to the different degradation path.

The resistance measured by HPPC shows a good relationship with SOH in all the analyzed cases. No significant differences are observed between measurements obtained at different SOC levels. However, an error decrease is observed for longer pulse durations, obtaining RMSE below 3% for calendar aging cells and below 4.5% in the case of cycling aging cells.

The accuracy of this method is similar to that obtained by EIS, however, in the case of HPPC a resistance dependence on aging conditions is observed, which makes SOH estimation more complex and less convenient when the aging history is unknown.

Table 4.2: Statistic metrics of R_{1s}, R_{10s} and R_{18s} as SOH estimators at different SOC levels.

Calendar Aging					Cycling Aging				
SOC	**t**	**R^2**	**MAE**	**RMSE**	**SOC**	**t**	**R^2**	**MAE**	**RMSE**
	1s	0.91	3.23	4.12		**1s**	0.87	4.61	5.97
10%	**10s**	0.95	2.45	3.16	**10%**	**10s**	0.92	4.28	4.79
	18s	0.96	2.16	2.71		**18s**	0.93	4.16	4.5
	1s	0.91	3.06	4.13		**1s**	0.92	3.4	4.47
50%	**10s**	0.95	2.29	3.03	**50%**	**10s**	0.92	3.37	4.43
	18s	0.96	2.34	2.96		**18s**	0.93	3.21	4.19
	1s	0.88	3.4	4.85		**1s**	0.92	3.4	4.45
90%	**10s**	0.97	1.95	2.56	**90%**	**10s**	0.92	3.52	4.61
	18s	0.95	2.24	2.93		**18s**	0.92	3.49	4.53

4.2 Open Circuit Voltage Based Estimation

The open circuit voltage (OCV) is another widely used parameter to determine battery degradation. The voltage response depends on the cathode and the anode, as well as on the phase transformations they undergo during charging and discharging. With aging, variations in the electrochemical reactions occur, producing changes in the OCV curve.

The study of the voltage curves not only allows to estimate the state of health but also provides information about the main degradation mechanisms that occur in the cell. [67–70]. OCV variations are usually studied through incremental capacity analysis (ICA) [20, 21] or differential voltage analysis (DVA) [71, 72]. In the literature, different works have exposed that test conditions such as temperature [73, 74] or charging rate [69, 75] are key factors when implementing this method. Hence, these factors should be studied in order to obtain accurate and reliable estimates. The generalization from cell to vehicle is another challenge, since in the vehicle battery pack there are additional elements such as wiring or battery management system (BMS) that may produce deviations in the obtained results [76].

Methodology

The batteries used in this research come from commercial electric vehicles, more specifically the so-called B-cells from the BMW i3 with 63 Ah, the C-cells from the second-generation Nissan Leaf with 57.5 Ah, and the D-cells similar to the ones used in vehicles such as Tesla Model S [77], with 4 Ah capacity.

In order to evaluate the performance of this method, several cells were subjected to different aging conditions. The test matrix and the results from the aging tests are detailed in Chapter 2.

The IC curves of cells and vehicles are obtained from the voltage curve during charging. Figure 4.15 shows the typical vehicle charging process, which consists of two phases, the first at constant current (CC) until the voltage reaches its maximum and the second at constant voltage (CV) until the current reaches the cut-off value. The IC curves are obtained from the constant current phase.

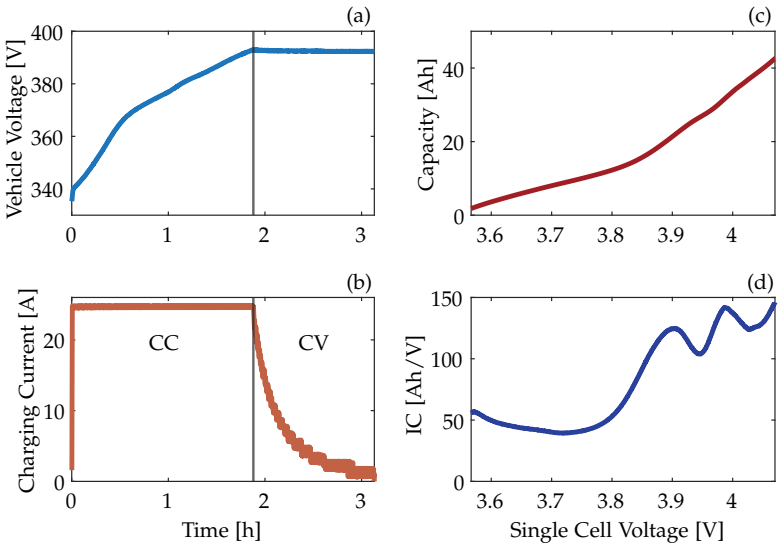

Fig. 4.15: Vehicle test procedure: (a) voltage response, (b) current profile (c) charge capacity during the CC stage, (d) incremental capacity scaled down to cell level. Adapted from [J2].

In this work the current and voltage measurements were recorded at a sampling frequency of 1 Hz (f_s). Raw data would produce a noisy IC curve, making it difficult to identify the features of interest (FOIs) such as peaks and valleys. Therefore, data is first smoothed using a moving average filter that can be expressed as in Equation 4.8:

$$v_{ma,j} = \sum_{i=j-\frac{m}{2}}^{j+\frac{m}{2}} \frac{v_i}{m}; \quad m = f_s t_{ma}. \tag{4.8}$$

Where v_i is the voltage measurement, v_{ma} is the filtered voltage and m is the number of samples in the averaging window (t_{ma}). Hence each voltage value is defined as the average of its m nearest neighbors. With the smoothed data, the IC is calculated, which is defined as the derivative of the capacity (dq) with respect to the voltage (dv), as described in Equation 4.9. A fixed voltage interval (Δv) is used to make the calculation [78].

$$IC = \frac{dq}{dv} \approx \frac{\Delta q}{\Delta v}. \tag{4.9}$$

Both the averaging window and the interval voltage used to calculate the IC have an influence on the shape of the curves obtained. Very low values would produce noisy results, interfering with feature detection, while values that are too high would lead to over-smoothed curves causing severe deformations and loss of information. To determine the optimal values, in Paper J2 different values for t_{ma} and Δv are tested, as shown in Figure 4.16, with the aim of reducing noise and minimizing the loss of information from the IC curves. Hence, it was determined that the best results were obtained with an averaging window of 200 s and an interval voltage of 40 mV.

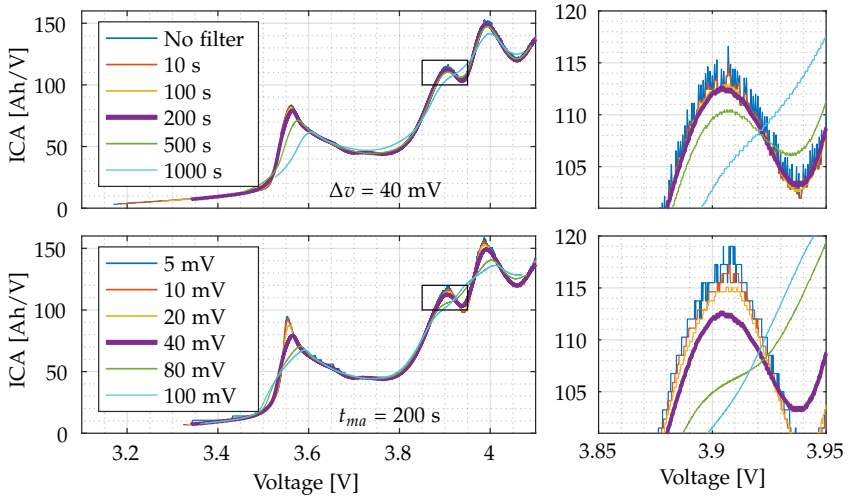

Fig. 4.16: Moving average window t_{ma} (top), and voltage increment Δv (bottom) comparison for IC processing. Adapted from [J2].

Temperature and Charging Rate Influence

The implementation of ICA in real-life applications such as the SOH estimation of EVs implies to overcome several challenges such as the effect of ambient temperature, temperature increase during charging or the need to reduce testing time and thus increasing the charging rate. In order to face this task, it is necessary to evaluate the impact of different test conditions on the IC curve. Paper J3 analyzes the effect of six temperatures (10ºC, 15ºC,

20ºC, 25ºC, 30ºC and 35ºC) and four charging rates (C/25, C/5, C/2 and 0.87C) on the shape of the curve and the position of the IC features of cell C.

With a charging rate of C/25, three peaks and two valleys can be observed at BOL state for this battery.

According to the literature, the shape of the IC curve can be altered by higher or lower rates and other parameters that affect battery kinetics and can broaden or sharpen the peaks [69, 75]. In addition to the IC curve shape, high currents and low temperatures affect the polarization, shifting the IC curve gradually to higher voltages.

However, this does not necessarily occur evenly throughout the entire voltage range. Figure 4.17 shows the IC variations as a function of charging rate and temperature. In this battery, opposite behaviors are observed in different features. The first peak (P1), is well defined at C/25, located at a voltage of 3.50 V. As the current and temperature gradually increase, P1 shifts to a voltage higher and flattens out being reduced to a shoulder.

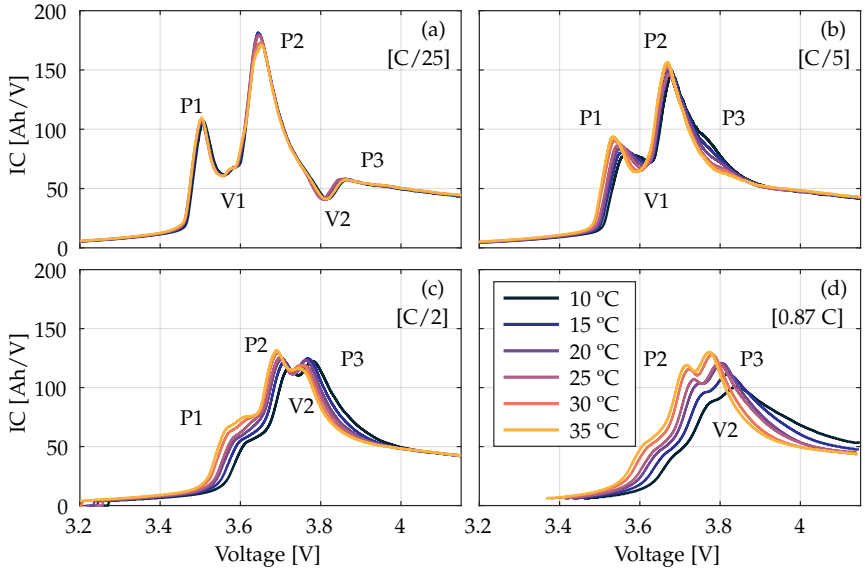

Fig. 4.17: IC curves obtained at BOL from cell C at different temperatures and charging rates; a) C/25, b) C/5, c) C/2, d) 0.87C; showing features P1, P2, P3 (peaks) and V1, V2 (valleys) Adapted from [J3].

On the contrary, when the trajectory of P3 is analyzed, it is observed that at C/25 it starts as the smallest of the three peaks, located at 3.85 V and at a height of 60 Ah/V. However, it becomes the main peak when the current is increased up to C/2, doubling its initial peak intensity. The peak can not be clearly observed between C/25 and C/2, instead a shoulder can be detected between 3.75 V and 3.85 V, at a lower voltage and increasing in size

as temperature decreases

Hence, it can be concluded that although there is a general trend towards a broadening and shifting of the curve with the increase of the charging rate this may not occur to all the peaks or features of the IC signature. Despite being under the same conditions, the different phase changes can diverge and cause opposite movements in the features of the resulting curve.

The lack of knowledge about IC behavior can lead to a misidentification of the features used for SOH estimation. Figures 4.17.b and 4.17.d show the same number of peaks, however these do not correspond to the same electrochemical processes. To support peaks identification, in Paper J3, half cells were set up from the anode and cathode of a fresh C-cell using metallic lithium as reference electrode.

Figure 4.18 shows the cathode, anode and full cell matching. The NMC cathode is represented in red, the graphite anode in blue, and the full cell in pink. There are some differences between the fresh full cell IC (solid pink) and the full cell IC calculated from the anode and cathode (dotted pink). This may be due to kinetic differences between full cell and half cells assembled in the laboratory.

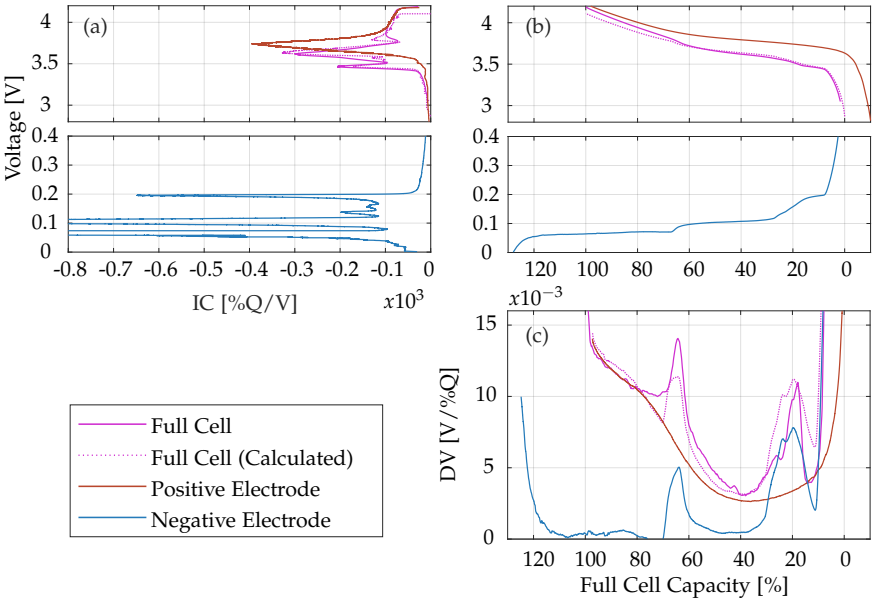

Fig. 4.18: Voltage curves of the tested electrodes corresponding IC and DV curves. Negative electrode (graphite) in blue, positive electrode (NMC) in red, full cell in pink (solid for the fresh full cell and dotted for the calculated from the separate electrodes). Adapted from [J3].

Figure 4.18.b shows the charge/discharge curve of the anode, cathode and full cell from which the IC and DV curves are derived and displayed in

Figures 4.18.a and 4.18.c respectively. The voltage plateaus observed in the voltage curves are produced by the phase transitions that occur during the discharge of the battery. Their quantity and position are easier to identify through ICA. In Figure 4.18.a, these phase transitions are observed as peaks, whose area represents the capacity stored in this process.

ICA allows to easily observe the effect of resistance increase with aging or due to charging current. However, the voltage difference between electrodes does not allow a direct visualization of the electrodes influence in the full cell curve.

The DV analysis allows to relate the phase transitions of both electrodes and their effect on the shape of the full cell curve, which can be calculated directly as the sum of the separate electrodes. In the DV curve, the peaks identify the phase equilibrium, while the valleys represent the transition between phases.

As explained in Paper J3, for cell C, three IC peaks are identified in the anode due to the interaction between different intercalation stages of Li+ in the graphite and the NMC phase transitions [69, 79, 80]. No phase equilibria are observed at the cathode, the transition between metal oxidation states occurs forming a single IC peak [81, 82]. Therefore, it is observed that the two-phase equilibria of the anode overlap with the voltage plateau of the cathode, forming the IC signature with three peaks and two valleys characteristic of this cell.

As already explained, the shape of the IC signature and therefore the location of the potential features is affected by test conditions. Furthermore, degradation also affects the IC curve unevenly, causing some FOIs to fade before others. Therefore, it is essential to analyze the evolution of the peaks and valleys as well as their behavior with test conditions to obtain a reliable and accurate SOH estimation in the entire range of conditions required.

In Paper J3, the effect of the current on the ICA is analyzed. Figure 4.19 shows the evolution of the IC curve for cell B-Cal-03 at two different charging rates, C/5 and C/2. At BOL, four peaks can be observed using C/5 while only three of them are visible at C/2. During the first aging stages, features P3 and P4 disappear when the upper voltage limit is reached due to the resistance increase and progressive shift of the entire curve towards higher voltages.

The first peak P1, initially located around 3.55 V, fades progressively with battery degradation, not being visible beyond 80% SOH. Upon reaching 60% SOH a new peak emerges in the path of the former P1, for practical reasons it is considered a different feature and renamed as P5.

The second peak P2, located at BOL around 3.9 V, shifts towards higher voltages with degradation. However, the height of this feature does not vary linearly with capacity. It is possible to observe it beyond 60% SOH at C/5, but at C/2 it shifts outside the voltage limits.

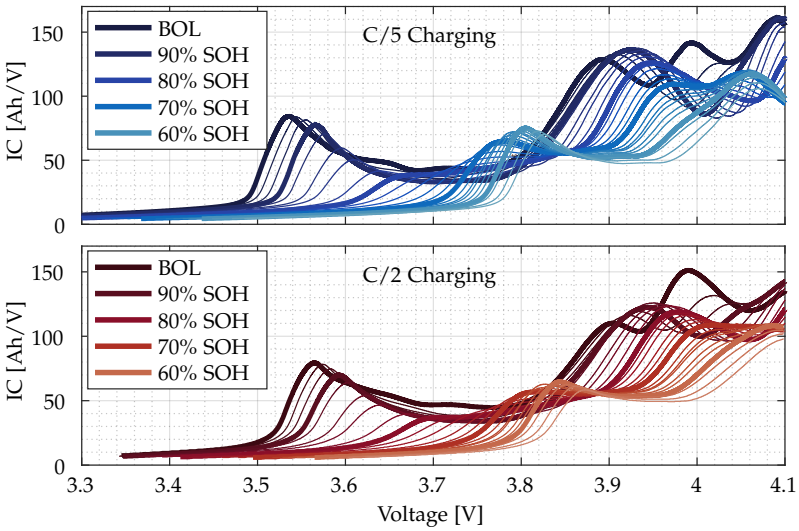

Fig. 4.19: IC curves evolution at different charging rates for cell B-Cal-03. Adapted from [J2].

Paper J3 studies the effect of temperature and charging rate on the ICA of cell C. Figure 4.20 shows the evolution of the IC signature of cell C-Cal-07 at three different charging rates (C/5, C/2 and 0.87C) and three different temperatures (10ºC, 25ºC and 35ºC).

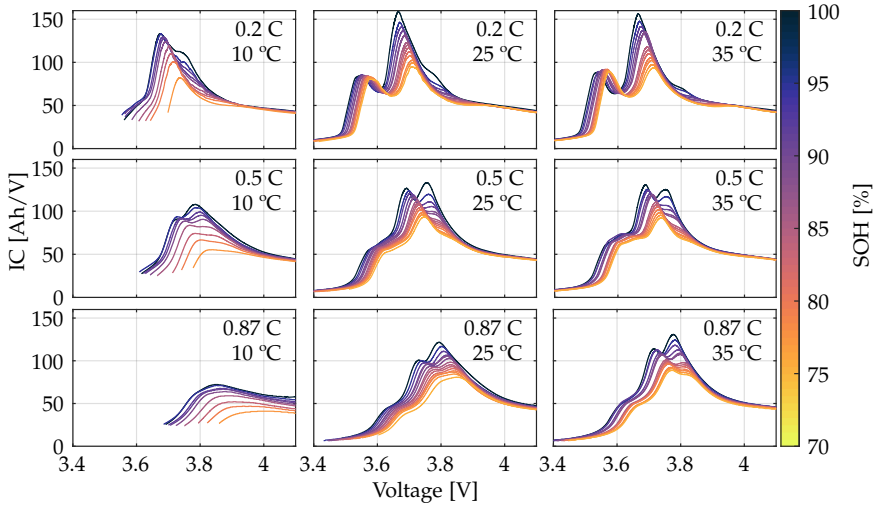

Fig. 4.20: IC curves evolution at different conditions of C-rate and temperature for cell C-Cal-07. Adapted from [J3].

In this case, contrary to the results shown at C/25 in Figure 4.17, a maximum of two peaks and one valley are observed simultaneously.

The results at 25ºC and 35ºC are very similar. P1 can only be clearly observed at a rate of C/5 and its height remains constant with aging, besides the shift towards higher voltages due to the internal resistance increase remains practically unchanged after 25% degradation. Under these conditions P2 is the main feature, however its size and shape become rather similar to P1 by the end of the test. Regarding P3 it can only be observed at BOL as a localized shoulder at 3.8V and being practically not perceptible at C/5. However, when the charging rate is increased up to C/2, P3 matches its height with P2, though its height decreases at a faster rate with aging than P2. P3 becomes the main feature at 0.87C and as the cell degrades it reaches the same peak intensity as P2 until they converge into a single wide peak. Overall, it can be observed that when temperature decreases or current increases features P1 and P2 flatten and shift towards higher voltages, even fading under some conditions. Nevertheless, P3 remains at almost the same voltage position at C/5 and 0.87C becoming more visible as charging rate increases.

Figure 4.21 shows the IC signature evolution from D-cal-06 cell for the nine combinations of charging rate and temperature.

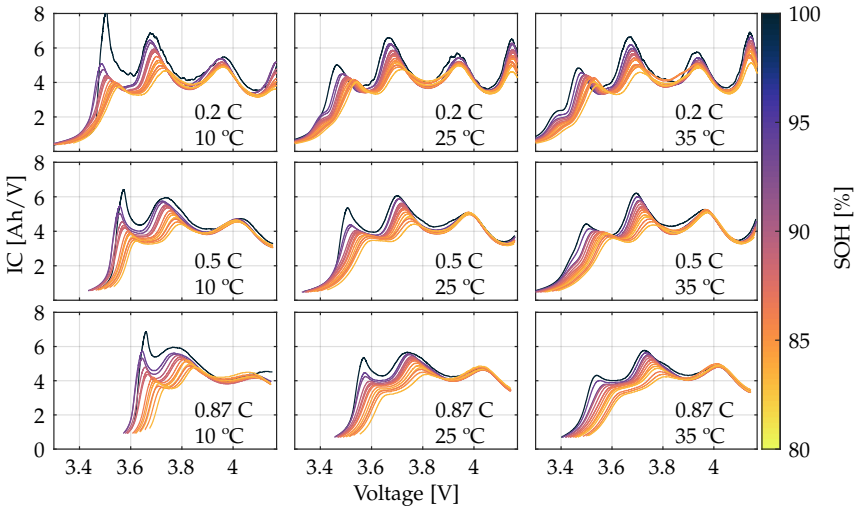

Fig. 4.21: IC curves evolution at different conditions of C-rate and temperature for cell D-Cal-06.

In this cell, it is possible to observe up to four peaks and three valleys, all with a similar height and area. However, P4 peak can only be observed at a low charging rate as it is close to the upper voltage limit.

On the other hand, P3 peak barely varies its voltage position or height with capacity, so it is not a good feature to estimate the SOH either. Finally,

both P1 and P2 are visible for all conditions analyzed. Both flatten and shift towards higher voltages, although under conditions of high charging rate and high degradation P1 begins to fade becoming a shoulder of P2.

The ICA of the three analyzed cells reveals the feasibility of this method to estimate the SOH for different batteries. In all three cases there is at least one feature that shows a relationship with the degradation in the test conditions analyzed.

When selecting the most suitable features for SOH estimation, it is important to consider their visibility under different conditions and their performance. In the case of cells D, it is observed that P2 and P3 seem to be the best features since they are present in most of the test conditions analyzed and show a marked variation with aging.

Features dependence on test conditions

The different charging rate and temperature conditions not only modify the position of the features but also their evolution with capacity, and consequently their performance as SOH estimator. Therefore, to get an accurate estimate it is necessary to select the appropriate features depending on the conditions. In Paper J3, the performance of different visible features in cell C is analyzed as a function of temperature and charging rate.

Figures 4.22 and 4.23 show the relationship between the peak intensity of P2 and P3 and the capacity of the cells for different charging rates and temperature conditions.

Figure 4.22 shows that P2 is a suitable feature at C/5 and C/2 for temperatures of 25ºC and 35ºC, with R^2 of 0.95 and 0.97, respectively. However, at 10ºC and C/5 the behavior becomes slightly non-linear and as the current increases to C/2, P2 ceases to be a good indicator. Figure 4.23 shows similar results for feature P3. Although P3 is not present at C/5, it seems to have a good relationship with capacity at C/2 and 0.87C. However, a limitation is again observed at 10ºC, since at 0.87C P3 can not longer be used as an SOH indicator.

It is hence concluded that the potential of a feature to estimate the SOH depends indeed on the test conditions and that for each set of conditions there may be different features that are the most suitable for estimation.

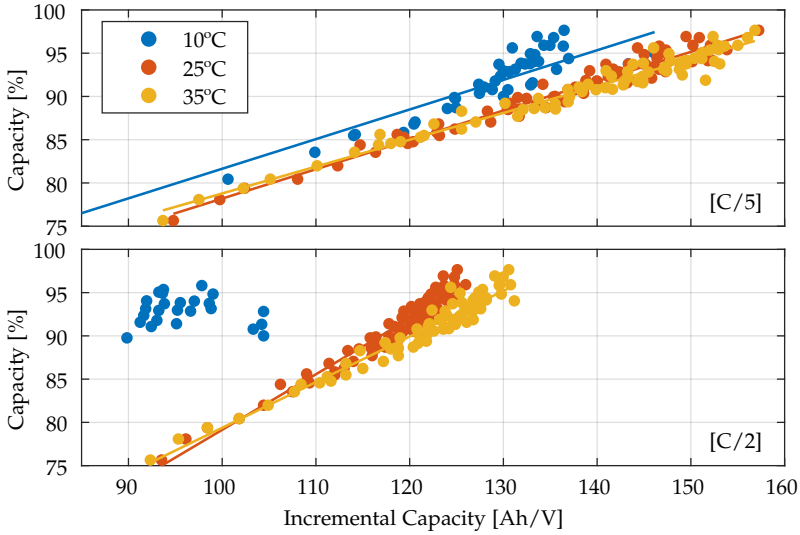

Fig. 4.22: Relationship between capacity and P2 peak intensity at different charging rates and temperatures.

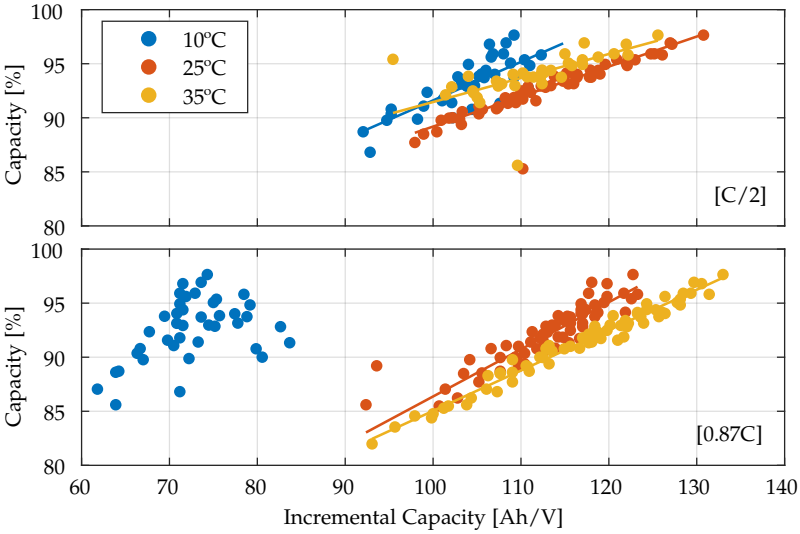

Fig. 4.23: Relationship between capacity and P3 peak intensity at different charging rates and temperatures.

Table 4.3 summarizes the performance results, comparing the R^2, Mean Absolute Error (MAE) and RMSE of features P2, P3 and V2 for different

Table 4.3: Statistic metrics of the analyzed FOIs at different conditions of current and temperature. Adapted from [J2].

		10ºC			25ºC			35ºC		
		R^2	**MAE**	**RMSE**	R^2	**MAE**	**RMSE**	R^2	**MAE**	**RMSE**
P2	0.2C	0.79	1.56	2.01	**0.95**	**0.71**	**0.98**	**0.97**	**0.65**	**0.84**
	0.5C	0.02	-	-	0.94	0.86	1.12	**0.94**	**0.83**	**1.08**
	0.87C	X	X	X	0.43	-	-	0.9	1.13	1.49
P3	0.2C	X	X	X	X	X	X	X	X	X
	0.5C	0.6	-	-	**0.95**	**0.44**	**0.49**	0.76	0.81	0.83
	0.87C	0.18	-	-	**0.86**	**0.95**	**1.17**	**0.97**	**0.49**	**0.64**
V2	0.2C	X	X	X	X	X	X	X	X	X
	0.5C	0.25	-	-	0.79	0.83	1.06	0.76	0.95	1.03
	0.87C	0.73	0.8	1.09	0.69	-	-	0.85	1.37	1.54

conditions of temperature and charging rate. The results in bold indicate the best estimator for each condition.

Vehicle tests

To validate if the ICA method can be generalized from cell level to vehicle level, a series of tests have been carried out on a sample of several vehicles with different mileage history.

Similarly to the cells, the batteries were discharged to the minimum voltage allowed by the vehicle and the tests were performed at a controlled temperature of 25ºC. In the automotive industry, the use of restricted voltage limits is more frequent for safety reasons and in order to extend battery life. Therefore, the capacity of a single cell cannot be directly compared to the capacity of an EV battery. Hence, to enable the comparison of results the "window capacity" is defined as the capacity measured between the lower and upper voltage limits of the vehicle during a constant current charge [78]. The scaled down voltage limits used in this dissertation are 3.60-4.08 V.

Figure 4.24 shows the IC curves of two BMW-i3 vehicles (cell B) with different mileage. For a one-month period, five and nine consecutive tests were carried out on each vehicle, respectively, obtaining maximum deviations of 1% window capacity. The tests were performed at a charging rate of 0.4C, obtaining an average window capacity of 41.1 Ah for the first vehicle and 39.2 Ah for the second, with higher mileage.

Due to more restrictive voltage limits, P1 is not visible in any of the vehicles tested. In the first vehicle, P3/V3 are still visible, which probably indicates, as discussed in Paper J2, that the battery experienced less than 5% capacity fade.

Figure 4.25 shows the IC curves obtained from a single vehicle Nissan Leaf (Cell C) over a 2-year time span.

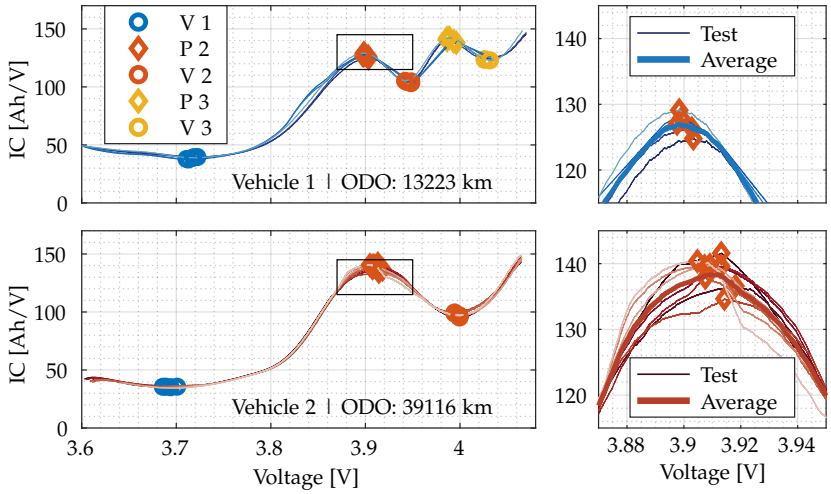

Fig. 4.24: IC curves obtained through multiple charges at 0.4C of two vehicles using cell-B. Adapted from [J2].

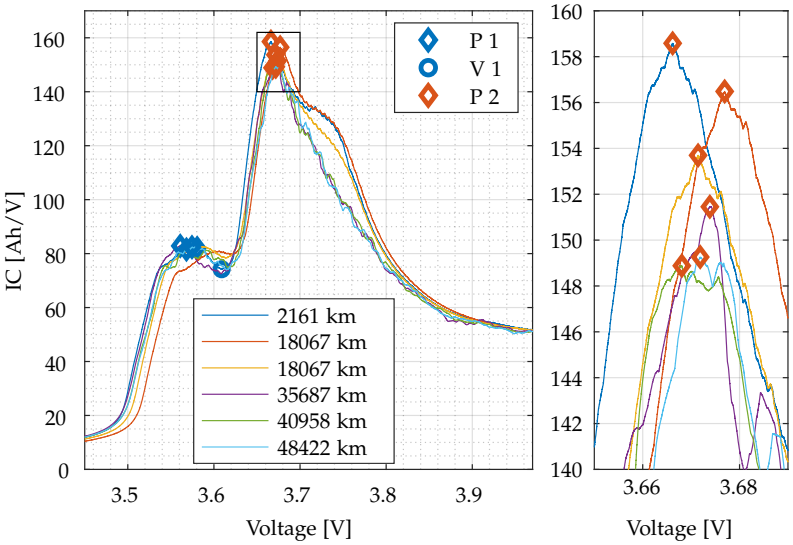

Fig. 4.25: IC curves obtained through multiple charges at 0.3C of a vehicle using cell-C.

The first test was carried out when the vehicle was practically new, with just 2,161 km, while for the last test the mileage of the vehicle amounted to

48,422 km. During this period, the window capacity was reduced from 39.1 Ah to 36.6 Ah, that is, 6.4% capacity fade. Two peaks can be observed in all the tests performed, though in the tests at the beginning of the vehicle life, it is also possible to observe a shoulder around 3.74 V corresponding to P3, which progressively flattened out with the degradation until it faded completely.

SOH Estimation

The features that best relate to capacity are selected to determine the SOH for both cells and vehicles. In the case of cell B, the best features to estimate the SOH are the voltage coordinates of P2/V2 and P5/V5. Figure 4.26 shows the relationship of these features with the window capacity of all the cells (calendar and cycling) and vehicles tested.

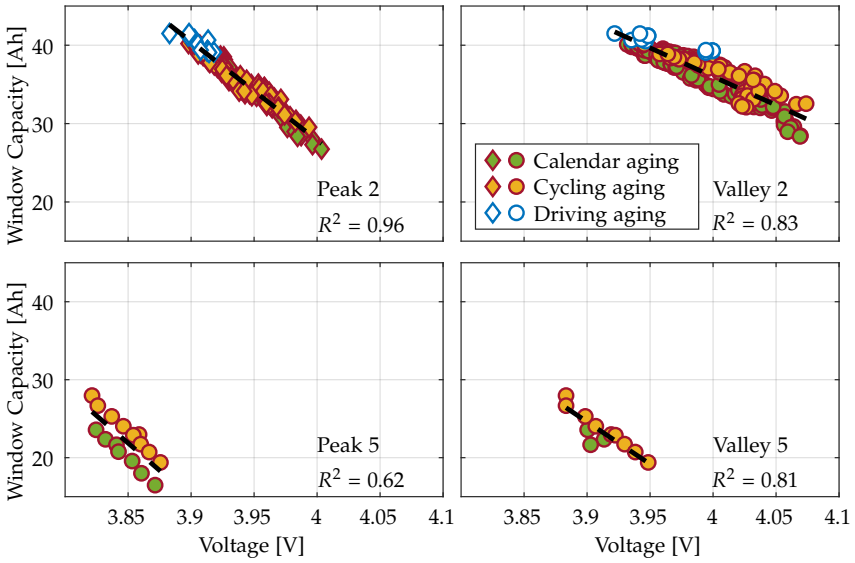

Fig. 4.26: The relationship between the window capacity and voltage, corresponding to Peak/Valley 2 (top) and Peak/Valley 5 (bottom). Adapted from [J2].

It is observed that P2 has a linear relationship with the window capacity, with an R^2 of 0.96 and without significant discrepancies between aging conditions. V2 also shows a linear relationship, however, a different slope is observed between the cells subjected to calendar and cycling aging. This could indicate the existence of different aging mechanisms occurring for both groups of cells and that this feature is aging path dependent.

Features P5 and V5 appear only after 70% SOH and therefore the number of samples is lower, because just a few cells reached that degradation level

during the tests. In the case of P5 it shows the same trend for the two groups of cells but with an offset of 4 Ah.

The SOH is estimated through multiple lineal regression of the available features. Figure 4.27 shows the SOH estimation results for cell B. The RMSE obtained from the set of eleven cells and the two vehicles is 2% with a maximum error below 6%. The results obtained are similar for cells subjected to calendar and cycling aging, although after 70% SOH the differences between them increase, since only P5 and V5 are available for estimation.

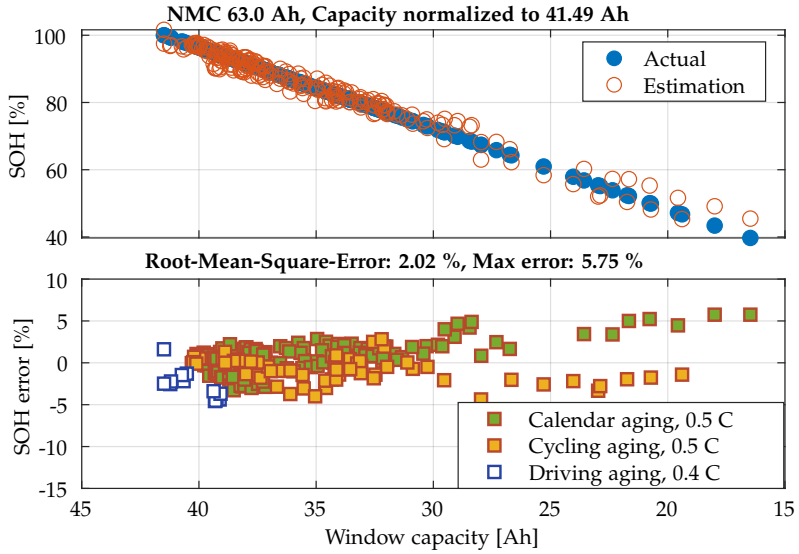

Fig. 4.27: SOH estimation from the IC measurements of cell-B by using FOIs P2,V2,P5,V5, at cell and vehicle level (top). Estimation error (bottom). Adapted from [J2].

In the case of cell C, the peak intensity of P2 and P3 are the best features for SOH estimation. Both are present at charging rates of C/2 or higher, although as the current increases, the performance of P3 outstrips P2. Finally, at C/5, P2 is the only valid feature.

Figure 4.28 shows the peak intensity relation of P2 and P3 with window capacity for different current conditions. Both features show a good trend with capacity regardless of aging conditions. However, a slightly nonlinear behavior is observed in P2 during the first aging stage. The feature P3 achieves good results as SOH estimator with high charging rates, obtaining an R^2 of 0.95 for 0.87C.

The SOH estimation results from cell C are shown in Figure 4.29. The RMSE obtained is 2.3% and the maximum error is 8%.

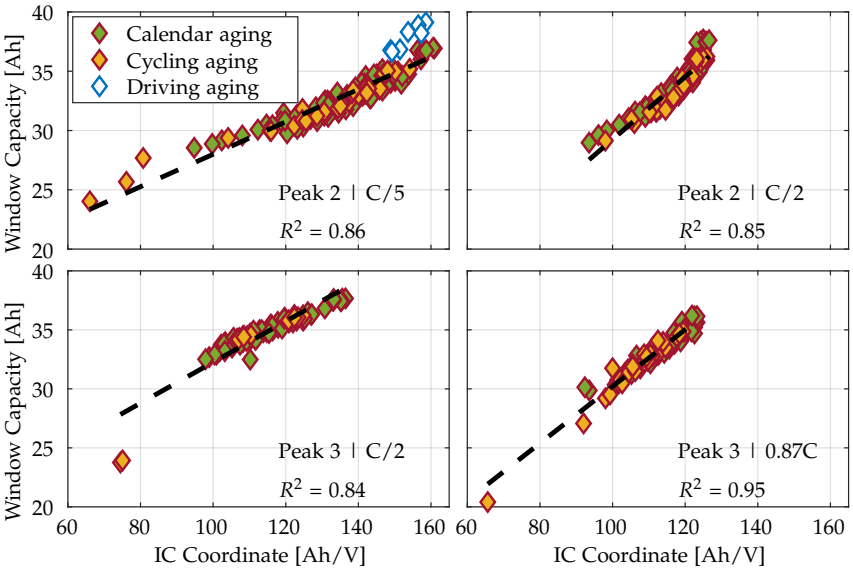

Fig. 4.28: The relationship between the window capacity and peak intensity at different C-rates, corresponding to Peak 2 (top) and Peak 3 (bottom).

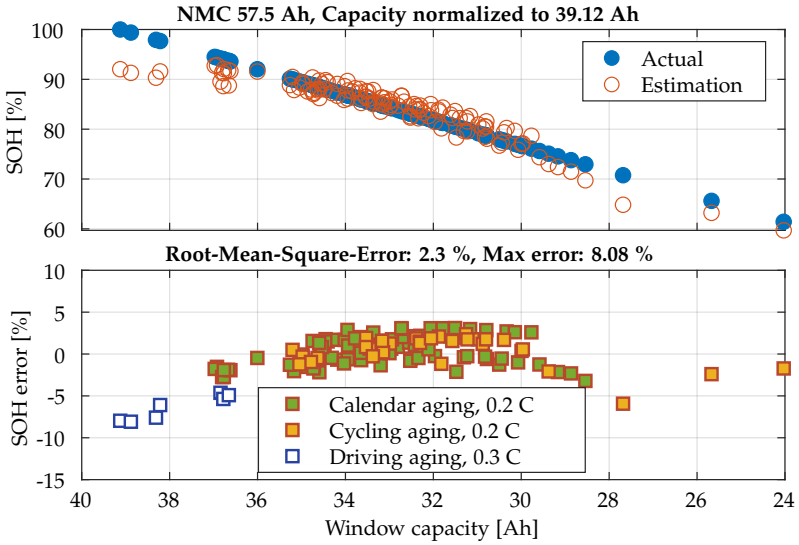

Fig. 4.29: SOH estimation from the IC measurements of cell-C by using FOI P2, at cell and vehicle level (top). Estimation error (bottom).

The results are rather similar between cells and with no significant differences due to aging conditions. However, the results obtained at vehicle level

are less accurate. The most probable reasons for the higher error could be that the capacity at BOL is slightly higher in the vehicle and that P2 shows a non-linear behavior just in that region.

4.3 Summary

This chapter studies the application of different SOH estimation methods on electric vehicle batteries. Firstly, using two of the main techniques to obtain impedance, EIS and HPPC, the relationship between the increase in internal resistance and capacity fade has been analyzed.

On the one hand, the EIS technique allows to obtain the impedance spectrum and also provides information on the aging mechanisms that occur in the cell. However, in this work, the only valid EEC parameter used was the ohmic resistance. Depending on the SOC used, the RMSE obtained in the SOH estimation through EIS ranged between 2.45% and 3.27%.

On the other hand, the HPPC also allows obtaining the internal resistance and is simpler to implement than the EIS. However, significant differences have been observed between cells at different aging conditions in which the duration of the pulse has a relevant role. By using longer pulses a higher internal resistance is obtained, since phenomena such as charge transfer resistance or diffusion processes are also measured and can be affected in different ways due to aging conditions. Nevertheless, for similar degradation paths, the pulse duration increase has a positive effect on the SOH estimation accuracy, obtaining RMSE below 3% with R_{18s} for cells subjected to calendar aging and 4.5% for cells subjected to cycling aging.

The use of ICA to determine the SOH both at cell and vehicle level has also been analyzed. Unlike impedance-based methods that require the injection of current pulses into the battery, ICA only requires the measurement of voltage and current during charging, making it the least intrusive of the investigated methods. Although this technique is usually used at very low currents and at room temperature, its implementation in electric vehicles implies variable working conditions. This work studied the effect of different temperatures and charging rates during cell charging, concluding that, although it is possible to raise the charging rate to values close to 1C, low temperature can be a limitation for some types of batteries. The method was applied to successfully estimate the SOH of two different cells subjected to different aging conditions, as well as of the vehicles in which they are used. Although some differences were found in the IC curves depending on the aging conditions, in all the cases analyzed, at least one independent feature with good qualities as SOH estimator was obtained. In this way, a combined RMSE between cells and vehicles below 2.3% was achieved for both types of cells analyzed.

Chapter 5

Conclusions and Future Work

This chapter summarizes the outcomes and conclusions of the research work carried out for the Ph.D. project "Electric Vehicle Batteries State Estimation Under a Wide Range of Test and Aging Conditions". The main contributions and future work are also detailed below.

5.1 Conclusions

First, the degradation performance of the four cells studied was analyzed in Chapter 2. To accomplish this task, the cells were subjected to calendar and cycling aging tests under different conditions of temperature, SOC and current profiles for a period between one and two years. The results showed an increasing capacity loss with storage temperature, in agreement with similar studies in the literature. Nevertheless, two different behaviors were detected depending on the SOC used in the calendar aging tests. Cells C and D showed a greater capacity fade for higher SOCs while cell B showed an unexpected accelerated capacity fade when combining high temperatures with medium SOC levels. The resistance measured showed, in general, a similar trend to the capacity loss. Cells C, however, presented a higher resistance increase for low temperature conditions (5ºC) or 10% SOC. Cell D despite showing similar capacity fade results to cell C, displayed an unusual resistance increase for high temperature and SOC conditions, doubling the resistance obtained in the same test of cell C. Regarding the cycling lifetime tests, an accelerated capacity loss at low temperature was observed in the tests performed at 10ºC, indicating that these conditions would be especially harmful in the case of cells C and D, for which the cycle life did not reach 500 cycles. Temperatures above 10ºC resulted in a moderate degradation rise at increasing temperatures, though substantial differences were found among the tested batteries. No significant effect of the C-rate or the mission profile

used was detected in the test performed.

In Chapter 3, the OCV curve was studied, analyzing the impact of aging, temperature and also the method used to obtain it in the SOC estimation. For this purpose, an extended Kalman filter was developed and implemented to compare the estimates obtained using different OCV curves. The results showed that, although the incremental method is the most accurate, at low rates of up to 0.25C the continuous method can also provide suitable results. The use of OCV obtained at BOL to estimate the SOC of a cell with a 7% capacity fade showed estimation errors four times higher than when using OCV corresponding with the current state of degradation. While the impact of temperature is practically negligible above 15ºC, lower temperatures severely alter the OCV. Therefore, it can be concluded that in order to maintain the same estimation accuracy at low temperatures or advanced degradation states, it is advisable to obtain the OCV as a function of these variables. The voltage characterization was later used in the implementation of a SOC and SOH estimation method based on Coulomb counting and OCV. Also, the effect on the efficiency of charging and discharging of different working conditions was studied in order to enable SOC estimation during battery operation under variable conditions. The use of the OCV avoided cumulative Coulomb counting errors regardless of the SOC, achieving estimate errors below 3%. Moreover, the proposed method estimates the capacity every time the vehicle is at rest, obtaining a SOH error below 1.5% during the 140-hour test performed on three different cells.

Chapter 4 studied the application of different SOH estimation methods for electric vehicles based on two different parameters, the impedance and the open circuit voltage. Two different techniques to obtain the impedance, EIS and HPPC, and their performance to estimate the capacity fade from the variation of the internal resistance were compared. Through EIS, the impedance spectrum was obtained and adjusted to an EEC model, achieving a maximum fitting error below 1%. From the analysis of the evolution of the different parameters of the equivalent circuit, it was concluded that the ohmic resistance was the only variable that presented a consistent evolution with the capacity fade. However, other parameters showed a relationship with the aging conditions and could therefore be used to identify different aging modes. Depending on the SOC at which the EIS is performed, it was possible to estimate the SOH regardless of the aging conditions with an RMSE between 2.45% and 3.27%. HPPC is faster and easier to implement, however it offers less information than EIS. The effect of SOC, rate and pulse length on the results obtained was studied. While SOC and rate did not appear to have a significant influence on the results, pulse duration did show a considerable impact. Short pulses of 1 second (R_{1s}) showed results close to the ohmic resistance obtained through EIS. Nevertheless, as the pulse duration increased, different trends were obtained depending on the aging conditions, although

the estimation accuracy increased for cells with a similar degradation path. Using R_{18s}, an RMSE below 3% was obtained for cells subjected to calendar aging, and 4.5% for cells subjected to cycling aging. Finally, ICA was used to determine the SOH in both cells and vehicles. Of the three methods analyzed, this is the least intrusive as it only requires collecting current and voltage measurements during charging. The effect of temperature and charging rate on IC features was analyzed, obtaining accurate SOH estimation with rates up to 0.87C. However, ICA showed a poor performance at low temperatures for some of the analyzed cells. The SOH of two different cells under different aging conditions and also of the corresponding vehicles was successfully estimated through this method, finding at least one independent feature as a strong indicator for SOC estimation in all the cases analyzed. For both types of cells analyzed, the combined RMSE between cells and vehicles achieved was below 2.3%.

5.2 Main Contributions

- Performance-degradation assessment of four different EV Li-ion cells subjected to calendar and cycling aging.
- Evaluation of the capacity, internal resistance and voltage response of the cells under a wide range of testing conditions.
- Assessment of the parameters affecting the open circuit voltage and their impact on the accuracy of the SOC estimation.
- SOC and SOH estimation method using Coulomb counting and the open circuit voltage.
- Assessment of the accuracy of impedance based methods for SOH estimation considering different operating conditions.
- In-depth analysis of the origin and behavior of different IC features validated through both experiments and simulation of the cell electrodes.
- SOH estimation method using incremental capacity analysis validated through extensive cell and vehicle tests in a wide range of test conditions.

5.3 Future Work

This Ph.D. research project has investigated the application of different battery state estimation methods on EVs, however from its results other possible lines of research have emerged that could improve this work, some of them are described below:

- Validate online estimation algorithms with real operation profiles and implement them in real vehicles.
- In-depth study of the degradation diagnosis to estimate not only the capacity but also the loss of lithium inventory and loss of active material, allowing a comprehensive understanding of the state of the cell.
- Validate the proposed methods in a larger number of vehicles and with a wider range of degradation.

References

[1] European Commission, "Fit for 55: delivering the EU's 2030 Climate Target on the way to climate neutrality," COM(2021) 550 final, Brussels, 2021. [Online]. Available: https://ec.europa.eu/info/sites/default/files/chapeau_communication.pdf

[2] ——, "Determining the environmental impacts of conventional and alternatively fuelled vehicles through LCA," doi = 10.2834/91418, Brussels, 2020. [Online]. Available: https://ec.europa.eu/clima/system/files/2020-09/2020_study_main_report_en.pdf

[3] European Environmental Agency (2020), "Air Quality in Europe – 2020 Report," EEA Report No. 09/2020, EEA, Copenhagen, 2020.

[4] European Commission, "Amending Regulation (EU) 2019/631 as regards strengthening the CO2 emission performance standards for new passenger cars and new light commercial vehicles in line with the Union's increased climate ambition ," 2021/0197 (COD), Brussels, 2021. [Online]. Available: https://eur-lex.europa.eu/resource.html?uri=cellar:870b365e-eecc-11eb-a71c-01aa75ed71a1.0001.01/DOC_1&format=PDF

[5] S. McBain and E. Bibra, "Electric Vehicles," IEA, Paris, 2021. [Online]. Available: https://www.iea.org/reports/electric-vehicles

[6] M. Abdelbaky, J. R. Peeters, J. R. Duflou, and W. Dewulf, "Forecasting the EU recycling potential for batteries from electric vehicles," *Procedia CIRP*, vol. 90, pp. 432–436, 1 2020.

[7] J. Zhu, I. Mathews, D. Ren, W. Li, D. Cogswell, B. Xing, T. Sedlatschek, S. N. R. Kantareddy, M. Yi, T. Gao, Y. Xia, Q. Zhou, T. Wierzbicki, and M. Z. Bazant, "End-of-life or second-life options for retired electric vehicle batteries," *Cell Reports Physical Science*, vol. 2, p. 100537, 8 2021.

[8] K. Vanherle and R. Vergeer, "Data gathering and analysis to improve the understanding of 2nd hand car and LDV markets and implications for the cost effectiveness and social equity of LDV CO2 regulations," 24 Avenue de Beaulieu, B-1040 Brussels, 2016. [Online]. Available: https://ec.europa.eu/clima/system/files/2016-11/2nd_hand_cars_en.pdf

[9] A. König, L. Nicoletti, D. Schröder, S. Wolff, A. Waclaw, and M. Lienkamp, "An Overview of Parameter and Cost for Battery Electric Vehicles," *World Electric Vehicle Journal*, vol. 12, p. 21, 2 2021. [Online]. Available: https://www.mdpi.com/2032-6653/12/1/21

[10] J. D. Graham and E. Brungard, "Consumer Adoption of Plug-In Electric Vehicles in Selected Countries," 2021. [Online]. Available: https://doi.org/10.3390/futuretransp1020018

[11] G. Krishna, "Understanding and identifying barriers to electric vehicle adoption through thematic analysis," *Transportation Research Interdisciplinary Perspectives*, vol. 10, 6 2021. [Online]. Available: https://doi.org/10.1016/j.trip.2021.100364

[12] F. H. Gandoman, J. Jaguemont, S. Goutam, R. Gopalakrishnan, Y. Firouz, T. Kalogiannis, N. Omar, and J. V. Mierlo, "Concept of reliability and safety assessment of lithium-ion batteries in electric vehicles: Basics, progress, and challenges," *Applied Energy*, vol. 251, p. 113343, 10 2019.

[13] C. Pastor-Fernández, T. F. Yu, W. D. Widanage, and J. Marco, "Critical review of non-invasive diagnosis techniques for quantification of degradation modes in lithium-ion batteries," *Renewable and Sustainable Energy Reviews*, vol. 109, pp. 138–159, 7 2019. [Online]. Available: https://linkinghub.elsevier.com/retrieve/pii/S136403211930200X

[14] D. Zhang, S. Dey, H. E. Perez, and S. J. Moura, "Real-Time Capacity Estimation of Lithium-Ion Batteries Utilizing Thermal Dynamics," *IEEE Transactions on Control Systems Technology*, vol. 28, no. 3, pp. 992–1000, 2020.

[15] M. Berecibar, I. Gandiaga, I. Villarreal, N. Omar, J. V. Mierlo, and P. V. D. Bossche, "Critical review of state of health estimation methods of Li-ion batteries for real applications," *Renewable and Sustainable Energy Reviews*, vol. 56, pp. 572–587, 4 2016.

[16] L. Chen, Z. Lü, W. Lin, J. Li, and H. Pan, "A new state-of-health estimation method for lithium-ion batteries through the intrinsic relationship between ohmic internal resistance and capacity," *Measurement: Journal of the International Measurement Confederation*, vol. 116, pp. 586–595, 2 2018. [Online]. Available: https://doi.org/10.1016/j.measurement.2017.11.016

[17] M. Galeotti, L. Cinà, C. Giammanco, S. Cordiner, and A. D. Carlo, "Performance analysis and SOH (state of health) evaluation of lithium polymer batteries through electrochemical impedance spectroscopy," *Energy*, vol. 89, pp. 678–686, 9 2015.

[18] D.-I. . Stroe, V. . Knap, and E. Schaltz, "State-of-Health Estimation of Lithium-Ion Batteries based on Partial Charging Voltage Profiles," *ECS Transactions*, vol. 85, pp. 379–386, 2018.

[19] E. . Schaltz, D.-I. . Stroe, K. . Nørregaard, B. . Johnsen, A. Christensen, E. Schaltz, D.-I. Stroe, K. Nørregaard, and B. Johnsen, "Partial Charging Method for Lithium-Ion Battery State-of-Health Estimation," vol. 17, 2019. [Online]. Available: https://doi.org/10.1109/EVER.2019.8813645

[20] D.-I. Stroe and E. Schaltz, "Lithium-Ion Battery State-of-Health Estimation Using the Incremental Capacity Analysis Technique," *I E E E Transactions on Industry Applications*, vol. 56, pp. 678–685, 2020. [Online]. Available: https://doi.org/10.1109/TIA.2019.2955396

[21] E. Schaltz, D.-I. Stroe, K. Nørregaard, L. S. Kofod, and A. Christensen, "Incremental Capacity Analysis Applied on Electric Vehicles for Battery State-of-Health Estimation," *I E E E Transactions on Industry Applications*, vol. 57, pp. 1810–1817, 2021. [Online]. Available: https://doi.org/10.1109/TIA.2021.3052454

[22] G. L. Plett, "Extended Kalman filtering for battery management systems of LiPB-based HEV battery packs Part 2. Modeling and identification," *Journal of Power Sources*, vol. 134, pp. 262–276, 2004. [Online]. Available: http://mocha-java.uccs.edu.

[23] P. Shrivastava, T. K. Soon, M. Y. I. B. Idris, and S. Mekhilef, "Overview of model-based online state-of-charge estimation using Kalman filter family for lithium-ion batteries," *Renewable and Sustainable Energy Reviews*, vol. 113, 10 2019. [Online]. Available: https://doi.org/10.1016/j.rser.2019.06.040

[24] M.-K. Tran, A. Dacosta, A. Mevawalla, S. Panchal, and M. Fowler, "Comparative Study of Equivalent Circuit Models Performance in Four Common Lithium-Ion Batteries: LFP, NMC, LMO, NCA," 2021. [Online]. Available: https://doi.org/10.3390/batteries7030051

[25] J. Xu, R. D. Deshpande, J. Pan, Y.-T. Cheng, and V. S. Battaglia, "Electrode Side Reactions, Capacity Loss and Mechanical Degradation in Lithium-Ion Batteries," *Journal of The Electrochemical Society*, vol. 162, pp. A2026–A2035, 7 2015. [Online]. Available: https://iopscience.iop.org/article/10.1149/2.0291510jeshttps://iopscience.iop.org/article/10.1149/2.0291510jes/meta

[26] "USABC electric vehicle Battery Test Procedures Manual. Revision 2." [Online]. Available: https://www.osti.gov/biblio/214312

[27] M. Dubarry, C. Truchot, B. Y. Liaw, K. Gering, S. Sazhin, D. Jamison, and C. Michelbacher, "Evaluation of commercial lithium-ion cells based on composite positive electrode for plug-in hybrid electric vehicle applications. Part II. Degradation mechanism under 2C cycle aging," *Journal of Power Sources*, vol. 196, pp. 10 336–10 343, 12 2011.

[28] C. R. Birkl, M. R. Roberts, E. McTurk, P. G. Bruce, and D. A. Howey, "Degradation diagnostics for lithium ion cells," *Journal of Power Sources*, vol. 341, pp. 373–386, 2 2017. [Online]. Available: http://creativecommons.org/licenses/by/4.0/

[29] M. Dubarry, N. Qin, and P. Brooker, "Calendar aging of commercial Li-ion cells of different chemistries - A review," 2018. [Online]. Available: www.sciencedirect.com

[30] J. Olmos, I. Gandiaga, A. S. de Ibarra, X. Larrea, T. Nieva, and I. Aizpuru, "Modelling the cycling degradation of Li-ion batteries: Chemistry influenced stress factors," *Journal of Energy Storage*, vol. 40, p. 102765, 8 2021. [Online]. Available: https://doi.org/10.1016/j.est.2021.102765

[31] D. Stroe, M. Swierczynski, A. I. Stan, and R. Teodorescu, "Accelerated lifetime testing methodology for lifetime estimation of Lithium-ion batteries used in augmented wind power plants," *2013 IEEE Energy Conversion Congress and Exposition, ECCE 2013*, pp. 690–698, 2013.

[32] V. Knap, D.-I. Stroe, R. Purkayastha, S. Walus, D. J. Auger, A. Fotouhi, and K. Propp, "Reference Performance Test Methodology for Degradation Assessment of Lithium-Sulfur Batteries," *Journal of The Electrochemical Society*, vol. 165, pp. 1601–1609, 2018.

[33] S. huang Wu and P. H. Lee, "Storage fading of a commercial 18650 cell comprised with NMC/LMO cathode and graphite anode," *Journal of Power Sources*, vol. 349, pp. 27–36, 5 2017.

[34] S. K. Rechkemmer, X. Zang, W. Zhang, and O. Sawodny, "Calendar and cycle aging study of a commercial limn2o4 cell under consideration of influences by cell progress," *Journal of Energy Storage*, vol. 30, p. 101547, 8 2020.

[35] T. Bank, J. Feldmann, S. Klamor, S. Bihn, and D. U. Sauer, "Extensive aging analysis of high-power lithium titanate oxide batteries: Impact of the passive electrode effect," *Journal of Power Sources*, vol. 473, p. 228566, 10 2020.

[36] S. F. Schuster, T. Bach, E. Fleder, J. Müller, M. Brand, G. Sextl, and A. Jossen, "Nonlinear aging characteristics of lithium-ion cells under different operational conditions," *Journal of Energy Storage*, vol. 1, pp. 44–53, 2015.

[37] L. D. Sutter, G. Berckmans, M. Marinaro, J. Smekens, Y. Firouz, M. Wohlfahrt-Mehrens, J. V. Mierlo, and N. Omar, "Comprehensive Aging Analysis of Volumetric Constrained Lithium-Ion Pouch Cells with High Concentration Silicon-Alloy Anodes," 2018. [Online]. Available: www.fivevb.eu

[38] M. F. Zia, E. Elbouchikhi, and M. Benbouzid, "Optimal operational planning of scalable DC microgrid with demand response, islanding, and battery degradation cost considerations," *Applied Energy*, vol. 237, pp. 695–707, 3 2019.

[39] C. Strange, S. Li, R. Gilchrist, and G. D. Reis, "Elbows of Internal Resistance Rise Curves in Li-Ion Cells," *Energies 2021, Vol. 14, Page 1206*, vol. 14, p. 1206, 2 2021. [Online]. Available: https://www.mdpi.com/1996-1073/14/4/1206/htmhttps://www.mdpi.com/1996-1073/14/4/1206

[40] P. Keil, S. F. Schuster, J. Wilhelm, J. Travi, A. Hauser, R. C. Karl, and A. Jossen, "Calendar Aging of Lithium-Ion Batteries," *Journal of The Electrochemical Society*, vol. 163, p. A1872, 7 2016. [Online]. Available: https://iopscience.iop.org/article/10.1149/2.0411609jeshttps://iopscience.iop.org/article/10.1149/2.0411609jes/meta

[41] K. S. Ng, C.-S. Moo, Y.-P. Chen, and Y.-C. Hsieh, "Enhanced coulomb counting method for estimating state-of-charge and state-of-health of lithium-ion batteries," *Applied Energy*, vol. 86, no. 9, pp. 1506 – 1511, 2009. [Online]. Available: http://www.sciencedirect.com/science/article/pii/S0306261908003061

[42] G. L. Plett, *Battery management systems*. Artech House, 2016, vol. 2.

[43] T. Wang, L. Pei, R. Lu, C. Zhu, and G. Wu, "Online Parameter Identification for Lithium-Ion Cell in Battery Management System," in *2014 IEEE Vehicle Power and Propulsion Conference (VPPC)*, 2014, pp. 1–6.

[44] H. Pan, Z. Lü, H. Wang, H. Wei, and L. Chen, "Novel battery state-of-health online estimation method using multiple health indicators and an extreme learning machine," *Energy*, vol. 160, pp. 466–477, 10 2018.

[45] G. won You, S. Park, and D. Oh, "Real-time state-of-health estimation for electric vehicle batteries: A data-driven approach," *Applied Energy*, vol. 176, pp. 92–103, 8 2016.

[46] X. Feng, C. Weng, X. He, X. Han, L. Lu, D. Ren, and M. Ouyang, "Online State-of-Health Estimation for Li-Ion Battery Using Partial Charging Segment Based on Support Vector Machine," *IEEE Transactions on Vehicular Technology*, vol. 68, pp. 8583–8592, 9 2019.

[47] K. Huang, Y. F. Guo, M. L. Tseng, K. J. Wu, and Z. G. Li, "A Novel Health Factor to Predict the Battery's State-of-Health Using a Support Vector Machine Approach," *Applied Sciences 2018, Vol. 8, Page 1803*, vol. 8, p. 1803, 10 2018.

[Online]. Available: https://www.mdpi.com/2076-3417/8/10/1803/htmhttps://www.mdpi.com/2076-3417/8/10/1803

[48] European Commission, "Supplementing Regulation (EC) No 715/2007 of the European Parliament and of the Council on type-approval of motor vehicles with respect to emissions from light passenger and commercial vehicles (Euro 5 and Euro 6)," C/2017/3521, Brussels, 2017. [Online]. Available: https://eur-lex.europa.eu/legal-content/EN/TXT/?uri=CELEX:32017R1151

[49] M. A. Roscher and D. U. Sauer, "Dynamic electric behavior and open-circuit-voltage modeling of LiFePO4-based lithium ion secondary batteries," *Journal of Power Sources*, vol. 196, pp. 331–336, 1 2011.

[50] M. Petzl and M. A. Danzer, "Advancements in OCV measurement and analysis for lithium-ion batteries," *IEEE Transactions on Energy Conversion*, vol. 28, pp. 675–681, 2013.

[51] F. Baronti, W. Zamboni, N. Femia, R. Roncella, and R. Saletti, "Experimental analysis of open-circuit voltage hysteresis in lithium-iron-phosphate batteries," *IECON Proceedings (Industrial Electronics Conference)*, pp. 6728–6733, 2013.

[52] V. J. Ovejas and A. Cuadras, "Effects of cycling on lithium-ion battery hysteresis and overvoltage," *Scientific Reports*, vol. 9, 12 2019.

[53] F. Baronti, W. Zamboni, R. Roncella, R. Saletti, and G. Spagnuolo, "Open-circuit voltage measurement of Lithium-Iron-Phosphate batteries," *Conference Record - IEEE Instrumentation and Measurement Technology Conference*, vol. 2015-July, pp. 1711–1716, 7 2015.

[54] Y. Cui, P. Zuo, C. Du, Y. Gao, J. Yang, X. Cheng, Y. Ma, and G. Yin, "State of health diagnosis model for lithium ion batteries based on real-time impedance and open circuit voltage parameters identification method," *Energy*, vol. 144, pp. 647–656, 2 2018.

[55] J. Meng, L. Cai, G. Luo, D. I. Stroe, and R. Teodorescu, "Lithium-ion battery state of health estimation with short-term current pulse test and support vector machine," *Microelectronics Reliability*, vol. 88-90, pp. 1216–1220, 9 2018.

[56] J. Jiang, Z. Lin, Q. Ju, Z. Ma, C. Zheng, and Z. Wang, "Electrochemical Impedance Spectra for Lithium-ion Battery Ageing Considering the Rate of Discharge Ability," *Energy Procedia*, vol. 105, pp. 844–849, 5 2017.

[57] W. Waag, S. Käbitz, and D. U. Sauer, "Experimental investigation of the lithium-ion battery impedance characteristic at various conditions and aging states and its influence on the application," *Applied Energy*, vol. 102, pp. 885–897, 2 2013.

[58] U. Tröltzsch, O. Kanoun, and H. R. Tränkler, "Characterizing aging effects of lithium ion batteries by impedance spectroscopy," *Electrochimica Acta*, vol. 51, pp. 1664–1672, 1 2006.

[59] D. I. Stroe, M. Swierczynski, A. I. Stan, V. Knap, R. Teodorescu, and S. J. Andreasen, "Diagnosis of Lithium-Ion Batteries State-of-Health based on Electrochemical Impedance Spectroscopy Technique," *2014 IEEE Energy Conversion Congress and Exposition, ECCE 2014*, pp. 4576–4582, 11 2014. [Online]. Available: https://vbn.aau.dk/en/publications/diagnosis-of-lithium-ion-batteries-state-of-health-based-on-elect

[60] C. T. Love, M. B. Virji, R. E. Rocheleau, and K. E. Swider-Lyons, "State-of-health monitoring of 18650 4S packs with a single-point impedance diagnostic," *Journal of Power Sources*, vol. 266, pp. 512–519, 11 2014.

[61] S. Gantenbein, M. Weiss, and E. Ivers-Tiffée, "Impedance based time-domain modeling of lithium-ion batteries: Part I," *Journal of Power Sources*, vol. 379, pp. 317–327, 3 2018.

[62] D. Andre, M. Meiler, K. Steiner, C. Wimmer, T. Soczka-Guth, and D. U. Sauer, "Characterization of high-power lithium-ion batteries by electrochemical impedance spectroscopy. I. Experimental investigation," *Journal of Power Sources*, vol. 196, pp. 5334–5341, 6 2011.

[63] Y. F. Pulido, C. Blanco, D. Anseán, V. M. García, F. Ferrero, and M. Valledor, "Determination of suitable parameters for battery analysis by Electrochemical Impedance Spectroscopy," *Measurement*, vol. 106, pp. 1–11, 8 2017.

[64] ISO Central Secretary, "Electrically propelled road vehicles –Test specification for lithium-ion traction battery packs and systems – Part 4: Performance testing," International Organization for Standardization, Geneva, CH, Standard ISO 12405-4:2018, 2018. [Online]. Available: https://www.iso.org/standard/71407.html

[65] H. He, R. Xiong, and J. Fan, "Evaluation of Lithium-Ion Battery Equivalent Circuit Models for State of Charge Estimation by an Experimental Approach," *Energies 2011, Vol. 4, Pages 582-598*, vol. 4, pp. 582–598, 3 2011. [Online]. Available: https://www.mdpi.com/1996-1073/4/4/582/htmhttps://www.mdpi.com/1996-1073/4/4/582

[66] M. Mathew, S. Janhunen, M. Rashid, F. Long, and M. Fowler, "Comparative Analysis of Lithium-Ion Battery Resistance Estimation Techniques for Battery Management Systems," *Energies 2018, Vol. 11, Page 1490*, vol. 11, p. 1490, 6 2018. [Online]. Available: https://www.mdpi.com/1996-1073/11/6/1490/htmhttps://www.mdpi.com/1996-1073/11/6/1490

[67] M. Dubarry, M. Berecibar, A. Devie, D. Anseán, N. Omar, and I. Villarreal, "State of health battery estimator enabling degradation diagnosis: Model and algorithm description," *Journal of Power Sources*, vol. 360, pp. 59–69, 8 2017.

[68] M. Dubarry, C. Truchot, and B. Y. Liaw, "Synthesize battery degradation modes via a diagnostic and prognostic model," *Journal of Power Sources*, vol. 219, pp. 204–216, 12 2012.

[69] Y. Chen, L. Torres-Castro, K.-H. Chen, D. Penley, J. Lamb, M. Karulkar, and N. P. Dasgupta, "Operando detection of Li plating during fast charging of Li-ion batteries using incremental capacity analysis," *Journal of Power Sources*, vol. 539, p. 231601, 8 2022. [Online]. Available: https://linkinghub.elsevier.com/retrieve/pii/S0378775322006048

[70] M. Dubarry, G. Baure, and A. Devie, "Durability and Reliability of EV Batteries under Electric Utility Grid Operations: Path Dependence of Battery Degradation," *Journal of The Electrochemical Society*, vol. 165, pp. A773–A783, 3 2018. [Online]. Available: https://iopscience.iop.org/article/10.1149/2.0421805jes

[71] J. Sieg, M. Storch, J. Fath, A. Nuhic, J. Bandlow, B. Spier, and D. U. Sauer, "Local degradation and differential voltage analysis of aged lithium-ion pouch cells," *Journal of Energy Storage*, vol. 30, p. 101582, 8 2020.

[72] M. Berecibar, M. Garmendia, I. Gandiaga, J. Crego, and I. Villarreal, "State of health estimation algorithm of LiFePO4 battery packs based on differential voltage curves for battery management system application," *Energy*, vol. 103, pp. 784–796, 5 2016.

[73] B. Jiang, H. Dai, and X. Wei, "Incremental capacity analysis based adaptive capacity estimation for lithium-ion battery considering charging condition," *Applied Energy*, vol. 269, 7 2020. [Online]. Available: https://www.researchgate.net/publication/341524458_Incremental_capacity_analysis_based_adaptive_capacity_estimation_for_lithium-ion_battery_considering_charging_condition

[74] M. Maures, R. Mathieu, A. Capitaine, J.-Y. Delétage, J.-M. Vinassa, and O. Briat, "An Incremental Capacity Parametric Model Based on Logistic Equations for Battery State Estimation and Monitoring," 2022. [Online]. Available: https://doi.org/10.3390/batteries8050039

[75] Y. Lin, B. Jiang, and H. Dai, "Battery Capacity Estimation Based on Incremental Capacity Analysis Considering Charging Current Rate," *World Electric Vehicle Journal 2021, Vol. 12, Page 224*, vol. 12, p. 224, 11 2021. [Online]. Available: https://www.mdpi.com/2032-6653/12/4/224/htmhttps://www.mdpi.com/2032-6653/12/4/224

[76] T. Kalogiannis, D.-I. Stroe, J. Nyborg, K. Nørregaard, A. E. Christensen, and E. Schaltz, "Incremental Capacity Analysis of a Lithium-Ion Battery Pack for Different Charging Rates," *ECS Transactions*, vol. 77, pp. 403–412, 7 2017. [Online]. Available: https://vbn.aau.dk/en/publications/incremental-capacity-analysis-of-a-lithium-ion-battery-pack-for-d-2

[77] G. Baure and M. Dubarry, "Synthetic vs. Real Driving Cycles: A Comparison of Electric Vehicle Battery Degradation," *Batteries 2019, Vol. 5, Page 42*, vol. 5, p. 42, 5 2019. [Online]. Available: https://www.mdpi.com/2313-0105/5/2/42/htmhttps://www.mdpi.com/2313-0105/5/2/42

[78] E. Schaltz, D. I. Stroe, K. Norregaard, L. S. Ingvardsen, and A. Christensen, "Incremental Capacity Analysis Applied on Electric Vehicles for Battery State-of-Health Estimation," *IEEE Transactions on Industry Applications*, vol. 57, pp. 1810–1817, 3 2021.

[79] C. Xu, P. J. Reeves, Q. Jacquet, and C. P. Grey, "Phase Behavior during Electrochemical Cycling of Ni-Rich Cathode Materials for Li-Ion Batteries," *Advanced Energy Materials*, vol. 11, p. 2003404, 2 2021. [Online]. Available: https://onlinelibrary.wiley.com/doi/full/10.1002/aenm.202003404

[80] R. Carter, T. A. Kingston, R. W. Atkinson, M. Parmananda, M. Dubarry, C. Fear, P. P. Mukherjee, and C. T. Love, "Directionality of thermal gradients in lithium-ion batteries dictates diverging degradation modes," *Cell Reports Physical Science*, vol. 2, p. 100351, 3 2021.

[81] R. Jung, M. Metzger, F. Maglia, C. Stinner, and H. Gasteiger, "Oxygen Release and Its Effect on the Cycling Stability of LiNixMnyCozO2 (NMC) Cathode Ma-

terials for Li-Ion Batteries," *Journal of The Electrochemical Society*, vol. 164, pp. A1361–A1377, 2 2017.

[82] B. G. Hudson and S. E. Mason, "Metal Release Mechanism and Electrochemical Properties of Lix (Ni1/3 Mn1/3 Co1/3)O2," *Applied Sciences (Switzerland)*, vol. 12, 4 2022.

Part II

Papers

Paper J1

Recursive State of Charge and State of Health Estimation Method for Lithium-Ion Batteries Based on Coulomb Counting and Open Circuit Voltage

Alejandro Gismero, Erik Schaltz and Daniel-Ioan Stroe

The paper has been published in
Energies Vol. 13(7), pp. 1811–1822, 2020.
DOI: 10.3390/en13071811

© 2020 by the authors. Licensee MDPI, Basel, Switzerland. This article is an open access article distributed under the terms and conditions of the Creative Commons Attribution (CC BY 4.0) license.

Paper J2

Electric Vehicle Battery State of Health Estimation Using Incremental Capacity Analysis

Alejandro Gismero, Kjeld Nørregaard, Bjarne Johnsen, Lasse Stenhøj, Daniel-Ioan Stroe and Erik Schaltz

The paper has been submitted to
Journal of Energy Storage 2022.

Paper J3

Influence of Test Conditions in the Incremental Capacity Analysis for the State of Health Estimation of Lithium-ion Batteries for Electric Vehicles

Alejandro Gismero, Matthieu Dubarry, Jia Guo, Daniel-Ioan Stroe and Erik Schaltz

The paper has been submitted to
Applied Energy 2022.

Paper C1

Calendar Aging Lifetime Model for NMC-based Lithium-ion Batteries Based on EIS Measurements

Alejandro Gismero, Daniel-Ioan Stroe and Erik Schaltz

The paper has been published in
2019 Fourteenth International Conference on Ecological Vehicles and Renewable Energies (EVER) Vol. 13(7), pp. 1–8, 2019.
DOI: 10.1109/EVER.2019.8813635

© 2019 IEEE. Reprinted, with permission, from A. Gismero, D. -I. Stroe and E. Schaltz, "Calendar Aging Lifetime Model for NMC-based Lithium-ion Batteries Based on EIS Measurements," *2019 Fourteenth International Conference on Ecological Vehicles and Renewable Energies (EVER)*, May 2019.

Paper C2

Comparative Study of State of Charge Estimation Under Different Open Circuit Voltage Test Conditions for Lithium-Ion Batteries

Alejandro Gismero, Daniel-Ioan Stroe and Erik Schaltz

The paper has been published in
IECON 2020 The 46th Annual Conference of the IEEE Industrial Electronics Society, pp. 1767-1772, 2020.
DOI: 10.1109/IECON43393.2020.9254429

© 2020 IEEE. Reprinted, with permission, from A. Gismero, D. -I. Stroe and E. Schaltz, "Comparative Study of State of Charge Estimation under Different Open Circuit Voltage Test Conditions for Lithium-Ion Batteries," *IECON Proceedings (Industrial Electronics Conference)*, October 2020.

ISSN (online): 2446-1636
ISBN (online): 978-87-7573-813-7

AALBORG UNIVERSITY PRESS